Toward modeling traffic-induced forest road erosion: field investigations and process-based model conceptualization

Amanda Alvis

A dissertation

submitted in partial fulfillment of the

requirements for the degree of

Doctor of Philosophy

University of Washington

2024

Reading Committee:

Erkan Istanbulluoglu, Chair

Charles Luce

Julie Dieu

Program Authorized to Offer Degree:

Civil & Environmental Engineering

University of Washington

Abstract

Toward modeling traffic-induced forest road erosion: field investigations and process-based
model conceptualization

Amanda Alvis

Chair of the Supervisory Committee:
Erkan Istanbulluoglu
Civil & Environmental Engineering

Though abundant anecdotal and empirical evidence of increased erosion on forest roads due
to traffic exists, the literature lacks a holistic treatment of the ways in which traffic and other
important contextual covariates influence runoff and erosion on forest roads. The main goal
of my dissertation is to examine the relationship between forest road erosion, traffic, and po-
tential erosion control treatments through literature synthesis, small-scale field experiments,
and the conceptualization of a comprehensive process-based model. In Chapter 2, I discuss
current hypotheses of how traffic affects forest road erosion, what data are required to vali-
date those hypotheses, and present the motivation for developing a process-based model of
forest road erosion. In Chapter 3, I evaluate the efficiency of multiple roadside ditch line
erosion control treatments using ditch line roughness, discuss the theory behind using rough-
ness as an efficiency metric, describe the methodology of the experiment, and present results
from the experiment. In Chapter 4, I use unoccupied aerial vehicle (UAV) structure-from-

motion (SfM) technology to examine how wheel ruts evolve on mainline logging forest roads following maintenance of the road surface. The implications of said rut formation on the road surface drainage system and erosion potential are discussed in detail. Finally, in Chapter 5, I lay the theoretical foundation for a process-based model that includes mathematical conceptualizations of traffic-induced local sediment production as well as road-segment-scale sediment transport.

TABLE OF CONTENTS

LIST OF FIGURES

LIST OF TABLES

ACKNOWLEDGMENTS

I have to open this with an apology: I'm sorry. I have no doubts that I am missing someone (or multiple someones) in these acknowledgements, but I promise that does not mean I am not grateful!

First and foremost, I would like to express my deepest gratitude to my advisor, Dr. Erkan Istanbulluoglu. Working with you has expanded my understanding of the world, scientifically and personally. I doubt you envisioned the sheer number of emails you were going to receive from me, and I am immensely grateful that you answered most (if not all) of them. Thanks for taking a chance on a hydrologically-intrigued physicist from the Midwest almost 8 years ago. I also could not have undertaken this journey without the support from my supervisory committee: Dr. Steven Walters, Dr. David Shean, Dr. Charlie Luce, and Dr. Julie Dieu. Steven, thank you for agreeing to be the GSR on my committee and for teaching me all I know about GIS. David, thank you for your reminders that the application of my drone surveys is "super freaking cool"; they have done wonders for my confidence in my work. Charlie, thank you for the endless conversations about road erosion and constantly making me feel like the work I do is valued. Julie, thank you for making fun of my skinny jeans and "city-girl shoveling" in the field (because, honestly, I needed that wake-up call) and for always, ALWAYS answering every question I throw at you, no matter how silly.

All of the work presented in my dissertation was made possible by public funding through the Cooperative Monitoring, Evaluation, and Research (CMER) Committee within the Washington State Department of Natural Resources Adaptive Management Program. I am deeply indebted to my colleagues on the CMER Roads Prescription-Scale Effectiveness Monitoring Project: Erkan Istanbulluoglu (again), Charlie Luce (again), Julie Dieu (again), Alexander Prescott, Tom Black, and Jenelle Black. Your endless help and support have made my dissertation not only possible but enjoyable, too! I feel so lucky to be part of this team filled with some of the smartest people I have ever met. From long days in the field to countless virtual meetings to drinking wine on the patio of a motel, you all have made this journey incredible.

I am extremely grateful for the camaraderie I found among other students (graduate and otherwise!) and faculty in Civil & Environmental Engineering at UW. Specifically, I want to thank Sai Nudurupati for being the mentor I needed in my first years of graduate school; Michelle Hu for being my GSAB co-chair, saner counterpart, and dear friend; and Lauren Wittkopf for being the most excellent undergraduate research assistant I could possibly have asked for. I also want to thank Dr. Nirnimesh Kumar for believing in me as a scientist

before I believed in myself. I miss you every day, and I wish you could be here.

Of course, I wouldn't be where I am today without my family and friends. Your love and support have meant the world to me. To Mom: Thank you for showing me that being a rad scientist doesn't preclude you from embracing your femininity. To Dad: Thank you for instilling in me a love of writing, goofiness, and terrible puns. To the A(nxious) Team (Andy, Abby, and Adam): not everyone can say that their siblings are their best friends, and I'm elated because I can. Thank you for being there for me for my whole life, but especially these past 8 years. To my incredible in-laws (mothers, siblings, et al.): How did I get lucky enough to marry into one of the coolest families of all time that also supports me in all of my endeavors?? To my friends (who I won't even try to name because there are so many of you): I can finally travel and hang out and play video games again. Let's do something fun. (Also, I promised Matthew Hinze a special shout-out because he sat with me for days as I did Pomodoro timers, cursed at my code, and asked "what's another word for ____ ?" countless times. You made this last month more fun than it had any right to be.)

Last, but certainly not least: Sebastian Alvis. My husband. My best friend. My whole entire heart. Words aren't enough to express my gratitude for everything that you've done and everything that you are. 9 years ago in November, we started dating, and a month later we were applying for grad schools in the same places because we knew that we didn't want to do long distance and that we were it for each other. This dissertation, this LIFE, wouldn't be possible without you. I love you. Thank you.

DEDICATION

To everyone who took the road less traveled by.

Chapter 1

INTRODUCTION

1.1 Background and motivation

Erosion of unpaved forest roads, and the relative impacts thereof, has been a topic of research for decades (*Bilby et al.*, 1989; *Boston*, 2016; *Dubé et al.*, 2010; *Foltz and Burroughs*, 1990; *Luce and Black*, 1999; *Megahan and Kidd*, 1972b; *Ramos-Scharrón and Macdonald*, 2005; *Reid*, 1981; *Reinhart et al.*, 1963; *Sheridan and Noske*, 2007; *Trimble and Sartz*, 1957; *Ziegler et al.*, 2001a). Throughout the years, we have learned that the majority of forest road erosion occurs on high-traffic, near-stream (HTNS) forest roads, specifically those associated with timber production. In Oregon and Idaho, *Black et al.* (2013) found that 90% of sediment delivered to nearby streams came from less than 10% of drainage points, with the majority of those drainage points existing on HTNS roads.

Though abundant anecdotal and empirical evidence of increased erosion of forest roads due to traffic exists (e.g., *Luce and Black*, 2001a; *Reid and Dunne*, 1984; *Sheridan et al.*, 2006; *Sugden and Woods*, 2007; *Ziegler et al.*, 2001b), the substantial literature lacks a comprehensive treatment of the ways in which traffic and other important contextual covariates influence erosion and runoff. To address sediment production from forest roads in a more efficient way, we need to advance our understanding of the erosion processes and potential

mitigation strategies.

One way to do this is to improve upon the current collection of forest road erosion models. Most forest road erosion models rely on empirical equations based on limited field data and require a more objective and process-based incorporation of traffic and other important contextual covariates. The main goal of this dissertation is to examine the relationship between forest road erosion, traffic, and potential erosion control treatments to help inform future models through literature synthesis, small-scale field experiments, and the conceptualization of a comprehensive process-based model.

1.2 Organization of dissertation

The chapters outlined below are part of a continuing collaborative effort funded by the Cooperative Monitoring, Evaluation, and Research (CMER) Committee within the Washington State Department of Natural Resources Adaptive Management Program to examine the effectiveness of forest road best management practices in western Washington.

Chapter 2 provides the extensive underlying motivation for Chapters 3, 4, and 5. In this chapter, I and my collaborators review the existing literature regarding interactions between traffic and road erosion, including a discussion of knowledge gaps, and we propose the need for a process-based modeling framework. We also present a limited factor framing that relates the ratios of erosion-sediment supply and transport capacity-sediment supply, similar to the Budyko hypothesis used in hydrometeorology.

Chapter 3 discusses using roughness as a metric to evaluate roadside ditch line erosion

control treatment efficiency. We present a small-scale field experiment that measured various hydraulic parameters of roadside ditch lines to examine roughness as an efficiency metric. This chapter provides the basis for the parameterization of a roadside ditch line in future versions of a process-based model presented in Chapter 5.

Chapter 4 discusses using unoccupied aerial vehicle (UAV) structure-from-motion (SfM) technology to examine how wheel ruts evolve on mainline logging roads following road grading and the implications of said rut formation on the road surface drainage system and erosion potential. This chapter provides potential parameterization information for the road surface in future versions of a process-based model presented in Chapter 5.

Chapter 5 lays the theoretical foundation for a process-based model that incorporates local processes of sediment production, as well as road-segment-scale sediment transport. Sediment production is proposed to be driven by four traffic-induced erosion-enhancing processes: crushing, pumping, scattering, and rutting. This chapter includes proof-of-concept examples and a discussion of future model versions.

Chapter 2

HOW DOES TRAFFIC AFFECT EROSION OF UNPAVED FOREST ROADS?

Abstract

The relationship between traffic and forest road erosion has been studied for decades, and the answer to the question "what happens when traffic is present on these unpaved forest roads?" is simple: erosion increases. However, the answer to the question "why does it increase?" is complex and requires us to consider forest road erosion through an integrated lens. Fully understanding how traffic affects forest road erosion will allow us to control forest road erosion effectively. In this synthesis, we look at forest road erosion literature and focus the discussion on the interactions between traffic and erosion. Specifically, we explore four main hypotheses that have been proposed to explain how traffic affects erosion. These hypotheses are discussed in detail, including what data and information are required to evaluate them. In addition to the specific traffic-erosion interactions, we review important factors that interact with traffic to enhance erosion. Finally, we propose a framework that

describes forest road erosion as a combination of all limiting factors. This framework can help guide future data collection needs, allow us to form a more holistic understanding of forest road erosion, and ultimately improve predictions of erosion from forest roads.

2.1 Introduction

Erosion from forest roads is a long-standing environmental problem (e.g., *Bilby et al.*, 1989; *Kochenderfer*, 1970; *Lane and Sheridan*, 2002; *Megahan and Kidd*, 1972a; *Packer*, 1967; *Sheridan and Noske*, 2007; *Trimble*, 1959; *Trimble and Sartz*, 1957), with ongoing contention over how best to prevent road-derived sediments from entering streams (e.g., *Aust et al.*, 2015; *Boston*, 2012; *Brown et al.*, 2015). Forest streams are generally cleaner than their counterparts in urban, suburban, and agricultural settings, making the impacts of turbid water from forest roads readily apparent. The set of standard best practices for managing sediment from roads includes protecting ditches with vegetation, placing sturdier rock on road surfaces, limiting traffic, and placing roads as far from streams as practical. Even so, locations exist where roads must cross or are located close to streams, and some of these near-stream roads carry substantial traffic. In these locations, options for erosion control are more limited, resulting in impacts that, from a practical standpoint, seem unavoidable. However, where protected fish species are affected, this unavoidability is better framed as an issue of economics and tradeoffs.

Erosion control solutions are commonly presented as two potential options: paving the road surface and limiting traffic on the road. These solutions been applied to varying loca-

tions where the value of both timber and fisheries are high (e.g., *Cederholm and Reid*, 1987). However, these two practices are expensive for forest land managers (e.g., *Edwards et al.*, 2016). Framing the management choices as stopping traffic or paving roads is too coarse, and more gradations in treatment choices need to be articulated. Certainly, we could express degrees of traffic limitation, such as an acceptable number of loaded trucks per unit time (e.g., *Croke and Hairsine*, 2006) or condition traffic on other factors, such as precipitation (e.g., *Dent et al.*, 2003). Similarly, engineering approaches like reduced tire pressure (e.g., *Foltz*, 1994; *Foltz and Elliot*, 1997), geotextiles placed in the subgrade (e.g., *Visser et al.*, 2017), and harder rock (e.g., *De Witt et al.*, 2020) have all been shown to help reduce sediment production and erosion on forest roads.

Unfortunately, the substantial literature covering the interactions between traffic and erosion lacks a holistic treatment of the various ways in which traffic influences sediment and runoff production from forest roads. Research does indicate that the presence of traffic increases forest road erosion (e.g., *Luce and Black*, 2001a; *Reid and Dunne*, 1984; *Sheridan et al.*, 2006; *Sugden and Woods*, 2007; *Ziegler et al.*, 2001a) though in a broad sense and with little quantitative accounting for context. Multiple hypotheses have been put forth regarding what traffic-induced processes are driving sediment production and erosion, including pumping, scattering, rutting, and crushing. However, these hypotheses are typically—often individually—invoked as a potential explanation of erosion (e.g., *Foltz et al.*, 2000; *Reid and Dunne*, 1984; *Swift*, 1984a), sometimes without a detailed mechanism being defined or providing quantitative expectations of effect. Some authors have gone further than others,

but research is still missing how these mechanisms interact with one another and how they are affected by other treatments for sediment reduction. If we want to address sediment production from high traffic roads in a more fine-tuned and efficient way, it is necessary to advance our understanding of these different effects on roads. The hypotheses that have been put forth need more specific definition, particularly so that quantitative models can be constructed to guide the data collection needed to test the models and hypotheses.

In this synthesis, we focus on the relationship between traffic and erosion by examining the current state of the literature and including a discussion of hypotheses and knowledge gaps. Additionally, we present a potential contextual framing for the erosion process with respect to traffic and other factors and discuss how we can further our understanding of erosion on unpaved forest roads. We begin by focusing on the specific ways in which traffic affects erosion from roads; we then discuss the ways in which erosion is enhanced by the interactions between traffic and contextual climate, topographic, and road characteristics; and we complete the discussion with a conceptualization that generalizes forest road erosion in terms of sediment supply and transport energy to quantify contextual interactions and expectations for treatments.

2.2   *Traffic-induced, erosion-enhancing processes*

Traffic is one of the most frequently cited drivers of erosion on unpaved forest roads. Disturbance of the road surface by heavy vehicles—leading to an increase in fine sediment supply and changes in the energy available for sediment transport—has been observed in many

studies (e.g., *Bilby et al.*, 1989; *Coker et al.*, 1993; *Luce and Black*, 2001a; *MacDonald et al.*, 2001; *Reid et al.*, 2016; *Reid*, 1981; *Swift*, 1984a; *Van Meerveld et al.*, 2014; *Ziegler et al.*, 2001b). These studies investigate the effects of traffic on erosion from a broad perspective, generally noting that erosion is highly correlated with the presence of traffic. This general understanding has motivated the development of hypotheses regarding the mechanics of traffic-induced erosion processes.

Observations and anecdotal evidence of the influence of traffic on erosion are multitudinous, but more information is needed to understand how and why traffic has such an influence, particularly if erosion caused by traffic is to be accurately represented in a model. Researchers have hypothesized multiple traffic-induced erosion processes: 1) crushing, 2) pumping, 3) scattering, and 4) flow rerouting. However, available datasets to evaluate these hypotheses are limited. In the next few sections, we address these processes in more depth and present a discussion of what we know and what we have yet to learn.

2.2.1 Crushing

Crushing occurs when a heavy vehicle, such as a loaded logging truck, drives over an aggregate-covered road surface, and the aggregate breaks down. The downward force exerted by the vehicle onto a brittle material causes breakage, increasing the supply of fine sediment available for transport (Figure 2.1a). Shifting of grains against one another under heavy loading causes chipping and abrasion of particles, which we lump conceptually in the term crushing. Crushing is posited to be influenced by aggregate quality, as well as frequency

and type of traffic. Because of its relation to other factors and plentiful anecdotal evidence (Figure 2.1b), crushing is one of the most cited traffic-induced erosion mechanisms in the literature (e.g., *Dawson and Kolisoja*, 2006; *Dubé et al.*, 2010; *Foltz and Truebe*, 1995, 2003; *Kemp et al.*, 2016; *Luce and Black*, 2001a; *Reid and Dunne*, 1984; *Rhee et al.*, 2018; *Toman and Skaugset*, 2011; *Ziegler et al.*, 2001b).
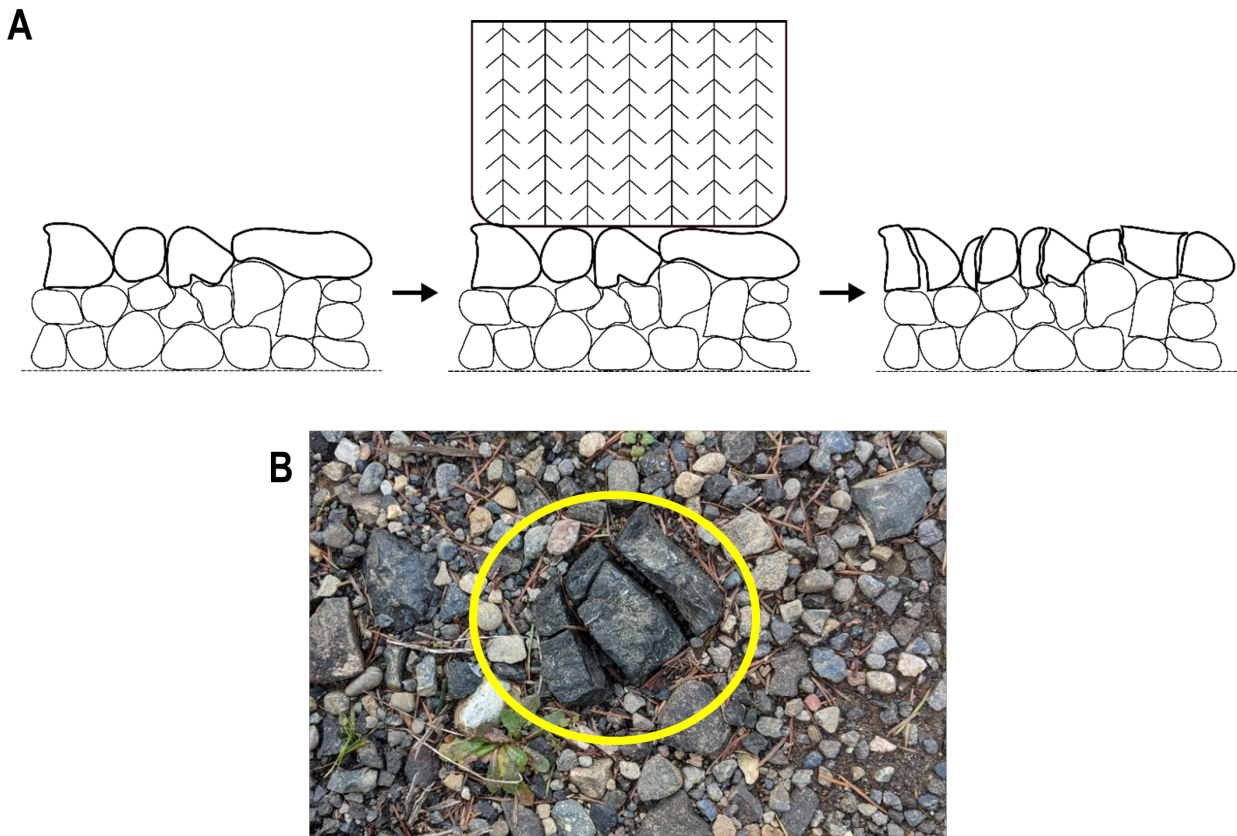
Figure 2.1: (a) Schematic of the crushing process. On a typical road surface aggregate (left) when vehicles drive over the road (center) the larger sediment breaks down into finer sediment (right). Image not to scale. (b) Image of forest road with evidence of crushing (circled in yellow).

Crushing is so closely connected with other factors affecting erosion that few data re-

garding the process of crushing—why and how it occurs—have been collected. Most field studies related to crushing focus on aggregate strength rather than the role that traffic plays with respect to aggregate. However, in a recent paper, *De Witt et al.* (2020) describe a field experiment in which they isolated different qualities of road surface aggregate in cylindrical geotextile bags to observe degradation after traffic had driven over the segment. The cylindrical geotextile parcels of aggregate were placed within the road surface and were subject to a different number of truck passes. The authors looked at the aggregate after 500, 950, and 1500 passes of a loaded dump truck and found that most of the degradation occurred within the first 500 truck passes for all aggregate qualities.

The results of this study confirm that crushing relates to traffic volume and frequency, but the observation resolution is still too low to capture the nonlinearities in the crushing rate. The authors recommend a future experiment with earlier and more frequent observations (i.e., check the aggregates after 100, 250, 350 truck passes) to capture the initial aggregate degradation rate and how it changes. Such an understanding would allow us to represent this diminishing rate process more accurately in a model.

2.2.2   Pumping

Pumping is the process by which fine sediment is forced upwards toward the surface of the road. When a vehicle passes over a gravel road surface, larger sediment is pushed down, which, in turn, displaces fine sediment, moving it upwards (Figure 2.2a). As this process is repeated, fine sediment makes its way to the surface of the road where it is readily available

for sediment transport, thus increasing the supply. Pumping has been suggested as a traffic-induced erosion process in many studies (e.g., *Dawson and Kolisoja*, 2006; *Foltz and Truebe*, 2003; *Luce and Black*, 2001a; *Ramos-Scharrón and Macdonald*, 2005; *Reid*, 1981; *Swift*, 1984b; *Ziegler et al.*, 2001b) and anecdotal evidence is abundant (Figure 2.2b).
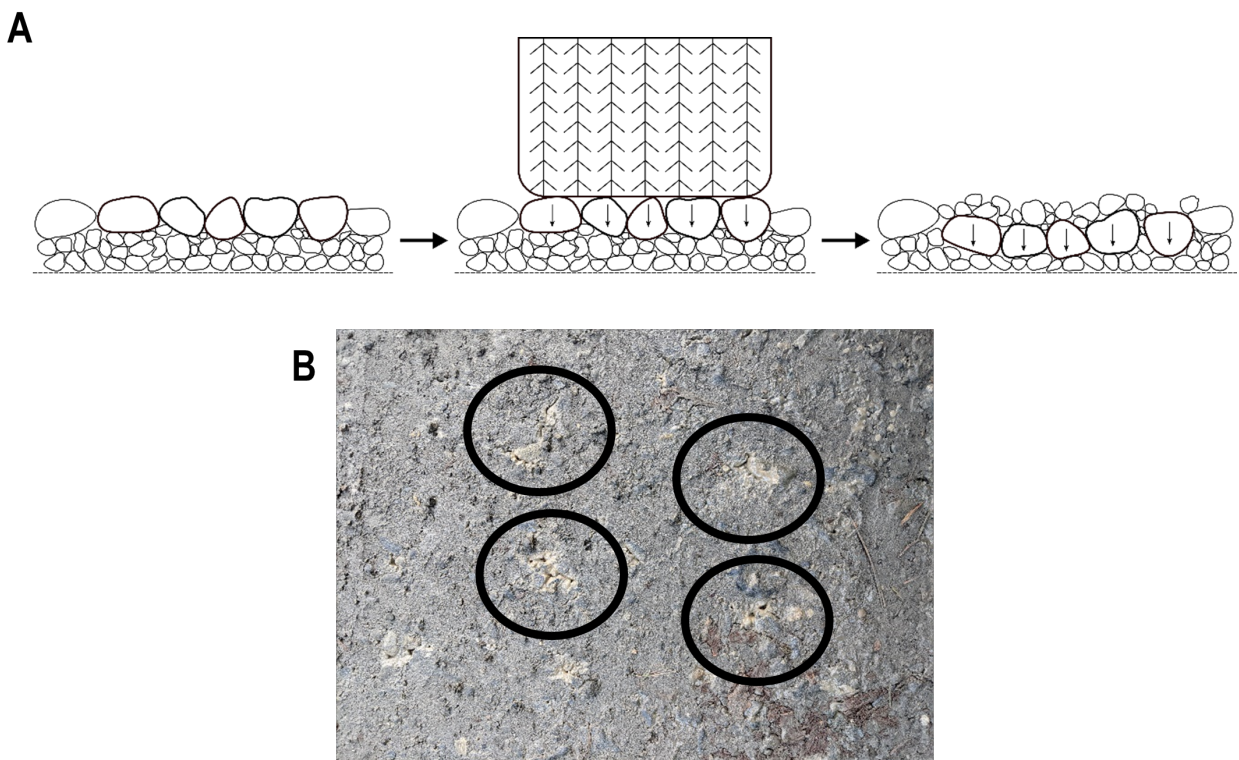
Figure 2.2: (a) Schematic of the pumping process. Larger sediment over finer sediment (left) gets pushed down due to the weight of the vehicles (center), which forces the finer sediment upwards (right). Image not to scale. (b) Image of forest road with evidence of pumping, light colored deposits of fine sediments around edges of holes (circled in black).

Because pumping is a difficult process to isolate, only a few studies investigated the process further than qualitative field observations and conjecture. One study attempted to investigate pumping by examining the utility of three different treatments to reduce fine

sediment production, which was hypothesized to be caused by pumping at the surfacing-subgrade interface (*Toman and Skaugset*, 2011). The three different treatments included: 1) placing geotextile between the subgrade and road surfacing; 2) increasing the depth of the road surfacing; and 3) installing a geocell pavement structure. All three treatments were meant to hinder the pumping process at the surfacing-subgrade interface and were compared to control segments.

This study was carried out on recently built spur roads designed for short-term use in three locations. Measurements of sediment runoff were made over a single winter haul season. The authors concluded that pumping was not a significant source of fine material on the roads they tested based on the fact that sediment production did not differ significantly between treated and control road segments. Rather, they concluded that the fine material was either already present in the new road surface aggregate or was generated by crushing of the surface aggregate.

Extrapolation of these findings to more established roads may not be applicable because the study focused on short-term use roads that were recently built and were monitored only one winter season. Recently built roads have a settling period in which existing fine sediment is flushed away, armoring the road surface (*Megahan*, 1974). This armoring phenomenon is also observed in roads that have been disturbed by other means, such as road maintenance (*Luce and Black*, 2001a). As such, the study's findings—that the road surface aggregate was the main source of fine material—may well be a feature of the newly-built road's settling period.

Experimental evidence for pumping has been demonstrated on more established unpaved forest roads. *Rhee et al.* (2018) carried out a study in Clearwater National Forest, Idaho in which they inferred different processes (i.e., crushing, pumping, scattering) from changes in the particle size distribution of different vertical layers of the road after varying amounts of traffic (i.e., none, light, heavy). Coarsening of the middle and bottom layers of these roads provides evidence of pumping, while fining provides evidence of crushing. Significant evidence of pumping (i.e., a coarsened particle size distribution) was found in the bottom layer of the heavy traffic road. Further investigation is warranted to help us understand the rate at which pumping occurs under different conditions.

2.2.3   Scattering

Road surface armoring occurs when readily available fine sediment is flushed away, leaving only larger sediment that forms a protective layer (*Megahan*, 1974). Scattering is the displacement of the larger sediments that have armored the road surface and is caused by a disturbance thereof, such as traffic. Disturbing this armor layer exposes the fine sediments below, increasing the amount of sediment that is readily available for transport (Figure 2.3).

This process has been both posited by researchers and observed in the field (e.g., *Foltz et al.*, 2000; *Gnanendran and Beaulieu*, 1999; *Johnson*, 2003). *Rhee et al.* (2018) is one of the few studies that demonstrated the scattering process in a field study—referred to as "sweeping" in their study. They were able to infer that scattering was a dominant process on the shoulder section of the light traffic road in their study based on an increase in the particle
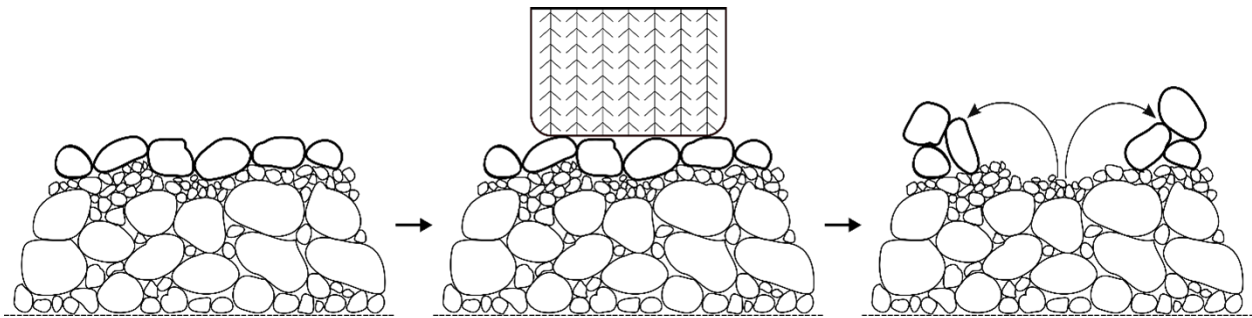
Figure 2.3: The road surface develops an armor layer of larger sediments (left). Once the road is disturbed by traffic (center), the armor layer is scattered, exposing fine sediments below (right). Image not to scale.

size distribution (i.e., coarsening) at that location on the road. They note that evidence of scattering outside of the tire tracks (i.e., the coarsening of material outside the tire tracks) is more significant than evidence of scattering inside the tire tracks (i.e., the fining of material inside the tire tracks). This suggests that reduced erosion of medians and shoulders can be attributed to traffic but that increased erosion in tire tracks—caused by reduced rock cover therein—might be less clearly attributable to scattering of an armor layer by traffic.

Most other evidence of scattering is largely anecdotal (Figure 2.4). More empirical evidence of scattering, as well as quantification thereof, is required if we are to separate the effects of different processes on the supply of fine sediments and to prescribe treatments to mitigate traffic effects. Quantification of scattering under different circumstances (e.g., weather, traffic speed, tire pressure) will help us further understand the process and potential solutions.

Figure 2.4: Image of a forest road with evidence of scattering.

2.2.4 Flow rerouting

Flow rerouting occurs when traffic deforms a road surface and diverts the flow pathways. On a non-deformed road, runoff leaves the road as sheet flow and flows either into a roadside ditch line or onto the fill slope below the road. Traffic-induced road deformation, however, reroutes the flow and changes its hydraulics. One specific traffic-induced road surface deformation is the development of wheel ruts. Ruts are small channels—like rills on a hillslope—that form on an unpaved road surface due to traffic. The formation of ruts is posited to be caused by a combination of factors, including, but not limited to, scattering, compaction, and plastic deformation of the surface (*Dawson*, 1997). Ruts tend to develop on either side of the crown of the road due to traffic straddling the center of the road (Figure 2.5a).

Once a rut has formed, a feedback loop begins where concentrated water flows in the rut (Figure 2.5b), leading to higher shear stress and, thus, more erosion and further channelization. This advective process would typically produce deep rill- or gully-like features in a

strongly consolidated material, but on heavily trafficked roads, the traffic acts as a diffusive process due to its spatially stochastic nature, which allows the ruts to maintain a relatively hydraulically wide shape. Even with the diffusive nature of traffic, the ruts that develop still have a greater capacity and competence to move sediment. This feedback loop of a dominant advective process and an ancillary diffusive process causes the hydraulically wide ruts to persist and deepen unless an outside force, such as grading of the road surface, occurs.
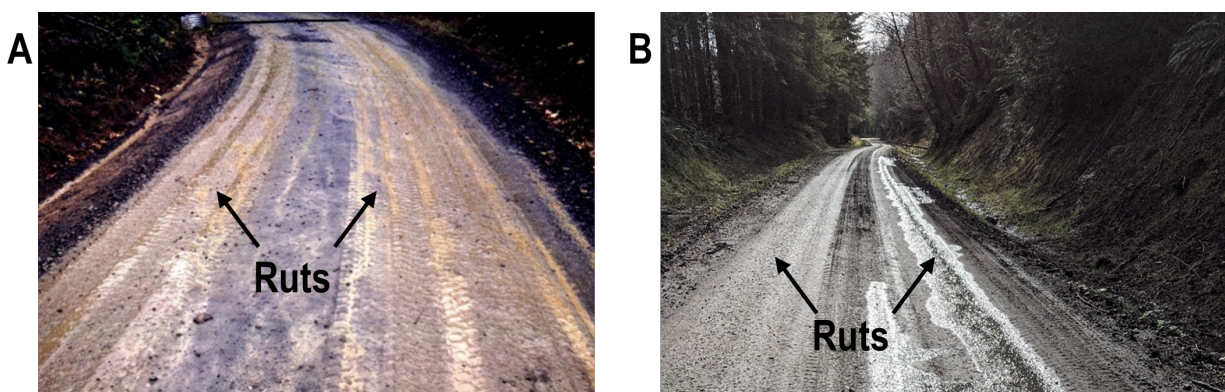
Figure 2.5: (a) Image of a rutted forest road. (b) Image of a rutted forest road with water flowing in one of the ruts rather than off to the ditch line.

The presence of wheel ruts can cause an effective increase in the supply of fine sediment available to be transported and an effective increase in the energy available to transport the sediment. This traffic-driven change in topology tends to route flow along the road surface instead of to the sides, which has its own implications for erosion. Where wheel ruts prevent out-slope drainage, they directly add to potential delivery through concentration of flow along the road instead of diffuse flow. Where wheel ruts capture flow bound for a ditch, they prevent the potential utility of ditchline best management practices (BMP)—such as grass

lining, wattles, or rock lining—that could reduce transport capacity and potentially yield less erosion.

The presence of ruts and their influence on erosion are anecdotally abundant (Figure 2.6). Additionally, empirical studies have found that roads with ruts can produce anywhere from 2 to 5 times more sediment than freshly graded roads (*Foltz and Burroughs*, 1990). However, distributing the weight of logging vehicles over a larger surface area (i.e., reducing tire pressure) can decrease rut development and, thus, erosion (*Bradley*, 1994; *Foltz*, 1994). Additionally, consistent maintenance of roads can minimize the impacts of ruts (*Sheridan et al.*, 2006). Though we have some knowledge about how to decrease rut development, additional information is needed about the formation of wheel ruts and other road surface deformations. Learning the rate at which the road deforms and the conditions under which the road deforms can give us more insight into how to prevent these deformations.

2.3 Important contextual covariates for traffic effects

Other factors that influence the erosion of unpaved forest roads include rainfall intensity, road topography and topology, aggregate quality, and subgrade strength. These factors can fall into one of two categories: supply-related or energy-related. As discussed in Chapter 2.2, traffic is one of the most-cited and least-understood factors affecting the erosion of forest roads that is both supply- and energy-related. Many other processes and characteristics of roads that influence forest road erosion exist and can be either supply-related or energy-related, but these factors also affect how traffic affects erosion. These additional factors are

Figure 2.6: Image of an extremely rutted road that receives little traffic.

largely related to traffic and each other, and as such, a discussion of all factors and their interaction is warranted to fully frame a discussion of unpaved forest road erosion and the dominant role of traffic therein.

2.3.1   Rainfall intensity

Rainfall initiates sediment transport on forest roads because it quickly turns into runoff due to low infiltration rates (e.g., *Luce and Cundy*, 1994; *Ziegler et al.*, 2000). The energy from the rain can contribute to displacement of sediment on the road through rain splash erosion as well. Thus, erosion caused by rainfall can be partitioned into two interconnected processes: hydraulic erosion and rain splash erosion.

Hydraulic erosion is largely energy-related and occurs due to Hortonian overland flow,

which is frequently seen on unpaved forest roads. As these roads are used, they can become heavily compacted, allowing for less infiltration, and thus increasing the amount of overland flow (*Ziegler and Giambelluca*, 1997). Hydraulic erosion is the agent through which sediment is transported away from the road prism. For areas in which sediment is readily available prior to a storm—through traffic, road maintenance, or other means—hydraulic erosion tends to be the dominant process at the beginning of a storm (*Ziegler et al.*, 2000).

Though hydraulic erosion is the transporter of sediment, rain splash erosion is another important supply-related piece in the rainfall-driven erosion process. Rain splash erosion increases the sediment supply that is readily available to be transported due to sediment displacement via rain drop impact, and once sediment is available for transport, hydraulic erosion occurs. For areas in which sediment is not immediately loose enough for overland flow transport alone (i.e., roads that have not been disturbed) rain splash erosion tends to dominate at the beginning of a storm (*Ziegler et al.*, 2000).

2.3.2   Road topography and topology

Road topography refers to the geometry, slope, and other spatial characteristics of the road (Figure 2.7). Topographical features such as road length and gradient are among the most cited and studied influences on road surface erosion and largely impact erosion from an energy perspective. Road length and gradient are interconnected topographical features that represent the space over which erosion can occur. Assuming a constant road length, increasing the road gradient significantly increases erosion (*Arnáez et al.*, 2004). The interaction

between road length and gradient leads to different effects on erosion. For example, increasing the length of a low gradient road has a smaller impact on erosion than increasing the length of a high gradient road. This relationship has been observed on established mainline logging roads (*Luce and Black*, 1999) and less-used unpaved forest roads (*Ramos-Scharrón and Macdonald*, 2005).
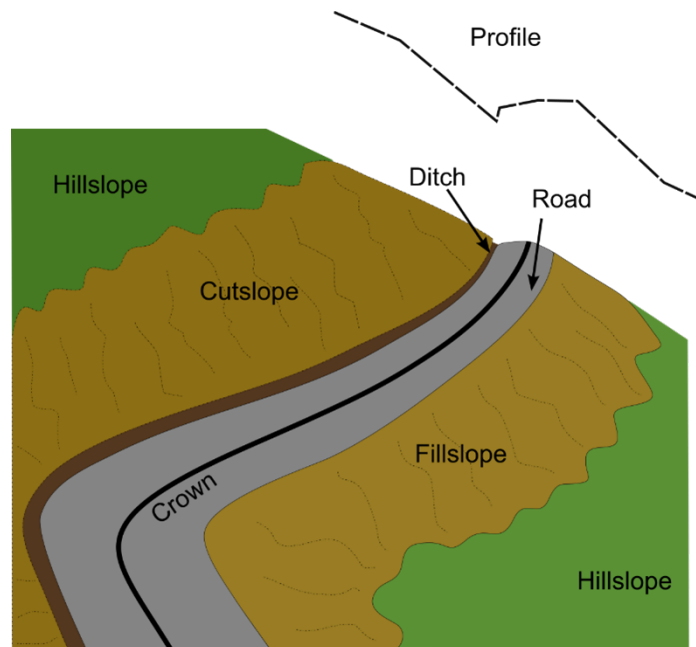
Figure 2.7: Schematic of a typical forest road and its surroundings.

Related to topography is the topology of the road. We can think of topology as how water navigates the topography of the road (e.g., across the road vs. along the road). Some roads are out-sloped, where sheet flow that forms during rainfall events is directed primarily toward the fillslope, with some along-road movement that depends on the road's slope. Similarly, some roads are in-sloped, where the water flows toward an inboard ditch that runs alongside

the road until a drainage feature, like a culvert, relieves the ditch. For maintenance and traffic reasons, many roads are crowned, with half of the road draining to the fillslope and half to the inboard ditch. A point of special interest discussed in Chapter 2.2.4 is that traffic can form wheel ruts that favor flow along the road surface before it reaches either the outer edge or the inboard ditch. Flow coming off out-sloped roads does not travel far because the road contributing area per unit discharge width is small. In contrast, runoff travelling along a road in a ditch or wheel rut becomes concentrated. When this concentrated runoff is discharged from a drainage feature, the likelihood of delivery to a stream increases (*Wemple et al.*, 1996).

In addition to water flow along and off of the road, cutslopes along the side of the road and their spatial characteristics have also been shown to affect erosion. *Arnáez et al.* (2004) point to mass-wasting and freeze-thaw cycles as being important processes that provide transportable sediment from cut slopes. Additionally, increases in the cut slope gradient causes erosion to increase (e.g., *Jordán and Martínez-Zavala*, 2008; *Jordán-López et al.*, 2009). However, cutslope height is not necessarily a significant influence on sediment yield from roads in some areas, perhaps because of vertical heterogeneity in cutslope material (*Luce and Black*, 1999; *Megahan et al.*, 2001). Cutslopes are also often sources of water, either as direct overland flow during high rainfall intensity events or through interception of subsurface flow (*Luce*, 2002; *Wemple and Jones*, 2003; *Ziegler et al.*, 2000). This water flows along the ditch when one is present, which lends itself to carrying sediment towards drainage features.

Some topographical and topological features of roads are commonly used to model road erosion because the features are easily obtained, either through field measurements or GIS software computations, and their relations to erosion are computationally simple. Modeling studies most often incorporate road drainage area and gradient, which is closely related to the concept of the slope-area product in geomorphology (e.g., *Istanbulluoglu et al.*, 2002, 2003). Because these features are easily extracted using GIS technologies and are shown to be correlated with road erosion, they are the basis of multiple models that use empirically based equations to estimate such erosion (e.g., *Akay et al.*, 2008; *Anderson and Macdonald*, 1998). Coefficients for these relationships can be empirically determined using existing data and, with additional experimentation, can be tied to climate, soil, and level of road disturbance.

2.3.3 Aggregate quality

Aggregate refers to the material used to surface an unpaved forest road (see Surfacing in Figure 8a). This surfacing aggregate provides a layer of protection to the native material underneath and decreases the amount of erosion that would otherwise be present without such protection (e.g., *Brown et al.*, 2013; *Kochenderfer and Helvey*, 1987). Though the presence of surfacing aggregate decreases erosion, aggregate quality must also be considered where traffic occurs. In general, aggregate quality is defined by how much the aggregate breaks down when it is exposed to different stressors, such as water, air, or traffic. The quality of surfacing aggregates is an important factor influencing erosion via the supply of fine sediment. Studies have observed that lower quality aggregate leads to more erosion

because of its susceptibility to breakdown (e.g., *Foltz and Truebe*, 1995; *Foltz et al.*, 2000).

What aggregate is used to surface a forest road depends on the landowner's main goal—cost reduction or erosion reduction—though that goal may change based on local availability of material. Generally, lower quality aggregates will be used to decrease cost, whereas higher quality aggregates will be used to reduce sediment loss. The quality of aggregate can be determined via either road managers' recommendations based on experience or physical tests of the aggregate. However, *Hanna and Boston* (2018) carried out a series of physical tests on aggregate obtained from quarries that road managers were also asked to classify as good or marginal sources of material. Results showed that road manager-recommended aggregates rarely met quality thresholds as established based on literature review, emphasizing the importance of testing aggregate prior to placing it on roads.

Two of the best tests to predict aggregate quality are the P20 portion of the Oregon air degradation test and the sand equivalent test (*Foltz and Truebe*, 2003). The P20 portion of the Oregon air degradation test assigns an index indicating the breakage resistance of the aggregate when exposed to both water and a jet of air, and the sand equivalent test assigns an index to the aggregate based on the amount of fine material present. The sand equivalent test is more common as it is less time- and equipment-intensive and is therefore easier to carry out in the field.

2.3.4   Subgrade strength

The subgrade is the base upon which forest roads are built and is generally composed of native soil and rock (see Subgrade in Figure 2.8a). Multiple studies have looked at the importance of subgrade strength with respect to the durability of the road. Overall, these studies have found that deformation of the road surface—poor aggregate performance and quality aside—can occur when the integrity of the subgrade is compromised (Figure 2.8b) and that road surface deformation is positively correlated with erosion. Therefore, lower subgrade strength can lead to increased erosion (e.g., *Bloser and Scheetz*, 2012). As such, subgrade strength influences erosion from a supply perspective.

The strength of the subgrade is highly dependent on both the level of compaction during road construction and the durability of the materials therein. Different levels of compaction can lead to different levels of material breakage, with an optimal range of compaction existing to minimize material degradation (e.g., *Indraratna et al.*, 2005; *Lackenby et al.*, 2007). Additionally, proper compaction of the subgrade can optimize subgrade strength and decrease the required amount of surface aggregate—and, therefore, cost—without compromising the integrity of the road (*Boston et al.*, 2008). Easy field measurements of subgrade strength in tandem with a simple correlation model can aid in the proper compaction of the road subgrade (*Pattison et al.*, 2010).

In addition to compaction of the subgrade, other reinforcements—such as geogrids or geotextiles—can be installed in or on the subgrade to increase road strength while decreasing the required amount of road surface aggregate (*Giroud and Han*, 2004). Geotextiles

are permeable textiles placed at the subgrade-aggregate interface to increase soil stability; geogrids are synthetic materials that reinforce the subgrade. *Visser et al.* (2017) looked at the cost-benefit of using geogrids with less road surface aggregate and found that doing so may be viable, specifically in cases which would otherwise require expensive or exorbitant amounts of road surface aggregate to maintain similar road strength.
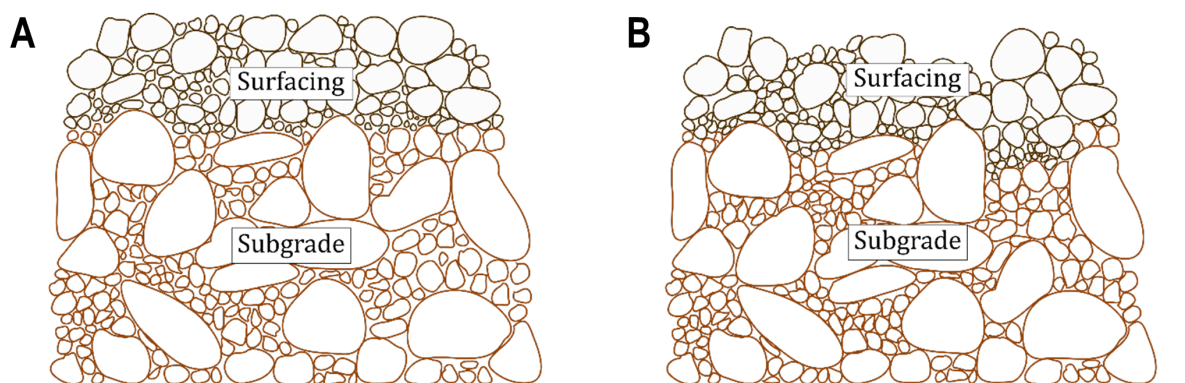
Figure 2.8: (a) Schematic of a road cross section. The surfacing (top layer) is the aggregate used to cover the forest road, and the subgrade (bottom layer) is the packed excess fill material from road excavation as well as the native material. (b) Schematic of a road cross section where the integrity of the subgrade has been compromised, causing surfacing deformation. This example demonstrates a case where the subgrade was improperly compacted (i.e., weak) when the road was installed, and repeated outside stressors (traffic) caused further subgrade compaction that deformed the road surface. Images not to scale.

2.4 A framework for future research

The role of traffic in forest road erosion is still poorly understood, which limits our ability to efficiently reduce its effects on erosion. The studies discussed in previous sections have given us tantalizing individual hints that further our understanding, but they are poorly integrated with one another and form a fragmented field of knowledge. As a result, we are left with

many fundamental questions: How does the rate of traffic affect these erosion processes? Which of these traffic-induced erosion processes is the most dominant under different field and climate conditions? Why do some heavily trafficked roads accumulate fine sediment on the surface while others do not? What is the role of compaction in traffic-induced erosion processes? Is the pumping process solely a function of traffic, or are time and moisture variables to be considered as well? What other factors contribute to the importance of these traffic-induced erosion processes? In other words, we want to know how much sediment is coming from which mechanisms under what circumstances—a three-fold problem. To answer these questions, we need an efficient path forward.

We can think of forest road erosion through the lens of supply and energy limitations, a framework commonly used in geomorphology. In the classic geomorphological sense and a very long time perspective, this framework would characterize forest roads as energy limited only. However, if we view a forest road as a closed system that exists under specific conditions, we can characterize the system as either supply or energy limited. Supply limiting factors include traffic (Chapter 2.2), aggregate quality (Chapter 2.3.3), and subgrade strength (Chapter 2.3.4), while energy limiting factors include traffic (Chapter 2.2), road topography (Chapter 2.3.2) and rainfall (Chapter 2.3.1), and all these factors are markedly interconnected. These factors, both individually and combined, determine where a forest road falls on an energy- vs. supply-limited spectrum.

At any point in time, depending on the context, a forest road, even the same segment of forest road, can be considered either a supply-limited or an energy-limited system, and

under different contexts, the state of the system may change. As such, we posit that the relationship between erosion, supply, and energy can be described using the concept of limiting factors (Figure 2.9). If the energy is less than the supply, the erosion of the system will be dependent on energy, making the erosion process energy limited (e.g., a muddy road storing fine sediment on the surface that has not yet been transported off the road). However, once the energy surpasses the supply, the erosion of the system will be equal to the supply available, making the erosion process supply limited (e.g., a rocky road).

A subset of this relationship can be seen in preliminary sediment and flow data collected in Washington state (Figure 10) as part of an ongoing study conducted by the Cooperative Monitoring Evaluation and Research (CMER) Committee within the Washington Department of Natural Resources Adaptive Management Program. In this ongoing study, a number of covariates are being measured. These covariates include the total annual flow of a road segment, which is measured using tipping buckets, and the total annual sediment mass, which is collected in settling basins connected to the same road segment. These preliminary data show the relationship between average annual flow x slope (a surrogate for transport capacity or "energy", T_c) and total annual mass of sediment (a measure of erosion, E) as a function of traffic level (a surrogate for supply, S). At field sites where traffic levels are high (purple circles in Figure 2.10), sediment supply is also high and the data show that E depends on T_c. These locations plot near the energy-limited line in the limiting factor space presented above. In contrast, the low traffic field sites (green squares in Figure 2.10) have a lower supply and the data show that E does not depend on T_c. These locations would plot close to
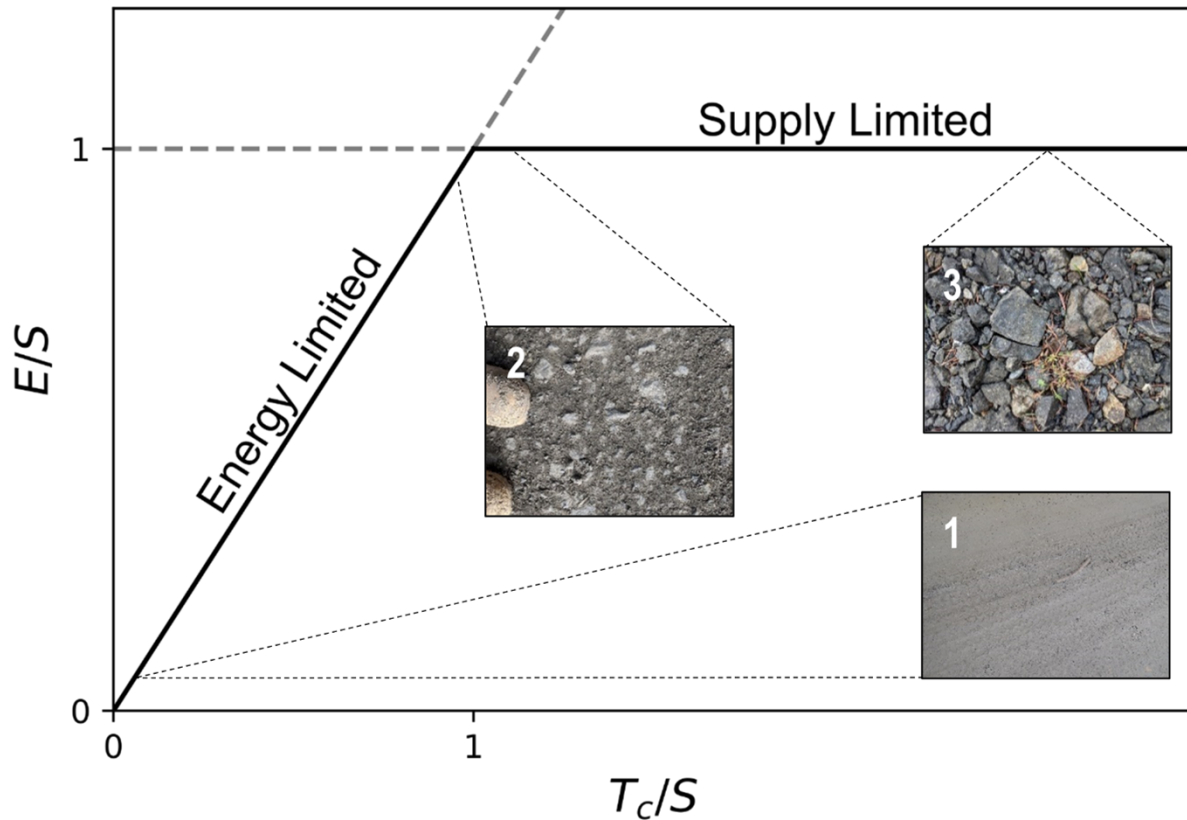
Figure 2.9: A limiting factor diagram for conceptualizing the relationship between erosion, energy, and supply. When the energy (T_c) is less than the supply (S), the erosion (E) depends on energy, and data from this road would plot along the energy limited line. When T_c surpasses S, E is equal to the supply, and data would fall along the supply limited line. Three examples of a forest road in different states are shown: 1) An energy limited road surface; 2) a road surface that is on the cusp between energy and supply limited; and 3) a supply limited road surface.

the supply-limited line in the limiting factor space. In this limiting factor space—where the response variable (i.e., erosion) is affected by multiple factors (i.e., the energy-supply balance and level of traffic)—quantile regression would be helpful to examine these data (*Cade and Noon*, 2003).
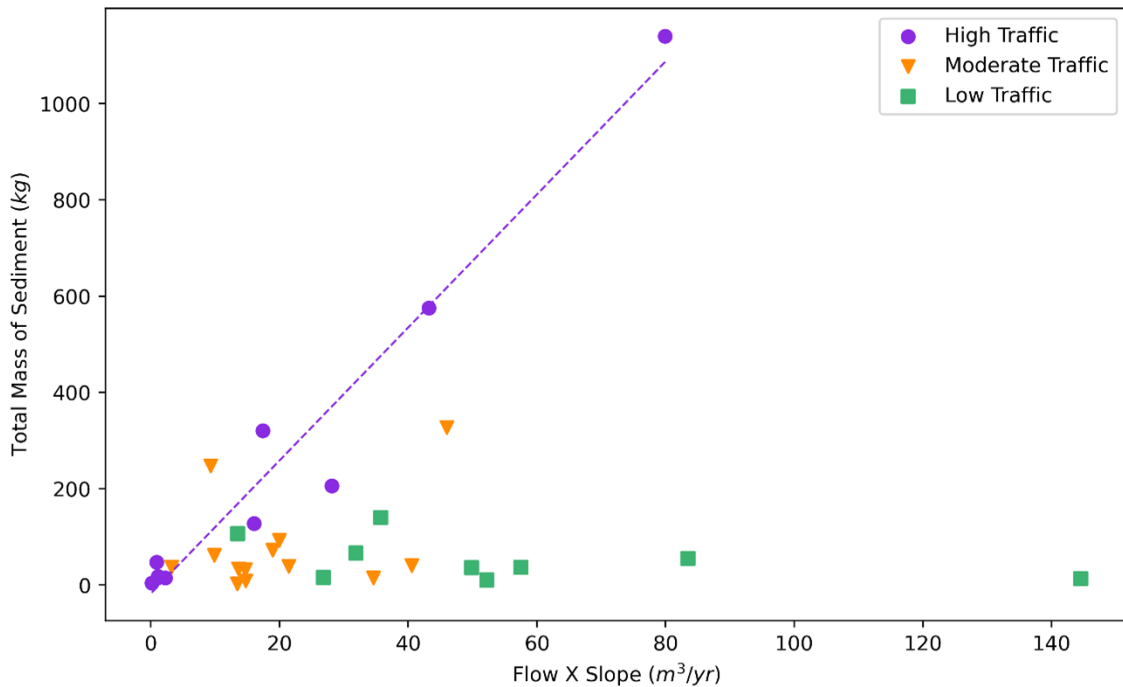
Figure 2.10: Preliminary data from western Washington field study showing the total annual mass of sediment (kg) vs. total annual flow x slope (m^3) for three different traffic levels. These data show that for high traffic sites (i.e., high supply sites; purple circles in figure), total annual mass of sediment (surrogate for erosion) is linearly related to total annual flow x slope (surrogate for transport capacity), whereas low traffic sites (i.e., low supply sites; green squares) show no significant dependence.

The framing of forest road erosion as a function of both supply and energy can help us focus further research, specifically with respect to the influence of traffic. As discussed above, we know that the role of traffic in this framework can be found in both the supply and energy limitations. For example, pumping and crushing can increase the available supply explicitly, while scattering can affect the available supply implicitly by either revealing or covering existing fine sediment on the road surface. Additionally, scattering can affect the available energy through road surface deformation, similar to rutting. Both rutting and scattering

lead to flow rerouting, which effectively increases the energy directed to transporting fine sediments. Rerouted flow will not necessarily reach the roadside ditches, which tend to offer more resistance to flow—through installation of grass or other ditch line best management practices—and therefore sediment transport. However, these effects depend on context, such as surfacing quality; subgrade strength; underlying geology; spatial characteristics of the road; wet weather; or freeze-thaw processes.

Thinking of traffic-induced erosion as a function of supply and energy and remembering context dependencies allows for interpretation and synthesis of targeted experiments to test hypotheses regarding these processes. One example experiment could include looking at short-time-scale interactions between traffic and an established mainline road to measure the magnitude of the pumping process. Another segment-scale experiment could include looking at changes in the hydraulics of flow in roadside ditch lines and road surface ruts to help characterize the effects of rutting on flow rerouting and, ultimately, erosion.

An important next step would be to use our current understanding and hypotheses to develop a process-based model that incorporates mathematical conceptualizations for the aforementioned processes. The development of such a model can, in turn, help us develop field studies to further understand these processes and parameterize our models. Currently, no model exists that looks at the multiple specific traffic-induced erosion processes. Some previous models incorporate the role of traffic via a traffic factor that changes erosion based on average road use (e.g., *Akay et al.*, 2008; *Dubé et al.*, 2004) or via increasing road "erodibility" with traffic over time (*Ziegler et al.*, 2001a), while other models note the importance of traffic

but do not consider it quantitatively. Therefore, a process-based unpaved forest road erosion model incorporating the four different traffic-driven processes (Chapter 2.2) and their context dependencies (Chapter 2.3) is warranted to guide data collection and analysis needs.

Advancing research regarding traffic-induced road erosion has multiple implications. Understanding how much supply is increased by pumping or crushing, and their dependencies on aggregate quality and subgrade integrity, can improve guidelines for traffic levels under particular conditions. Additionally, understanding how much energy increases by scattering or flow rerouting, and their dependencies on spatial road characteristics and weather, can allow for more informed recommendations regarding road maintenance. Overall, increased knowledge of traffic-specific processes and related factors will enable us to determine the most cost-effective steps to take to reduce forest road erosion.

2.5   Conclusion

The influence of traffic on forest road erosion has been studied from a broad and somewhat qualitative perspective, with the literature commonly focusing on increased erosion due to traffic and the effects thereof, without detailing and quantifying underlying mechanisms. Current research lacks comprehensive consideration of these mechanisms and related contextual covariates, but this research has provided the groundwork for development of quantitative hypotheses regarding four main traffic-induced erosion-enhancing processes: crushing, pumping, scattering, and flow rerouting. Quantifying these processes, and their relation to other important contextual covariates, is integral to furthering our understanding of forest

road erosion. To quantify these processes and covariates, we should start framing traffic and other influencing factors in terms of their roles in supply- and energy-limitations. If we focus future research using this framework, our capacity to evaluate the current hypotheses of traffic-induced erosion-enhancing processes will increase, and we will be able to establish the most effective and efficient ways to control forest road erosion.

Acknowledgements

Data availability

The data shown in Figure 10 of this chapter are not publicly available due to an agreement with the authors' funding agency but are available from the corresponding author upon reasonable request and approval from the funding agency.

Chapter 3

USING ADDITIONAL ROUGHNESS TO CHARACTERIZE EROSION CONTROL TREATMENT EFFECTIVENESS IN ROADSIDE DITCH LINES

Abstract

Forest roadside ditch lines capture and redirect road runoff and typically have erosion control treatments installed therein. Existing methods used to determine the effectiveness of roadside ditch line erosion control treatments estimate fixed fractional reductions in sediment yield. However, fixed fractional reductions do not describe dependence on any measurable physical property of treatment, climate, and the environment. Here we use additional flow roughness of erosion control treatments as a metric that can be used as the basis of estimating treatment effectiveness in varying contexts. We investigate its utility in small-scale field experiments in western Washington. We measured the physical characteristics of each ditch, and flow velocities and sediment concentrations for each treatment under multiple experimental discharges. We then used the concept of shear stress partitioning to relate sediment

yield from the ditch line erosion treatments to grain shear stress, which is a function of flow roughness (Manning's n) of the respective treatment. We found that 1) a given erosion control treatment produced consistent Manning's n values across multiple replications and sites, with a bare ditch (no treatment) yielding the lowest roughness (n=0.05) and a densely-wattled ditch yielding the highest roughness (n=0.75); 2) sediment load and calculated grain shear stress data yielded a single positive relationship when data from each experiment were combined, which suggests the effect of additional roughness on grain shear stress is a main driver in the reduction of ditch line sediment load; and 3) in our dataset, fractional erosion reduction had a variable and nonlinear sensitivity to low flow rates (99% of observed flows) for lower roughnesses. Our results demonstrate how additional flow roughness can be used as a general metric to help evaluate the effectiveness of ditch line erosion control treatments for a variety of physical conditions.

3.1 Introduction

Roadside ditch lines are crucial conduits for capturing and redirecting forest road runoff to mitigate the effects of forest road erosion. Erosion control treatments for dirt and gravel roads—especially those that are installed in roadside ditch lines—are essential to the protection of both transportation infrastructure and downstream water quality and aquatic habitat (e.g., *Cristan et al.*, 2016). Accurate estimates of erosion reduction from forest road surfaces and ditch lines are critical to developing regulations and assessing the cost effectiveness of erosion control treatments (e.g., wattles, gravel, vegetation; see e.g., *Boston*, 2016; *Dangle*

et al., 2019). Most of the current research evaluating the efficacy of these treatments has been done in the vein of randomized control trials (sensu *Cartwright*, 2007) and rely on empirical methods that quantify a fixed fractional reduction of sediment transport (e.g., *Aust et al.*, 2015; *Burroughs and King*, 1989; *Burroughs et al.*, 1984; *Cristan et al.*, 2019; *Edwards et al.*, 2016; *Luce and Black*, 1999; *Megahan*, 1974; *Megahan et al.*, 2001). The choice to use randomized control trials—rather than developing physics-based models and testing those models using experiments—is likely driven by a few key factors. For one, each erosion control treatment involves distinct mechanisms for reducing ditch line erosion. Rather than focusing on details of different process representations in models, empirical field methods can be used to determine reduction factors. Additionally, multiple treatments are commonly used within a single project to assess their efficacy, and the interactions among these treatments pose challenges for modeling due to their complex nature. Finally, a large portion of the motivation behind this research originates from practitioners rather than academics. Practitioners have preferred methods that can be easily implemented without the need for vast data collection and site characterization.

A major challenge in using fixed fractional reductions in erosion is in the generalization of the effects of the erosion control treatments to other contextual settings. For example, the fixed fractional reduction in sediment estimated from an experiment conducted in a place where high intensity rainstorms occur may not apply in places where snow melt generated runoff is more common. The results that are calculated from an experiment on a steep road will likely not be equivalent to those of a low-gradient road. The general applicabil-

ity of limited experimental results to a wide range of ditch conditions and treatments is hindered by the presence of thresholds and nonlinearities in the sediment entrainment and transport process (e.g., *Al-Hamdan et al.*, 2013; *Buffington and Montgomery*, 1997; *Govers*, 1992; *Nearing et al.*, 1989). To address the need for erosion predictions in a wide range of field conditions, differences in experimental controls or premises need to be accounted for in the development of models and/or methods. These differences can be considered either through conducting more randomized control trials in various experimental settings (a potentially slow and expensive process) or through a more process-based approach, where a simple physical parameter is used. We advocate for the latter by proposing to use additional roughness imparted by different ditch line erosion treatments as that simple physical parameter. Additional flow roughness is the increment in roughness affecting flowing water caused by placement or growth of materials/vegetation in the ditch. We then partition the shear stress acting on the water column between particles on the bed versus the added roughness elements. The concept of shear stress partitioning is a well-known method in sediment transport literature to represent how additional flow roughness elements on the bed reduce the shear stress acting on sediment particles (*Einstein and Banks*, 1950; *Einstein and Barbarossa*, 1952).

In practice, three main mechanisms help erosion control treatments reduce sediment transport and erosion in ditch lines: 1) increasing flow roughness, 2) binding, and 3) filtering. Increasing the roughness of the flow by placing additional roughness elements, such as grass and wattles, to slow down the flow velocity is well-grounded in observational evidence

(e.g., *Donald et al.*, 2013; *Edwards et al.*, 2016; *Li et al.*, 2020, 2022b; *Prosser et al.*, 1995; *Schussler et al.*, 2021; *Whitman et al.*, 2021). Other erosion control treatments approach erosion reduction through binding and filtering, both of which may involve additional physical mechanisms that decrease the erodibility of the bed material or reduce erosivity of flows. Binding refers to treatments that functionally increase the size of particles that would need to be transported. Examples of binding treatments include concrete lining, maintaining vegetative root mats, or spreading a binding agent (e.g., *Edwards et al.*, 2016; *Likitlersuang et al.*, 2020; *Sojka et al.*, 2007). Filtering treatments seek to capture particles that are in transport by passing them through some kind of sieving or settling element along a flow path. Examples of filtering treatments include constructed wetlands, straw bales, and rock check dams (e.g., *Collins and Johnston*, 1995; *Edwards et al.*, 2016; *Tollner et al.*, 1977; *Wright*, 2010). In the context of controlling erosion in the roadside ditches of rural and forest roads, most common treatments combine two or more of these effects to some degree. Not all erosion control treatments utilize binding and/or filtering, but all treatments do impart some degree of additional flow roughness, which affects shear stress partitioning. As a result, investigating the role of additional roughness—and therefore that of shear stress—on flow and sediment loads is a logical first step towards developing process-based modeling tools and conceptual frameworks to interpret field observations. Shear stress partitioning is a well-established method in the soil erosion literature of rangelands, landscape evolution, and fluvial geomorphology (e.g., *Al-Hamdan et al.*, 2022; *Darby et al.*, 2010; *Foster et al.*, 1989; *Istanbulluoglu et al.*, 2002, 2003; *Li et al.*, 2022a; *Yager et al.*, 2007; *Yetemen et al.*,

2019). However, such a method has not seen much attention in erosion control practices literature.

The idea of shear stress partitioning and its theory as developed by multiple researchers, particularly in fluvial environments (e.g., *Buffington and Montgomery*, 1997; *Einstein and Banks*, 1950; *Einstein and Barbarossa*, 1952; *Ferguson et al.*, 2019; *Manga and Kirchner*, 2000), provides the basis for quantification of changes in total vs. effective shear stress on grains with application of different treatments. Increased flow roughness (i.e., the addition of erosion control treatments) leads to deeper flows and thereby higher shear stress or stream power for sediment entrainment and transport. Consequently, a proportion of this shear stress is imparted on the added roughness elements rather than the bed sediment due to increases in friction around the immobile roughness elements. Effectively, the addition of erosion control treatments reduces the shear stress available for the bed, which decreases the frequency and magnitude of sediment mobilization and transport under a variable climate. A substantial body of literature already exists on shear stress partitioning and its effects on sediment transport that supports the use of additional roughness as a metric to determine reduction in sediment mobilization (e.g., *Istanbulluoglu and Bras*, 2005; *Le Bouteiller and Venditti*, 2015).

Critically, the roughness contributions from common ditch line erosion control treatments are unknown, and the literature provides scant recommendations to estimate additional flow roughness (i.e., Manning's n) contributed by erosion control treatments. Roughness is typically used as a calibration parameter in models (*Lane*, 2014) and is based on approximate

guidelines (e.g., *Arcement and Schneider*, 1989) offering large ranges in values. However, we posit that incremental roughness added by an erosion control treatment—a simple physical parameter—can be used as a measure or index of erosion control treatment effectiveness. We are left with multiple questions: What is the additional Manning's roughness due to different treatments? What is the influence of increased roughness on sediment load? Is increasing additional flow roughness the dominant mechanism for reducing sediment yields in select roadside ditch line erosion control treatments? Can additional flow roughness be used as a simple physical metric to generalize the effects of the treatments to other contextual settings?

In this paper, we examine several ditch line erosion control treatments through estimating their added roughness as well as measuring sediment transport in field experiments in western Washington. Using these measurements, as well as established theory around shear stress partitioning, we evaluate the utility of roughness as a quantitative characterization of ditch line erosion control treatments. Overall, this study offers potential simplification of determining erosion control treatment effectiveness through the leveraging of theory in hydraulics and sediment transport to reduce the dimensionality of the experimental measurements.

3.2 **Mathematical theory**

3.2.1   *Shear stress partitioning*

Sediment transport has been related to grain shear stress τ_g (the shear stress acting on sediment grains) in excess of critical shear stress τ_c (the shear stress threshold at which

sediment will begin to move) in a power-function form:

$$Q_s \sim (\tau_g - \tau_c)^m \tag{3.1}$$

When there are other obstructions in the channel aside from the substrate grains, the portion of shear stress acting on the sediment grains is responsible for transport. A shear stress partitioning ratio, f_g, can be used to determine this portion of the total boundary shear stress that acts on the channel bed substrate grains (e.g., *Tiscareno-Lopez et al.*, 1994).

$$\tau_g = \tau_t * f_g \tag{3.2}$$

Einstein and Barbarossa (1952) proposed to partition τ_t into various components such as τ_g and τ_a:

$$\tau_t = \tau_g + \tau_a \tag{3.3}$$

where τ_a is the shear stress acting on additional roughness in the channel (e.g., bed forms and vegetation). We write the total shear stress based on a force-balance derivation and equate it to the sum of drag forces acting on grains and additional roughness components (*Manga and Kirchner*, 2000).

$$\rho_w g R S = \rho_w C_{dg} U^2 + \rho_w C_{da} U^2 \tag{3.4}$$

where ρ_w is the density of water, g is the acceleration of gravity, R is the hydraulic radius of flow, S is the slope, C_{dg} is the drag coefficient for the sediment grains, C_{da} is the drag coefficient for additional roughness components, and U is the flow velocity. When additional roughness in not present, the equation can be solved for C_{dg}:

$$C_{dg} = \frac{gR_gS}{U^2} \tag{3.5}$$

where C_{dg} is assumed to remain constant within the same channel (ditch), even with the addition of any roughness elements. Here we would like to relate C_{dg} to Manning's n, which is widely used to represent channel roughness in hydraulic engineering applications. If we use Manning's equation for U ($U = \frac{1}{n}R^{2/3}S^{1/2}$), assume parabolic channel geometry, and express R from the equation of parabola, C_{dg} takes the following form (Appendix A):

$$C_{dg} = gn_g^{24/13}Q^{-2/13}S^{1/13}\left(\frac{6}{a}\right)^{1/13} \tag{3.6}$$

where n_g is grain roughness, a is a parabolic shape factor, and Q is channel flow. Following the logic of Eq. 3.3 and Eq. 3.4, the drag coefficient of the bare ditch can be added to the drag coefficient for added roughness elements to obtain a total drag coefficient (i.e., $C_{dg} + C_{da} = C_{dt}$). As such, we can write an equation for the total drag coefficient in a similar form:

$$C_{dt} = gn_t^{24/13}Q^{-2/13}S^{1/13}\left(\frac{6}{a}\right)^{1/13} \tag{3.7}$$

Substituting Eq. 3.6 and Eq. 3.7 into Eq. 3.4 to write equations for grain and total shear stress, we express the shear stress partitioning ratio in Eq. 3.2 as Eq. 3.8. Upon canceling the identical terms in the fraction, Eq. 3.8 reduces to Eq. 3.9:

$$f_g = \frac{\tau_g}{\tau_t} = \frac{\rho_w g n_g^{24/13} Q^{-2/13} S^{1/13} \left(\frac{6}{a}\right)^{1/13} U^2}{\left(\rho_w g n_t^{24/13} Q^{-2/13} S^{1/13} \left(\frac{6}{a}\right)^{1/13} U^2\right)} \tag{3.8}$$

$$\frac{\tau_g}{\tau_t} = f_g = \left(\frac{n_g}{n_t}\right)^{24/13} \tag{3.9}$$

In Appendix A, we show several methods for characterizing flow hydraulics in parabolic channels and derive variations of Eq. 3.9 with the exponent in the shears stress partitioning ratio ranging from 3/2 to 15/8 (1.5 to 1.875).

To obtain the shear stress partitioning ratio, we can characterize n_g from bare ditch lines and n_t from ditch lines with different erosion control treatments. The flow roughness (i.e., Manning's n or Manning's roughness) can be calculated by:

$$n = \frac{1}{U} R^{2/3} S^{1/2} \tag{3.10}$$

Again, if the channel geometry is assumed to be parabolic, R can be written in terms of other hydraulic and geometric properties (Appendix A), which turns Eq. 3.10 into:

$$n = \frac{Q^{4/9} S^{1/2}}{U^{13/9} \frac{6}{a}^{2/9}} \tag{3.11}$$

Given fixed Q, S, and a, U becomes the main variable that differentiates the actual roughness values for bare or erosion control treatment conditions, which can then be used in Eq. 3.9. Using Eq. 3.11, Manning's n obtained for a bare ditch gives us n_g, while that which is obtained for ditches with erosion control treatments gives us n_t.

As discussed above, the total shear stress can be divided into various components such as τ_g and τ_a (Eq. Eq. 3.3). Combining Eq. 3.3 and Eq. 3.9 and noting that $n_t = n_a + n_g$, we can visualize total shear stress and its division into various components as a function of additional channel roughness, n_a (Figure 3.1; see also figure 4 in *Manga and Kirchner* (2000) for a related perspective).
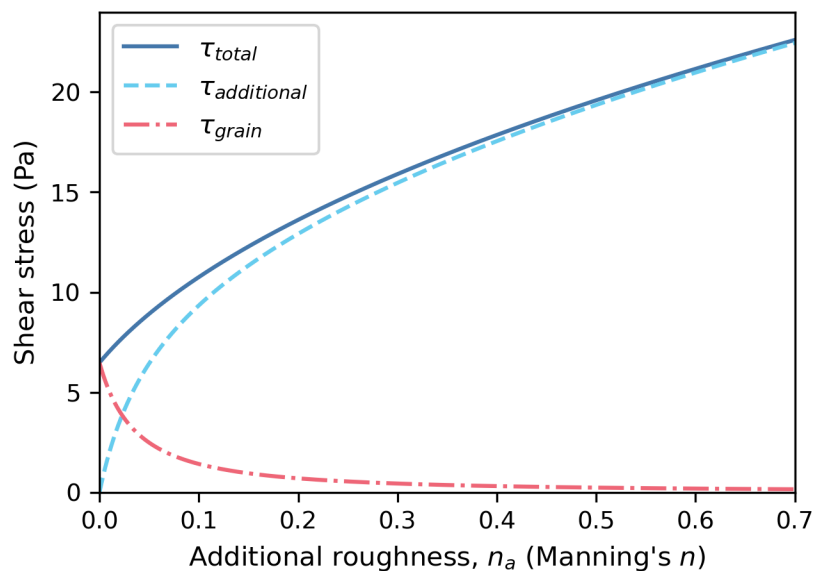
Figure 3.1: The theoretical effect of additional immobile roughness elements on shear stress and its partitioning.

3.2.2   Transport capacity of ditch flow

To evaluate the reductions of sediment transport of different erosion control treatments relative to bare ditch lines, we use an excess-shear-stress-dependent sediment transport equation developed for rills and overland flow on a non-cohesive substrate (*Govers*, 1992):

$$T_c = \frac{10^{-4.348}}{d_{50}^{0.811}} \left(\tau_g - \tau_c\right)^{2.457} \tag{3.12}$$

where T_c is the sediment transport capacity of the flow, d_{50} is the median grain size, τ_g is the grain shear stress, and τ_c is the critical shear stress.

3.2.3   Indicators of erosion control treatment effectiveness

To examine the effectiveness of erosion control treatments, we look at the contextually-determined fractional reduction in grain shear stress and the contextually-determined fractional reduction in sediment transport capacity (henceforth referred to in this experiment as "fractional reductions" as opposed to "contextually-determined fractional reductions," for clarity). We define the fractional reduction in grain shear stress, ϕ, as:

$$\phi = \frac{\tau_{g,bare} - \tau_{g,ect}}{\tau_{g,bare}} \tag{3.13}$$

where $\tau_{g,bare}$ is the bed shear stress of a bare ditch, or the shear stress acting on the sediment grains in a bare ditch, and $\tau_{g,ect}$ is the shear stress acting on the sediment grains in a ditch

with additional roughness from installed erosion control treatments. This metric allows us to quantify the proportion of reduction of $\tau_{g,bare}$ achieved by an erosion control treatment.

Similar to Eq. 3.13, we define the fractional reduction in sediment transport capacity, θ, as:

$$\theta = \frac{T_{c,bare} - T_{c,ect}}{T_{c,bare}} \tag{3.14}$$

where $T_{c,bare}$ is the transport capacity of flow in a bare ditch and $T_{c,ect}$ is the transport capacity of flow in a ditch with additional roughness from installed erosion control treatments.

3.3 Field study

3.3.1 Study area

We carried out an experiment to measure the Manning's roughness and sediment load of multiple roadside ditch line erosion control treatments in two regions of southwest Washington state: (1) a volcanic lithology near Mount Saint Helens and (2) a siltstone lithology near Aberdeen, WA. These regions contain multiple field sites with different ditch line treatments, which were selected to be on mainline logging roads as part of a broader study conducted by the Cooperative Monitoring Evaluation and Research Committee within the Washington Department of Natural Resources Adaptive Management Program. Each field site for this experiment consists of a 40-meter length of ditch line with a cross-drain culvert at the bottom of the ditch segment and has a slope between 4 and 6 percent (Figure 3.2a). The field sites in the volcanic lithology experience, on average, 1560 mm of annual precipitation, and the field sites in the siltstone province experience, on average, 2400 mm of annual precipitation

(*PRISM Climate Group*, 2023), with most of the precipitation occurring between October and April.
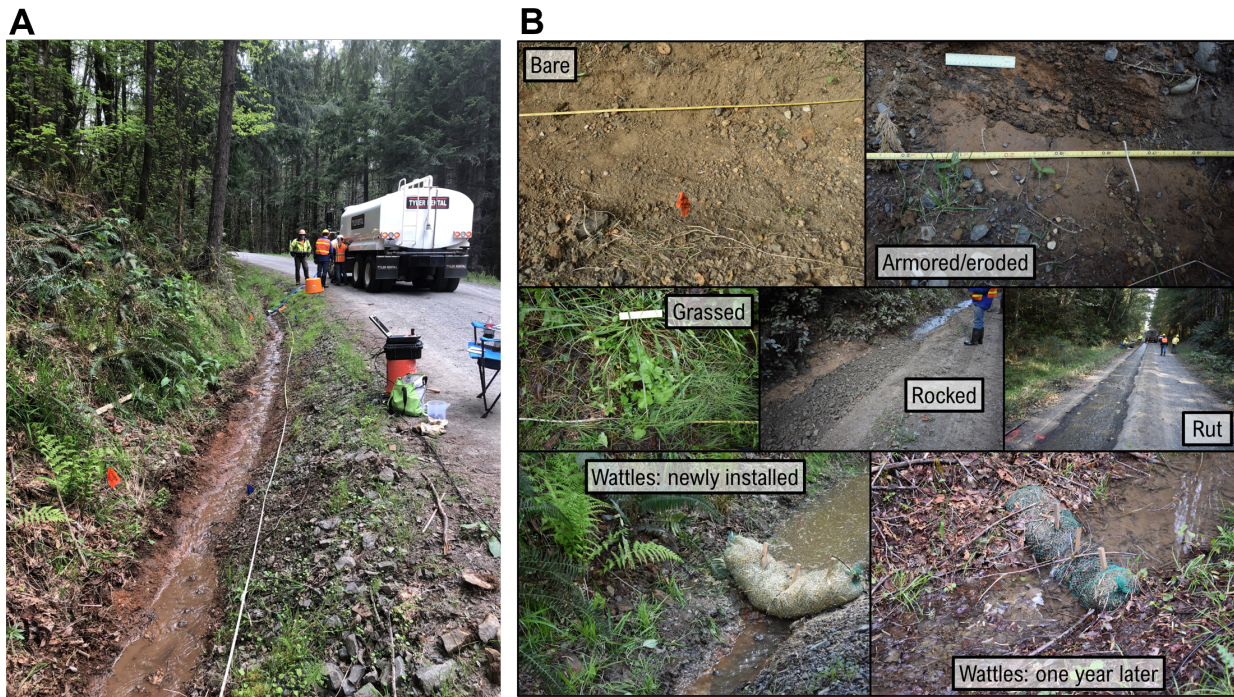
Figure 3.2: (a) Example experimental setup showing the roadside ditch line and water truck, and (b) example photos of each ditch line treatment tested.

The experimental runs were carried out in the volcanic region in May 2021 and May 2022 and in the siltstone region in May 2021, May 2022, and October 2022. In each region, multiple ditch treatments were tested (Table 3.1, Figure 3.2b):

Additionally, in the siltstone region, we performed the same experiment on a rut in the road surface to observe the hydraulic properties of ruts as well as their sediment-carrying effectiveness.

Table 3.1: Descriptions and locations for each ditch treatment tested.

Treatment	Description	Siltstone region	Volcanic region
Bare subsoil	freshly ditched and no treatment	x	x
Eroded/armored	not recently ditched with minimal grass recovery	x	
Grassed	not recently ditched with good grass recovery		x
Sparse wattles, initial installation	10 straw wattles		x
Sparse wattles, 1-year post-installation	10 straw wattles		x
Dense wattles, initial installation	19 straw wattles	x	
Rocked	3"-minus covering bottom of ditch	x	

3.3.2 Experiment

The goal of the experiment was to estimate Manning's roughness and sediment load for each ditch treatment. We examined changes in the hydraulics of flow, as well as sediment production and transport, in roadside ditch lines for multiple roughness-varying erosion control treatments. Each experimental run consisted of the following:

1. Measurements of the physical characteristics of the ditch line (e.g., shape, soil texture, slope).
2. Collection of surface sediment samples at each of five cross sections (measurement stations) in the ditch.
3. Use of a salt tracer to determine the velocity of flow for three given flow rates (*Moore*, 2005; *United States Bureau of Reclamation (USBR)*, 2001).
4. Collection of sediment samples at the downstream end of the ditch line throughout

each experimental run.

We determined the longitudinal profile (i.e., slope) of the ditch using a survey rod and a survey level and established measurement stations at 4-meter intervals from the ditch relief cross-drain culvert at the bottom of the ditch segment (origin; 0 meters) to the top of the experimental segment (40 meters up-ditch). Cross-sectional channel profiles were measured at every other measurement station from the bottom of ditch line (4 m above the pipe inlet, 12 m, 20 m, 28 m, 36 m) using a level and a metric ruler, with elevation-drop measurements being made at 0.1-meter intervals from the cutslope side of the ditch (0 meters) to the side of the road (1.1-1.2 meters) (Figure 3.3a).

Sediment was sampled at each of the five cross sections noted above to determine the existing grain size distribution in each experimental ditch. Sediment samples were taken from the surface because the expected transported sediment comes from the surface of the ditch, as flow was provided upstream of each ditch. These samples were originally processed such that we obtained a dispersed grain size distribution. However, because the material in our ditch lines had some cohesion, we took additional samples to obtain a water-stable aggregate grain size distribution for each site following the methods of *Kemper and Rosenau* (1986). The resulting median grain size was approximately 1 millimeter, which was used as the median grain size for further analysis (see Chapter 3.4). Photographs were taken at each of the five cross sections noted above to document the physical changes of the ditch line before and after the experimental runs (if any). Finally, to ensure minimal loss of water flow to infiltration during experimental runs, the ditch line was wetted by a water tank truck

providing flow at a slow rate (Figure 3.2a).

To provide known flow rates, we utilized a flow meter (Flomec G2 AI Turbine Flow Meter Model G2A15NQ9GMB) and hose attached at the water tanker outlet. The experimental runs were carried out at three flow rates for each ditch treatment, twice to thrice per flow rate: 57 liters per minute (lpm), 95 lpm, and 151 lpm. These three flow rates were chosen to reflect flows that have been observed in our broader study dataset of these magnitudes. More specifically, these three flow rates exist within the 99th to 100th percentile of empirical flow data recorded at one of our siltstone lithology sites between 2019 and 2021 (Figure 3.4). Those years experienced slightly drier-than-average climatic conditions (*PRISM Climate Group*, 2023). We used the high end of the flow rates as most sediment is transported within the wettest few days in ditch lines.

Conductivity probes (Campbell Scientific Model CS547A with a Campbell Scientific CR 1000 Data Logger) were placed in the ditch at just below 4 meters and just above 36 meters. The conductivity probes measured the passage of salt tracers, used to determine the velocity of the flow during our experimental runs.

Once the flow from the water tank truck stabilized in the ditch line, a known quantity of NaCl was added to the system, signaling the start of the experimental run, and was monitored via conductivity probes. The conductivity probes logged a reading every second. Once the NaCl level for both conductivity probes returned to their original values, the experimental run was considered complete. We repeated the addition of NaCl for each flow and treatment combination twice.

For each experimental run, a grab sample for sediment concentration was collected at the downstream end of the ditch line once the flow rate stabilized. We collected one main sediment concentration sample per run to give us an estimate of sediment transport occurring for each treatment prior to any ditch armoring occurring.

3.3.3   Data analysis

In order to calculate Manning's roughness values for each experimental run, we first estimated flow velocities from our salt tracer experiments. We measured the time it takes for the NaCl to travel from the upper sensor to the lower sensor (Figure 3.3b). With a known distance between the two sensors and the time of travel, we calculated the average velocity of the flow between the two sensors, which is taken as the average velocity for the ditch line flow.

The cross-sectional shape of our ditches for the experimental runs were mostly parabolic (e.g., Figure 3.3a). Given the estimated U and measured Q, we then characterized the parabolic shape factor, a. To calculate this shape factor, we took the average of the measurements of the ditch line cross-sectional channel profiles and characterized a representative cross-sectional shape of the ditch line. We fit each ditch with an equation for a parabola and estimated the shape factor a.

Given U, Q, a, and the measured mean profile slope of the ditch line, n is obtained from (Eq. 3.11). For each erosion control treatment (Figure 3.2b), we estimated the corresponding n (i.e., n_t) using the steps outlined above. We carried out an ordinary least squares regression analysis to help describe the observed relationship between n_t and flow (Table 3.2).
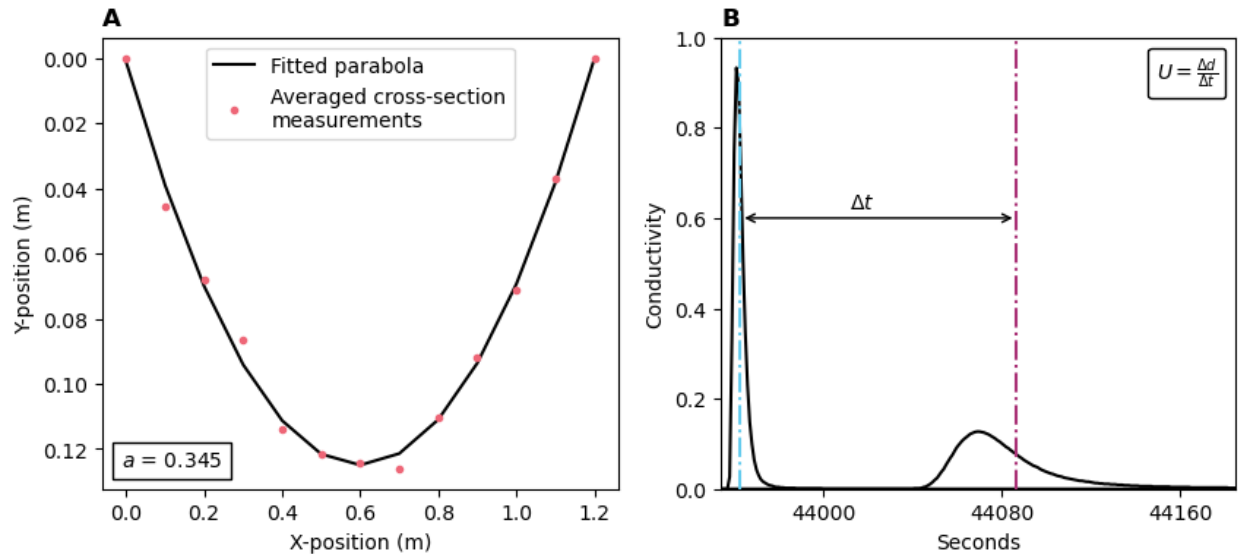
Figure 3.3: Examples of (a) average ditch cross-section measurements with a fitted parabola and shape factor and (b) a conductivity plot for two sensors from the salt tracer experiment. Δt is the time it takes for the salt tracer to get from the upper sensor to the lower sensor (average rate taken as 1/2 area under the curve) and is determined from the plot, and Δd is known.

Ultimately, we were interested in the response of the grain shear stress (i.e., shear stress partitioning) and the sediment transport capacity of the ditch line to additional Manning's roughness, which we calculated based on our measured and calculated experimental values following the logic in Chapter 3.2.

In addition to the roughness of each ditch and the grain shear stress of each experimental run, we used our sediment concentration grab samples from each experimental run to corroborate our estimates of shear stress partitioning and sediment transport capacity and test for whether additional factors other than roughness appeared to affect sediment transported along the bottom of the ditch line. Sediment concentrations were converted to sediment

transport per unit flow width, which is calculated as *sediment concentration* $* \frac{Q}{w}$ where Q is flow discharge and w is flow width obtained from the parabolic channel cross section assumption at the measured cross sectional area (Figure 3.3a).

We used two years of measured flow data (10/01/2019-09/30/2021) from one of our field sites to calculate flow durations to be applied (Figure 3.4) in estimating grain shear stress and sediment transport capacity. This allowed us to address questions about how much of the time sediment might be expected to be produced from the ditch, the expected distribution of sediment export rates, and the fractional reduction in sediment yields as a function of a treatment specified in terms of its added roughness. These flows were used to calculate grain shear stress (τ_g), sediment transport capacity (T_c), the fractional reduction in grain shear stress (ϕ) and the fractional reduction in sediment transport capacity (θ) for different erosion control treatments using their respective Manning's roughness values.

3.4 Results

3.4.1 Inferences from field observations

To address our first research question, we report estimated total roughness values (Manning's n) from our experiments (Figure 3.5). Erosion control treatment installation and natural armoring of a ditch line increased n_t as compared to a bare (recently disturbed) ditch. Three erosion control treatments—rocked, grassed, and sparse wattles 1-year post-installation—demonstrated a linearly decreasing relationship between the total roughness and flow (Table 3.2). Additionally, we performed the same experiment on a heavily defined
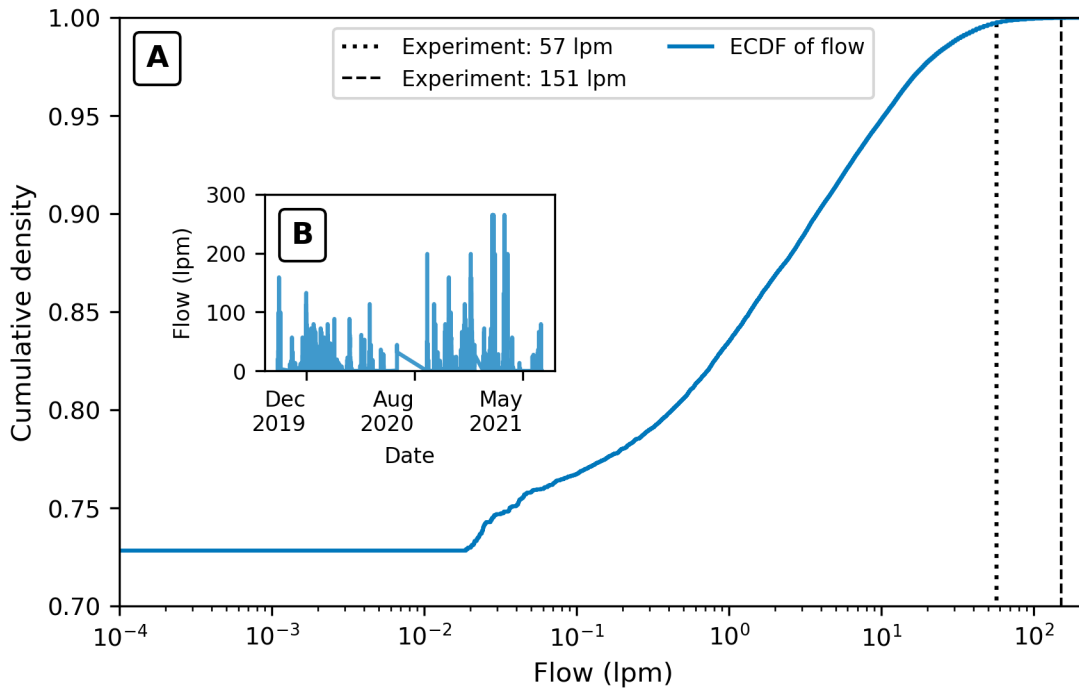
Figure 3.4: (a) Empirical cumulative distribution function of flow data from one of our siltstone lithology field sites in western Washington with vertical lines denoting two of the flows used in the small-scale experiment in liters per minute (57 lpm and 151 lpm). For this site, 57 lpm flows exist in the 99th percentile and 151 lpm flows exist in the 100th percentile. (b) The corresponding tipping bucket flow hydrograph for the 2020 and 2021 water years.

wheel rut on the road surface (Figure 3.2b) and found that the rut had similar roughness to a bare (recently disturbed) ditch. The observed increase in Manning's roughness with added erosion control treatments is consistent with the literature and the shear stress partitioning theory, further elaborated in the discussion section. The next logical question to address here is: What is the influence of increased roughness on sediment load? We address this question through our sediment concentration data.

Our grab samples provided us with sediment concentration values (Figure 3.6a) and
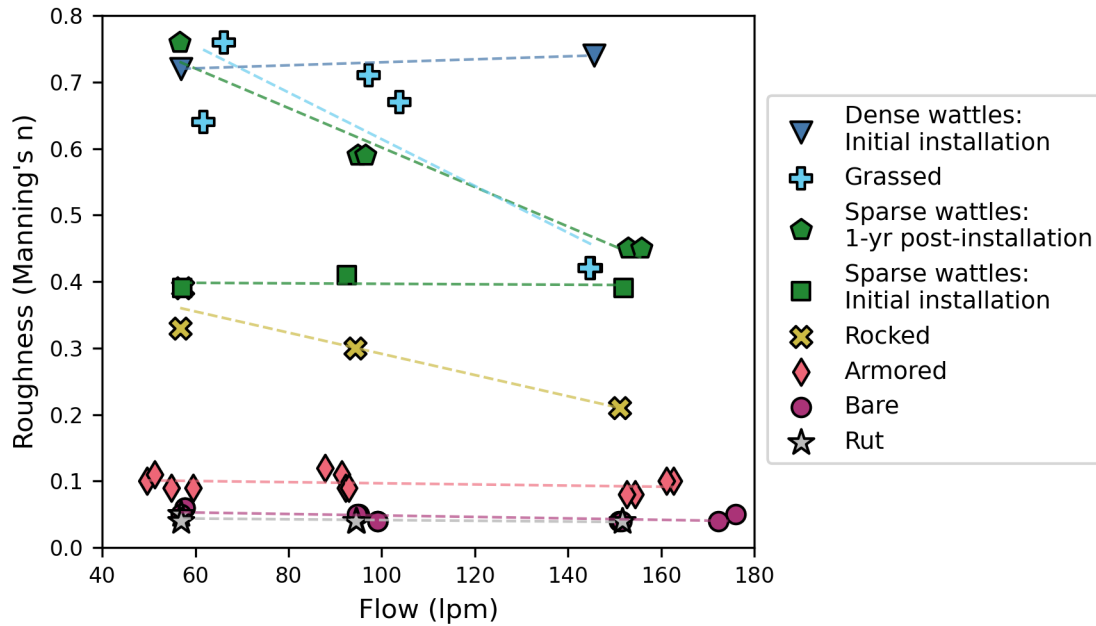
Figure 3.5: Roughness values (Manning's n) for each ditch condition and their relationship to flow.

sediment transport per unit width (Figure 3.6b) for each treatment and flow. All of our ditch treatments yielded some amount of sediment transport. The bare ditch and rut yielded the highest sediment concentrations and sediment transport, with an armored ditch yielding at least 1 order of magnitude less sediment. To provide a more direct comparison, we plot sediment transport from each erosion control treatment staged from low to high n_t, with nominal flow rates denoted by color (Figure 3.6c). As the roughness due to each treatment increases, sediment transport decreases, with the highest flow rate showing the most consistent reductions with increased roughness (Figure 3.6c).

One goal of this experiment was ultimately to determine the sediment reduction effects

Table 3.2: Statistical analysis results of trend lines shown that relate total roughness and flow.

Treatment	Slope	Coefficient of Variance	P-value
Dense wattles, initial installation	0.000*	1.000*	N/A*
Grassed	-0.0004	0.748	0.026
Sparse wattles, 1-yr post-installation	-0.0003	0.953	0.003
Sparse wattles, initial installation	0.000	0.021	0.907
Rocked	-0.002	0.890	0.057
Armored	0.000	0.099	0.319
Bare	0.000	0.405	0.035
Rut	0.000	0.240	0.402

*Only two data points

of erosion control treatments in roadside ditch lines using the concept of shear stress partitioning. To do so, we calculated—for each of the treatments—the total shear stress using the denominator of Eq. 3.8 and the grain shear stress using Eq. 3.9 solved for τ_g (Figure 3.7b). The merit of using shear stress partitioning to determine sediment reduction effects is well-illustrated by our data: the relationship between total shear stress and sediment transport is disjointed (Figure 3.7a). Despite a consistent increase in calculated total shear stress for different erosion control treatments, their associated sediment transport estimates were consistently lower than bare ditches and ruts (only under higher flow). This seemingly counterintuitive behavior can only be explained when effective (grain) shear stress is used, organizing the data points consistently along a curve, where all the erosion control treatment sediment fluxes are now pushed back to consistently small values, largely less than
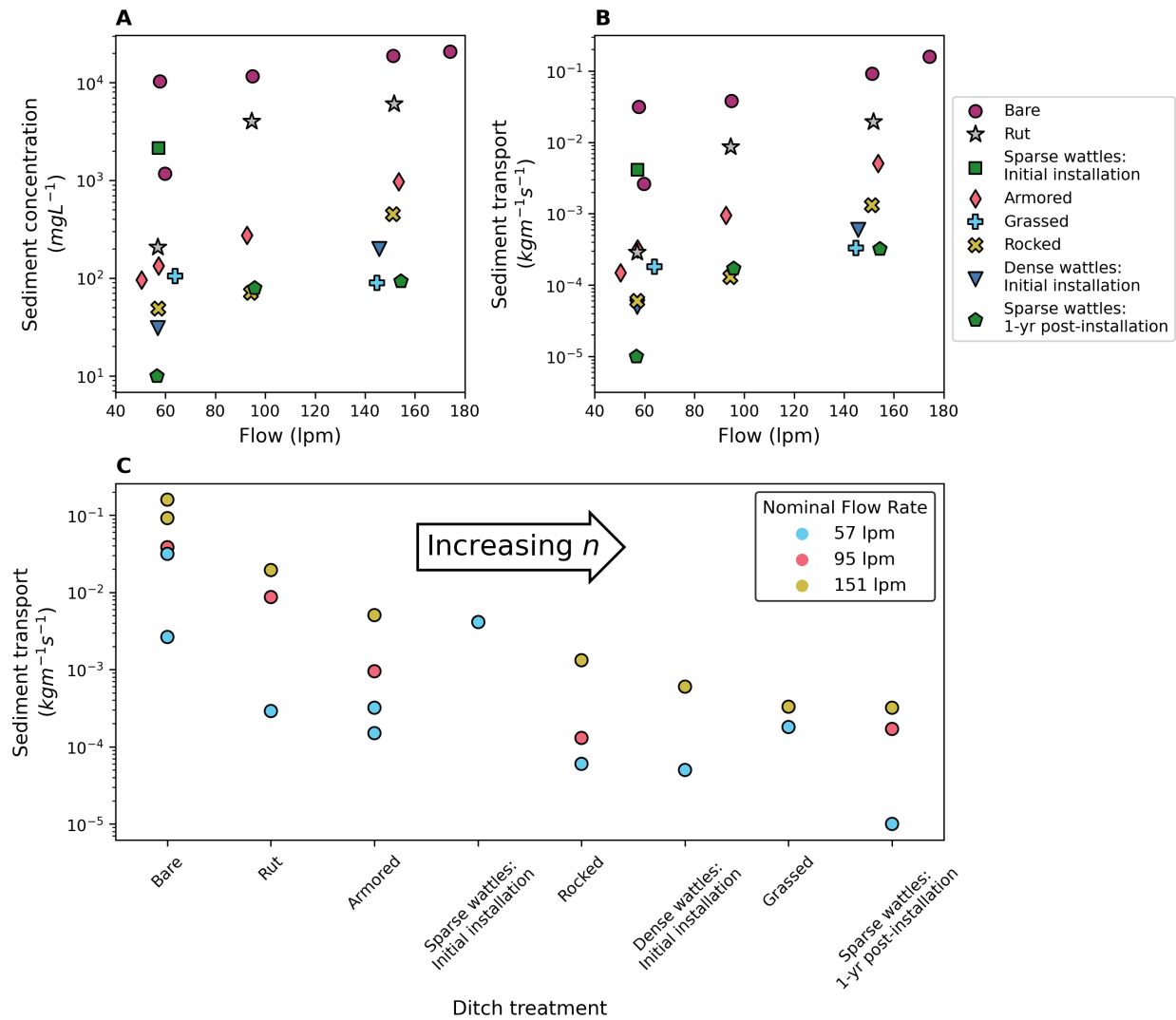
Figure 3.6: (a) Sediment concentration values for each ditch condition and their relationship to flow. (b) Sediment transport values for each ditch condition based on sediment concentration and flow width. (c) Strip plot showing the spread of sediment transport values for each ditch treatment. The nominal flow rates for each sediment transport value are denoted by different colors.

1 Pa, while bare plots remain constant ($\tau_g = \tau_t$). The relationship between grain shear stress and sediment transport aligns with the expectation that increased roughness results in decreased sediment transport (Figure 3.7b, c). Furthermore, if filtering were an additional

effect of some erosion control treatments, sediment yield from filtering treatments (grass, initial installation of wattles, rocking) might be systematically lower than the mean expectation based on the pattern of points (e.g., a fitted curve). No such pattern is observed in Figure 3.7c. As discussed above (Chapter 3.1), adding roughness elements to the ditch line (i.e., erosion control treatments) increases the total shear stress acting on the ditch due to the deepening and slowing of water flow. However, as also discussed previously, the resulting increase in friction around immobile roughness elements reduces the amount of grain shear stress available for sediment transport, which is illustrated by plotting total shear stress as a function of Manning's n due to additional roughness elements (Figure 3.1).

3.4.2 Erosion control treatment effectiveness in context of climate

Because sediment transport is a strongly nonlinear function of grain shear stress, we must consider potential sediment yield reductions from treatments in the context of not just a few flows, as done with the field study. Rather, we should consider potential sediment yield reductions in the context of an ensemble of flows as might be seen over a season of runoff (e.g., Figure 3.4).

We can see that with higher roughness values, the exceedance probabilities of grain shear stress decrease in a relatively consistent nature (Figure 3.8a), with substantial reductions in the fraction of time that sediment would likely be transported. The d_{50} of soil aggregate particles in the field sites is approximately 1 millimeter, which has a relatively high critical shear stress based on Shield's criteria (0.566 Pa) as compared to the distribution of grain
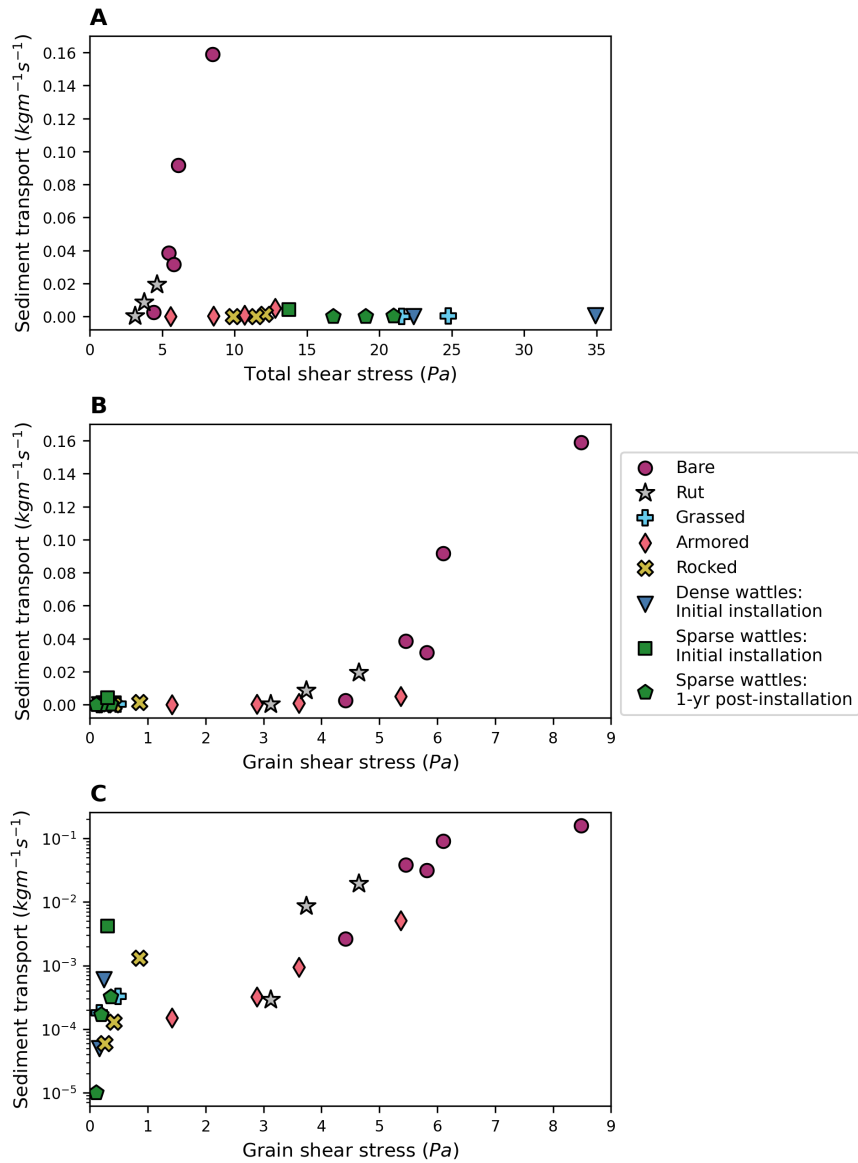
Figure 3.7: (a) Measured sediment transport values as a function of total shear stress, (b) measured sediment transport values as a function of grain shear stress, and (c) measured sediment transport values as a function of grain shear stress with a log-scale y-axis.

shear stresses estimated from observed flows and, as such, only yields modeled sediment transport for Manning's roughness values of up to 0.25 (Figure 3.8a). In Figure 3.4 and

Figure 3.8a, water flows (considered non-zero at a rate greater than 0.02 lpm) about 27%
of the time, and in freshly disturbed ditches, grain shear stress exceeds the critical shear
stress about 22% of the time (or about 80% of the time that water is flowing). In contrast,
by increasing the roughness to n=0.10 (armored condition), runoff from the ditch would be
expected to transport sediment only about 12% of the time (or 44% of the time there is
runoff), and with n=0.25 (rocked ditch), grain shear stress would exceed critical shear stress
less than 2% of the time (or 7% of the time that runoff occurs). The fractional reduction
in grain shear stress is constant for roughness values that do not vary with flow, whereas a
slight decrease occurs for roughness values that linearly decrease with flow (Figure 3.8b).

From our calculated grain shear stresses, and using Eq. 3.12 in Chapter 3.2, we mod-
eled the sediment transport capacity of ditch flow—when there was ditch flow—for different
roughness values. The resulting sediment transport capacity exceedance probabilities de-
crease dramatically as a function of increasing roughness (Figure 3.8c). For 5% of the time
(about 18 days per year) the transport capacity in a bare ditch (n=0.05) would exceed 0.1
$kg m^{-1}s^{-1}$, a rate that is almost never expected to occur in an armored ditch (n=0.10). At
the same time in an armored ditch 5% of the time transport capacity would be expected to
exceed 0.002 $kg m^{-1}s^{-1}$, which is about 2% of the rate in a bare ditch for that exceedance
probability. Integrating over the ensemble of flows, the bare ditch (n=0.05) would have a
transport capacity, T_c, of 61 $Mg\ m^{-1}yr^{-1}$, an armored ditch (n=0.10) would have a T_c of 2.8
$Mg\ m^{-1}yr^{-1}$, and the higher roughness of a rocked ditch (n=0.25) would have a T_c of about
0.04 $Mg\ m^{-1}yr^{-1}$. Actual erosion collected from a ditch would be smaller since available

sediment would eventually be depleted, but the contrast in transport capacity integrated over the year gives a more concrete sense of the effect of added roughness on sediment yield. One notable point is that for low flows (common), a total roughness of n =0.10 transitions from nearly complete reduction in sediment transport at 4 lpm or less to around 94% reduction at 57 lpm in a nonlinear way (Figure 3.8d). The modeled reductions are nearly 100% for a ditch with installed erosion control treatments (rocked ditch or stronger; n $\geq$ 0.25). In other studies, measurements of sediment yield from road segments with recently disturbed vs. armored ditches over a few months to years showed reductions ranging from 85% (*Luce and Black*, 1999, 2001b) to nearly complete reduction (*Luce and Black*, 2001a).

3.5   Discussion

Shear stress partitioning offers an effective way of characterizing the effect of forest road erosion control treatments in reducing sediment transport through the use of their associated Manning's roughness. Because Manning's roughness associated with shallow flow is typically an empirical value coming from limited studies with varying conditions and contexts, and few, if any, studies use Manning's n to evaluate erosion control treatment effectiveness, comparing all our measured Manning's roughness values to the literature is challenging. Our measured roughness values for bare soil (n$\simeq$ 0.05), grass (n$\simeq$ 0.45 to 0.75), and a rocked surface (n$\simeq$ 0.25 to 0.35) are reasonably consistent with previously established values for shallow flow (Figure 3.5; e.g., *Arcement and Schneider*, 1989; *Barros and Colello*, 2001; *Emmett*, 1970; *Engman*, 1986). While not comparable to established roughness values due
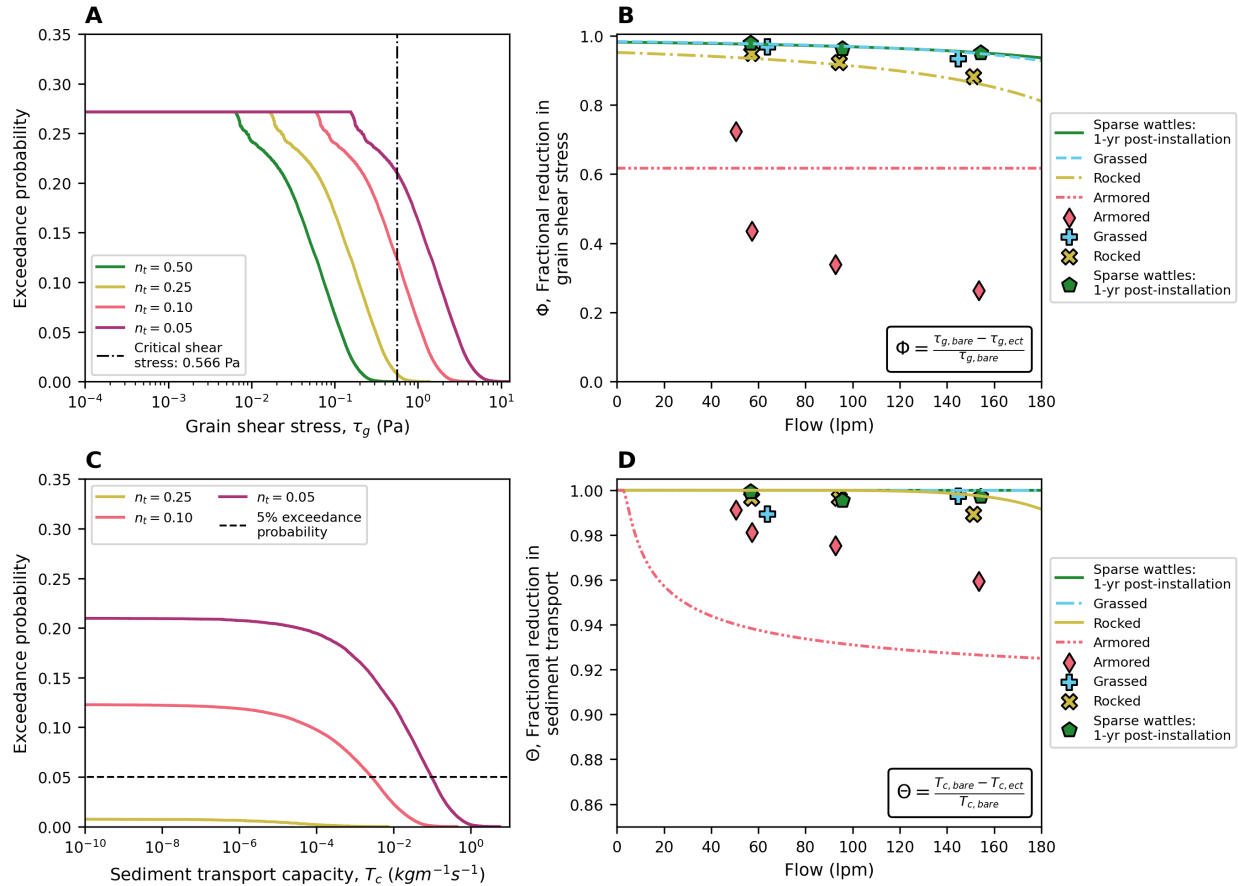
Figure 3.8: (a) Exceedance probabilities of grain shear stress, τ_g, for multiple n_t values calculated from Eq. 3.2 using observed ditch line flow hydrographs. Higher n_t values decrease grain shear stress. The critical shear stress threshold for a d_{50} of 1 mm is denoted by the vertical line. (b) Fractional reduction in grain shear stress, ϕ, for multiple ditch erosion control treatments. Erosion control treatments with n_t values that vary with flow provide less reduction in grain shear stress with higher flows. Experimental fractional reductions in grain shear stress are shown as points. (c) Exceedance probabilities of sediment transport capacity, T_c, for multiple n_t values. An exceedance probability of 5% is denoted by the horizontal line. (d) Theoretical fractional reduction in sediment transport capacity, θ, for multiple ditch erosion control treatments. Experimental fractional reductions in sediment transport are shown as points.

to limited studies, wattles do show comparable roughness values to grass. Measuring the roughness of a ditch line erosion control treatment offers an efficient and more general way to estimate the effectiveness of a given erosion control treatment, when used in a sediment transport equation driven by discharge, for differing conditions and contexts.

This final point is important—99% of observed flows that were > 0.02 lpm in this dataset were less than 57 lpm, and in this range of flows, there is a variable and nonlinear sensitivity of fractional sediment transport capacity reduction (θ) as a function of flow rate (Figure 3.8d). Any experiment that reports a fractional sediment reduction from a treatment equivalent to an armored ditch would need to qualify that the reduction is applicable to the particular flow rate used, and any study integrating sediment over a season would need to report the ensemble probability distribution of precipitation or flow. Directly transferring a fractional reduction from a mild rainy climate (e.g., northwest US, northern Europe) to one where high intensity storms are more common (e.g., tropics, southeast US) or places where snowmelt is more common is not necessarily a reasonable expectation. The change in roughness associated with an erosion control treatment, however, should be transferable through the use of shear stress partitioning in a sediment transport model.

While most erosion control treatments maintained constant total roughness with varying flow, three erosion control treatments had roughness decrease as flow increased (Figure 3.5): rocking, grass, and one-year-old wattles. Each of these treatments had unique physical characteristics that we hypothesize contribute to their decreasing relationship between roughness and flow (Figure 3.9).

For the site with a rocked ditch (approx. d_{50}= 38 mm), the decrease in roughness as flow increased can likely be attributed to the fraction of the cross-sectional area of flow navigating the immobile roughness elements. With low flow, the majority of the water is moving through the subsurface (the interstitial spaces between the rocks) of the channel, with minimal surface flow (Figure 3.9a). As the flow increases, the fraction of the water being slowed due to immobile roughness elements decreases (e.g., *Barros and Colello*, 2001; *Chen et al.*, 2015).

For the grassed site, the decrease in roughness with higher flows is similar to the rocked site: a decrease in the fraction of the cross-sectional area of flow experiencing immobile elements, but due to different mechanics. With lower flows, the water must flow through grass and vegetation stems. As the flow increases, the vegetation begins to bend, which effectively "smooths" these immobile roughness elements, causing the total roughness to decrease (Figure 3.9b; e.g., *Chen et al.*, 2015; *Jordanova and James*, 2003; *Nepf*, 2012).

The decrease in roughness with an increase in flow for the one-year-old sparse wattles site can likely be attributed to both the fraction of the cross-sectional area of flow navigating immobile roughness elements and the dam-and-reservoir effect seen during the experiment. The wattles at this site were initially installed in May 2020. During those initial wattle experimental runs, the flow never over-topped any of the wattles; rather, the flow went under or through the wattles (Figure 3.9c), which led to relatively consistent roughness values for varying flows. One year later, however, the wattles had not experienced any maintenance. Sediment and debris had built up inside of and behind each wattle, and, as such, the wattles
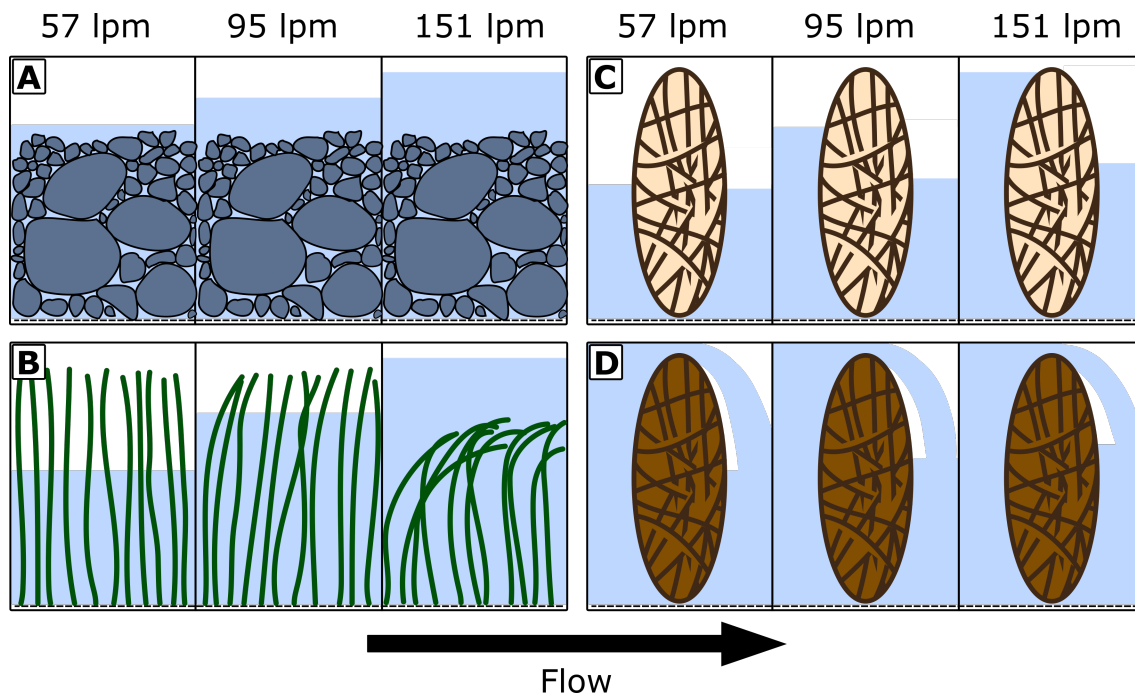
Figure 3.9: Drawings showing side views of: (a) The rocked ditch as flow increases. Once the flow gets to 151 lpm, the water far overtops the rocking, causing the fraction of the flow cross-sectional area being slowed by the immobile roughness to decrease. (b) The grassed ditch as flow increases. The highest flow causes the vegetation to bend, effectively smoothing the cross section. (c) The initial installation of straw wattles, where the flow went under or through the wattles, as they were brand new. (d) The wattles after they had been in the field for a year without any maintenance, causing them to become clogged with sediment. At all flow rates, the space behind the wattles fills up with water then overtops, producing a reservoir-and-dam effect, which slows the water down.

acted like a series of dams and reservoirs (see *Edwards et al.*, 2016). The initially high roughness values for the one-year-old wattles can likely be attributed to the severe slowing of water as it built up behind each wattle before spilling over. As the flow increased, that slowing had less of an effect, and the fraction of the flow seeing the immobile roughness element decreased (Figure 3.9d).

In conjunction with the roughness, the sediment concentration grab samples validated the

use of shear stress partitioning to evaluate reduced sediment transport effects due to erosion control treatment installation. This is demonstrated by the relationship between measured sediment transport and total shear stress (Figure 3.7a) and measured sediment transport and grain shear stress (Figure 3.7b). The trend between sediment transport and grain shear stress (Figure 3.7c) indicates that the increase in flow roughness due to additional immobile elements is likely the key driver in the reduction of sediment transport, rather than other mechanisms, such as binding effects of vegetation roots or filtering by wattles (which leads to rapid clogging with little internally-retained sediment in any event).

We estimated that a majority of ditch line erosion control treatments decreased calculated grain shear stress, and therefore modeled sediment transport, by almost 100%, producing fractional reductions near 1 (Figure 3.8d). In terms of measured sediment transport, we found that all treatments in our experimental runs produced some amount of sediment transport, including those with high roughness values. One site had a higher-than-expected sediment concentration value: sparse wattles during the initial installation (Figure 3.6). In the case of the sparse wattle initial installation, the measured sediment concentration value is high likely due to three factors: 1) the small amount of ditch below the final wattle had some erosion; 2) the ditch in which the wattles were installed had been recently disturbed and therefore had a larger amount of easily accessible sediment for transport; and 3) the wattles had a tendency to slightly float immediately after installation and, again, had a larger amount of easily accessible sediment for transport. Additionally, the sparse wattle installation had enough space between wattles that erosion and suspension of fine material

was possible therein, especially at lower flows. Indeed, the spatial heterogeneity in grain shear stress is not fully accounted for in our modeling approach, which assumes uniform roughness and grain shear stress.

Overall, the decrease in measured sediment transport and calculated sediment transport capacities with erosion control treatment installation emphasizes the importance of ditch line erosion control treatment installation both from the perspective of ditch erosion reduction and potential mitigation of sediment transport from other elements within the road prism. Erosion control treatment installation can help reduce large ditch line erosion events, particularly immediately after road ditch grading (e.g., Luce and Black, 2001b) or new road construction (e.g., *Megahan*, 1974). Additionally, roads that are crowned or insloped allow for sediment from the road surface to travel to the ditch line where erosion control treatments can mitigate the tread-derived sediment. However, due to traffic and road deformation, wheel ruts tend to form on the road surface, which can cause water and sediment to bypass ditch line erosion control treatments (*Alvis et al.*, 2023). As discussed above, a rut on the road (Figure 3.2b) has a similar roughness to a bare (recently disturbed) ditch and therefore has a high likelihood of carrying sediment in its rill-like flow. The interaction between the ditch line and other elements of the road prism is more complex and requires further exploration.

While the results from our experiment are promising, we have a limited number of observations for a limited number of erosion control treatments. However, we are not in the realm of conjecture, as both ample theory and empirical evidence exist for estimating the link between added roughness and sediment mobility and transport (e.g., *Kothyari et al.*,

2009; *Prosser et al.*, 1995; *Thompson et al.*, 2004). Geomorphologically, both shear stress partitioning and the relationship between roughness and sediment transport is commonly utilized to estimate erosion and sedimentation in rivers and on vegetated hillslopes (e.g., *Darby et al.*, 2010; *Ferguson et al.*, 2019; *Istanbulluoglu and Bras*, 2005; *Li et al.*, 2022a). Regardless, future studies to empirically validate the relationship between roughness measurements and ditch line erosion control treatment sediment reduction, especially for a larger range of contexts and conditions, are warranted.

3.6   *Conclusion*

Using the notion that the additional roughness of ditch line erosion control treatments can be used to examine their effectiveness—in conjunction with existing theory surrounding shear stress partitioning—we evaluated several ditch line erosion control treatments. We found that 1) each erosion control treatment yielded consistent Manning's n values across multiple replications and sites, with a bare ditch (no treatment) having the lowest roughness (n=0.05) and a densely-wattled ditch having the highest roughness (n=0.75); 2) when combined from each experiment, the sediment load and calculated grain shear stress data yielded a single positive relationship, which suggests the effect of additional roughness on grain shear stress is a main driver in the reduction of ditch line sediment load; and 3) our data demonstrated that fractional erosion reduction had a variable and nonlinear sensitivity to low flow rates (99% of observed flows) for lower roughnesses, which emphasizes the importance of context (i.e., climate, other conditions) in terms of fractional erosion reduction for a given treatment.

In contrast to the fixed sediment reductions determined through traditional engineering trials, the use of Manning's n and relevant established theory can allow for more rigorous extrapolation to other contexts and climates. Our study demonstrated that Manning's n, in tandem with shear stress partitioning in a sediment transport model, can be used in such a way for a few conditions and contexts. However, further research should be done to establish the use of roughness as a physical metric to evaluate erosion control treatment effectiveness for a wider range of conditions and contexts. Additionally, being able to characterize erosion control treatments with continuous numerical values would also pave the way for later empirical testing of the effect of additional ditch line roughness on overall road segment sediment production.

Acknowledgements

Data availability

The data presented in this chapter are not currently publicly available due to an agreement with the Cooperative Monitoring, Evaluation, and Research (CMER) Committee within the Washington State Department of Natural Resources Adaptive Management Program but are available from the corresponding author upon reasonable request and approval from CMER. Additionally, the data will be made publicly available in the future upon completion of the overarching project and CMER's approval of the final report.

Chapter 4

TEMPORAL EVOLUTION OF FOREST ROAD RUTTING AND FLOW PATHWAYS

This chapter is in preparation for submission to peer review.
Coauthors:
Charles Luce, Friedrich Knuth, Lauren Wittkopf, David Shean, Gregory Stewart, Erkan Istanbulluoglu

---

Abstract

Ruts are one of the most common types of surface deformation seen on unpaved forest roads. Historically, the rate and magnitude of rut development have been studied using cross-sectional analyses. While elevational cross sections are a straightforward way to examine the development of ruts, this type of analysis lacks spatial distribution. More recently, remote sensing techniques, such as structure-from-motion (SfM), have demonstrated their utility in detecting ruts on forest roads but applications of these data are limited. Here we used SfM to examine the development of ruts on forest roads in a spatially-comprehensive manner. We carried out a small-scale field experiment at two field sites in western Washington using unoccupied aerial vehicles (UAVs) to obtain digital elevation models (DEMs) of mainline logging road surfaces over three seasons. These UAV-derived DEMs were used in an elevation change analysis and in a simple flow routing model to examine the evolution of ruts, especially

with respect to the road surface flow pathways and erosion potential. We found that: (1) the cumulative rut incision for a given season and field site varied between 0.7 cm and 2.0 cm; (2) the relationship between rut incision and time since grading was nonlinear at both sites for all seasons with sufficient data; (3) as ruts develop, the overall flow pathways shift down-road; and (4) the erosion potential of our road surfaces tended to increase overall as ruts developed, with maximum increases of 30-120%. Our results demonstrate the advantage of using UAV-derived DEMs for analysis of rut evolution over cross-sections alone. Additionally, our results give us insight into how rutting may affect the utilization of erosion control treatments in roadside ditch lines and the sediment yield of the road surface.

4.1 Introduction

Forest roads are subject to a number of stressors that lead to road deformation, such as heavy traffic and rainfall. Road surface deformation commonly presents as ruts—rill-like incisions typically formed due to traffic—that straddle the centerline or crown of a road surface. Forest roads are typically crowned to allow water to drain as sheetflow to either side of the road (Figure 4.1a; Figure 4.2a). However, when ruts develop due to traffic, water on the road surface is instead diverted down the road (Figure 4.1b), which has multiple implications regarding forest road erosion. For one, water diverted down the road is unable to make use of any erosion control treatments in the roadside ditch lines (e.g., *Sheridan et al.*, 2006; Figure 4.2b). Additionally, ruts cause channelized flow, and thus have more capacity to carry sediment (*Foltz and Truebe*, 1995; *Ziegler et al.*, 2001b; Figure 4.2c).
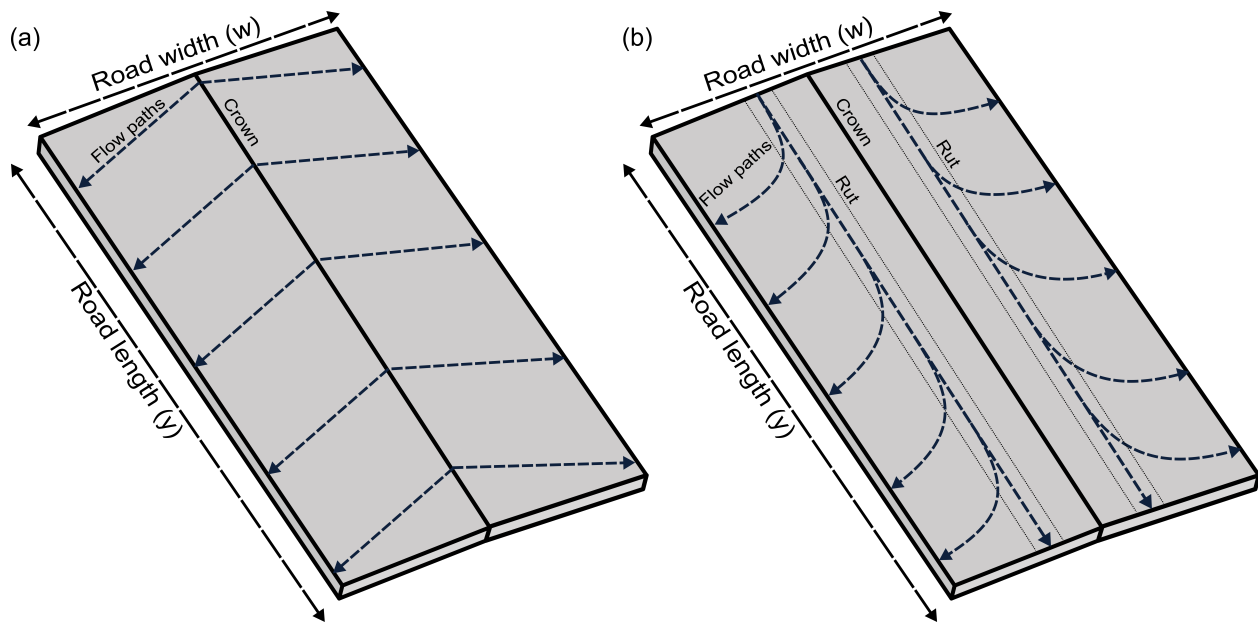
Figure 4.1: Schematic of a crowned road segment showing the flow pathways for (a) an idealized (i.e., perfectly smooth) road surface and (b) a rutted road surface.

The development and impact of rutting on forest roads has been the topic of study for decades. As early as the 1980s, ruts were denoted as a source of increased fine sediment on forest roads (e.g., *Burroughs and King*, 1989; *Reid and Dunne*, 1984), with later studies looking at maintenance techniques to mitigate rutting (e.g., *Bradley*, 1994; *Fannin and Sigurdsson*, 1996; *Foltz and Elliot*, 1997; *Sugden and Woods*, 2007). In more recent years, studies have shifted to focus on the development of rutting, specifically looking at how quickly or to what depth ruts form (e.g., *Akgul et al.*, 2017; *Nevalainen et al.*, 2017). In just the last few years, studies have begun to use remote sensing techniques, such as terrestrial LiDAR scanning (TLS) or photogrammetry techniques (e.g., *Cao et al.*, 2021; *Yurtseven et al.*, 2019), rather than more traditional physical measurements (e.g., *Fannin and Sigurdsson*,

Figure 4.2: Example photos of (a) an un-rutted road with flow heading to the ditch line from the center of the road; (b) water traveling down-road in a wheel rut instead of being directed to the roadside ditch; and (c) a heavily rutted road with channelized, sediment-laden flow heading down-road.

1996; *Foltz*, 1994).

However, whether using remote sensing or physical measurements, most studies evaluating ruts are either carried out on recently-built roads, or roads with soft soils where ruts develop deep and fast (e.g., *Fannin and Sigurdsson*, 1996; *Toman and Skaugset*, 2011), or on non-mainline roads such as skid trails or forest soils for logging operations (e.g., *Cambi et al.*, 2015; *Machuga et al.*, 2023; *Uusitalo et al.*, 2020; *Venanzi et al.*, 2023). Even if the studies are carried out on more established forest roads, their focus is typically on the advancement of data collection methods (e.g., *Aydin et al.*, 2019; *Dobson et al.*, 2014; *El Issaoui et al.*, 2021; *Hrůza et al.*, 2018; *Türk et al.*, 2022). Additionally, earlier studies use cross-sectional analyses to examine the magnitude (i.e., depth) of ruts (e.g., *Fannin and Sigurdsson*, 1996; *Foltz*, 1994), but such techniques offer no information regarding the fate of flow pathways on the road surface. Understanding the flow pathways on the road surface is critical for determining the effectiveness of maintaining the road surface to reduce sediment delivery from the established road network.

Mainline logging roads have heavy traffic and are some of the largest sources of anthropogenic sediment in nearby streams (*Cissel et al.*, 2014; *Megahan and Kidd*, 1972b; *Reid and Dunne*, 1984), and roads with ruts can produce 2 to 5 times more sediment than roads without ruts (*Foltz and Burroughs*, 1990). We lack detailed, quantifiable information about rut formation and their impacts on mainline logging roads, specifically with respect to the alteration of flow pathways on the road surface. Thus, information regarding rut formation and the alteration of flow pathways is important to plan for mainline logging road mainte-

nance to reduce fine sediment yields and assess the effectiveness of roadside ditch lines in trapping sediment.

To bridge this knowledge gap, we carried out a series of unoccupied aerial vehicle (UAV) structure-from-motion (SfM) surveys, with validation from TLS, to examine how wheel ruts evolve on mainline logging roads following road grading. We used differences between digital elevation models (DEMs) to assess the evolution of these ruts in terms of their incision and used a basic flow routing model to assess their impacts on the drainage system and erosion potential of the road segment. This paper presents the results from the aforementioned surveys to help us answer the following questions:

1. What are the depths and trends of rut formation on mainline logging roads?
2. How does rut evolution affect road surface flow pathways?
3. How do ruts affect the erosion potential of the road surface?

We first discuss the field study area and data acquisition methods, followed by the creation of DEMs and analyses of the elevation change, drainage system, and erosion potential. We present our results and finish with a discussion of the implications of this work.

4.2   Methods and data

4.2.1   Field study area

We carried out UAV and TLS surveys in two regions of southwest Washington state: (1) a volcanic lithology near Mount Saint Helens and (2) a siltstone lithology near Aberdeen, WA (Figure 4.3). Each region contains multiple field sites located on mainline logging roads as

part of a broad study conducted by the Cooperative Monitoring Evaluation and Research Committee within the Washington Department of Natural Resources Adaptive Management Program. One field site in each of the aforementioned regions was chosen for our UAV SfM and TLS surveys (KID-13 in the volcanic lithology and MEL-14 in the siltstone lithology). The field sites are relatively straight 80-meter segments of road delineated by 4.572-meter water bars placed at the top and bottom thereof to help drain the road surface to the roadside ditch line. KID-13 has an average gradient of 6% and is located approximately 278 meters (911 feet) above sea level. MEL-14 has an average gradient of 10% and is located approximately 185 meters (606 feet) above sea level. From our broader study, we obtained preliminary traffic count data for October 2021 to April 2022 at MEL-14 and November 2021 to June 2022 at KID-13. Over their respective durations, MEL-14 received heavy traffic (on average, 7 trucks per day), where heavy traffic is defined as five or more logging truck passes per day (*Reid*, 1981), and KID-13 received light traffic, where light traffic is defined as no logging trucks but some light vehicles (*Reid*, 1981). On average, KID-13 receives 1560 mm of annual precipitation, and MEL-14 receives 2400 mm of annual precipitation (*PRISM Climate Group*, 2023), with most of the precipitation occurring between October and April.

4.2.2   Data acquisition

UAV and TLS surveys were conducted over three subsequent seasons (wet, dry, wet) between November 2020 and June 2022 (Table 4.1). At the beginning of the first wet season (year 1, Wet1), each site had good quality aggregate added to the surface and was graded. Subsequent
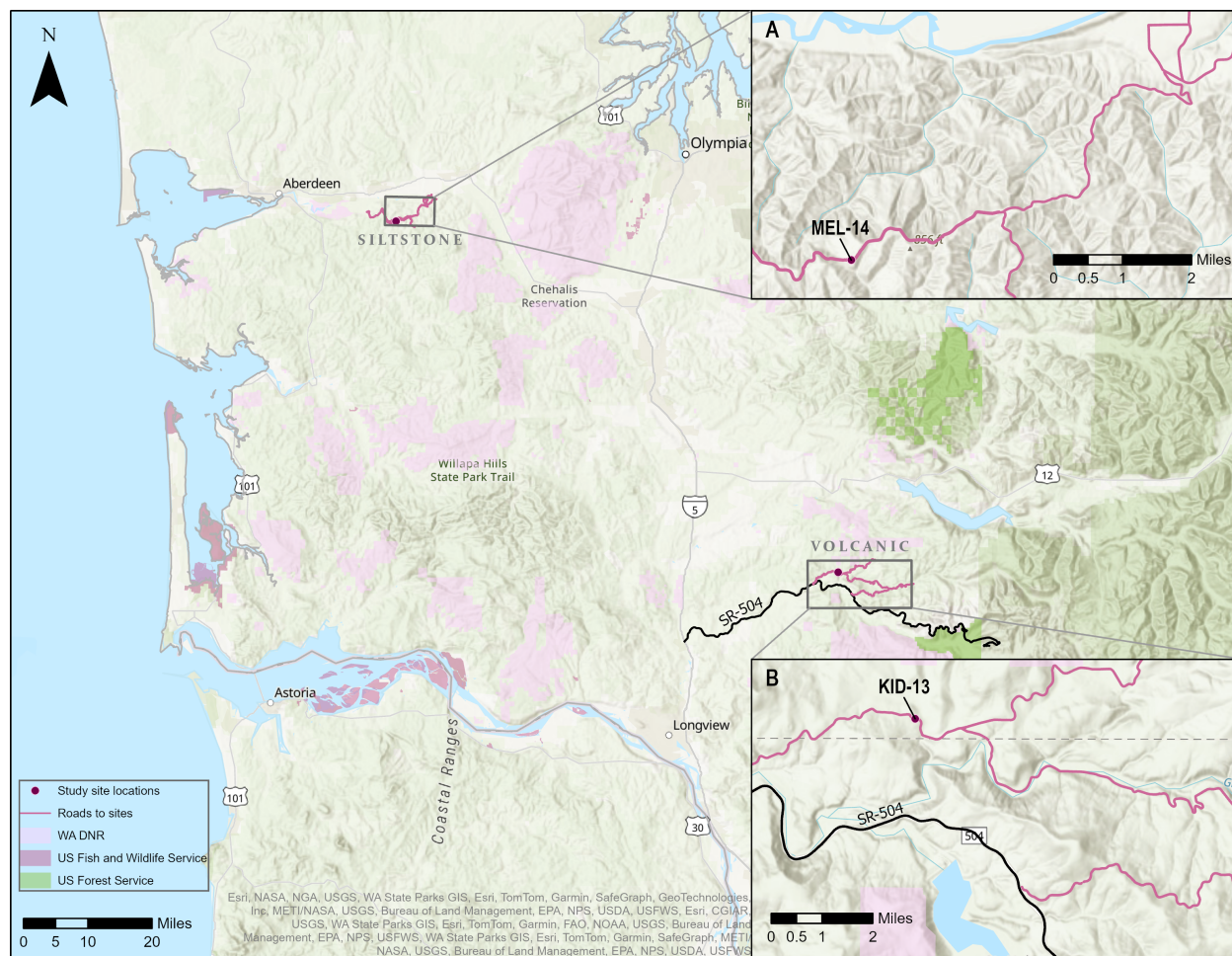
Figure 4.3: Map of field site locations in Washington state. Inset A shows MEL-14, the field site in the siltstone lithology and inset B shows KID-13, the field site in the volcanic lithology.

seasons (dry season year 1, Dry1; wet season year 2, Wet2) began once the road segments were regraded. At KID-13, all three seasons of surveys consisted of longer time periods between surveys (i.e., a range of 1-4 months between surveys) to look at the overall depth of rut development on a road segment. At MEL-14, the first two seasons consisted of longer time periods between surveys whereas the final season consisted of more frequent surveys (i.e., a range of 1-5 weeks between surveys) to look at the rate at which ruts develop on a road segment.

For ground-truthing of the UAV surveys and to align and coregister surveys at different time slices, 24 ground control points (GCP) were installed at each site. These ground control points were 10-inch nails hammered in along the sides of the road segments—12 on each side—and spray painted for extra visibility. The spatial coverage of GCPs was limited to the sides of the road segment as we could not guarantee the safety of traffic nor the stability of the GCPs if they were placed in the road prism itself. Two additional monuments were installed off the road at each site for TLS survey use.

The locations of the GCPs were measured in an arbitrary coordinate system at the beginning and end of a season using a Trimble SX10 Scanning Total Station to ensure that the GCPs had not migrated. At KID-13, the variation in repeat survey GCP locations was small (on average, less than 1 mm) and was assumed to be random error. As such, the mean survey location for each GCP was used for data processing at KID-13. At MEL-14, multiple GCPs were ripped out between seasons during grading, so the GCPs had to be reset at the beginning of each season. As such, locations recorded at the beginning of each season were

used for data processing at MEL-14.

To map rut formation on these road segments, UAV and TLS surveys were conducted in tandem. Multiple UAV surveys were conducted within each season, whereas the TLS surveys were conducted only at the beginning and end of each season (Table 4.1). The main goal was to use UAV SfM for analysis, with the initial TLS survey for each season serving as a reference baseline dataset, due to TLS inherently providing validated data (e.g., *Wilkinson et al.*, 2016). The TLS surveys used a Trimble SX10 Scanning Total Station and required three locations for scanning the full road surface. Each TLS survey yielded high-resolution point cloud data.

The UAV SfM surveys were carried out with a Phantom 4 Pro DJI drone with RC controller and all flights were done manually due to high tree cover and lack of good global navigation satellite system (GNSS) lock. Each UAV survey consisted of three flights: (1) lower flight elevation (∼5 meters above ground level) up and down the road segment with the camera nadir; (2) lower flight elevation (∼5 m agl) around the road segment with the camera at an angle; and (3) higher flight elevation (∼10-15 m agl) up the road segment with the camera nadir. The UAV SfM surveys collected high-overlap, high-resolution photographs to be processed using photogrammetric techniques.

4.2.3   TLS and UAV DEM post-processing

Post-processing of TLS and UAV data was done using CloudCompare and Pix4DMapper, respectively. The TLS data were processed such that the DEMs of the road surface had

Table 4.1: Survey seasons, dates, types, and times since baseline at each field site.

Site	Season	Date of survey	Type of survey	Time since baseline (months)
KID-13	Wet season year 1 (Wet1)	11/09/2020	UAV; TLS	0
		02/08/2021	UAV	3
		04/06/2021	UAV	5
		05/13/2021	UAV; TLS	6
	Dry season year 1 (Dry1)	06/04/2021	UAV; TLS	0
		08/19/2021	UAV	2.5
		09/13/2021	UAV; TLS	3.5
	Wet season year 2 (Wet2)	10/07/2021	UAV; TLS	0
		02/08/2022	UAV	4
		05/03/2022	UAV	7
		05/31/2022	UAV; TLS	8
MEL-14	Wet1	12/03/2020	UAV; TLS	0
		02/24/2021	UAV	2.5
		04/12/2021[*]	**UAV**[*]	**4.5**[*]
	Dry1	06/03/2021	UAV; TLS	0
		09/14/2021	UAV; TLS	3.5
	Wet2	03/09/2022	UAV; TLS	0
		03/16/2022	UAV	0.25
		03/24/2022	UAV	0.5
		04/11/2022	UAV	1
		04/28/2022	UAV	1.75
		06/01/2022	UAV; TLS	3

*This survey was rendered unusable due to unforeseen interim road work.

1 cm resolution in an arbitrary coordinate system. To process the UAV data and ensure accurate representation of the road surface, we manually selected high-precision GCP locations collected at each site. The data products of the UAV data post-processing included high-resolution orthoimages and UAV-derived DEMs with 1 cm resolution in an arbitrary coordinate system (Figure 4.4).

To analyze the development of wheel ruts over time, DEMs were reprojected on a common grid and subtracted from one another. The initial TLS-derived DEM for each season was only used as a reference dataset to coregister all UAV-derived DEMs. Following co-registration, the UAV-derived DEMs were subtracted from the baseline UAV survey of each season (Figure 4.5). Initial difference maps showed systematic error in the form of a longitudinal undulation pattern (Figure 4.5a). The longitudinal undulation artifacts seen in our datasets are presumably introduced during the initial alignment and camera model optimization step of data processing and create errors that can propagate to subsequent analysis steps (*Tarekegn and Sayama*, 2013). These artifacts likely arose from our UAV survey geometry (i.e., very low altitude flights due to canopy; e.g., *Mueller et al.*, 2023). Here we used a high-pass Gaussian filter, which is a common signal-processing technique used to remove undulation artifacts through attenuating low-frequency waveforms such that only the high-frequency waveforms (i.e., the elevation change signals) remain (Figure 4.5b).
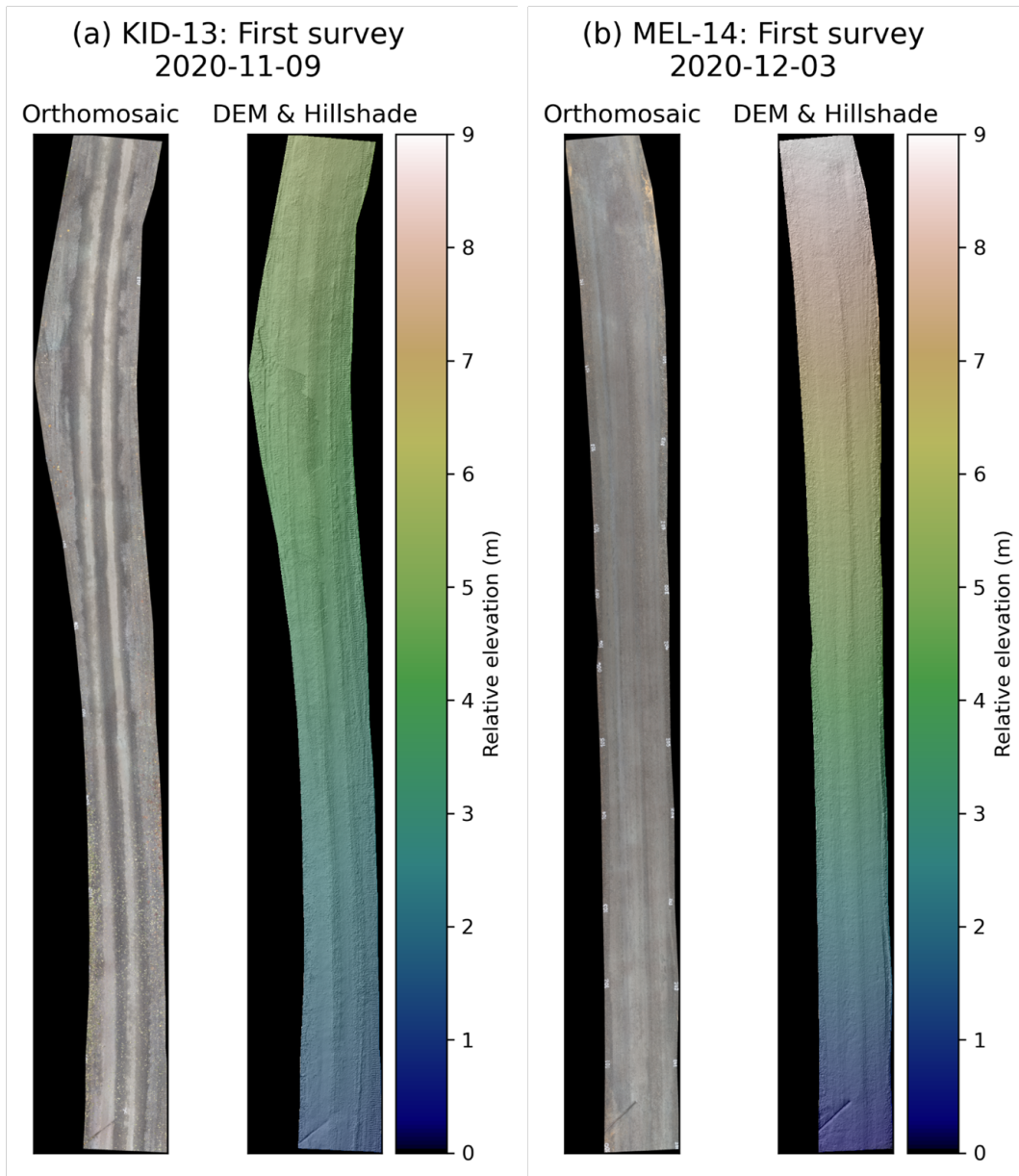
Figure 4.4: Example orthoimage (left) and color-shaded relief map (right) for the first UAV SfM survey at the (a) KID-13 and (b) MEL-14 sites.
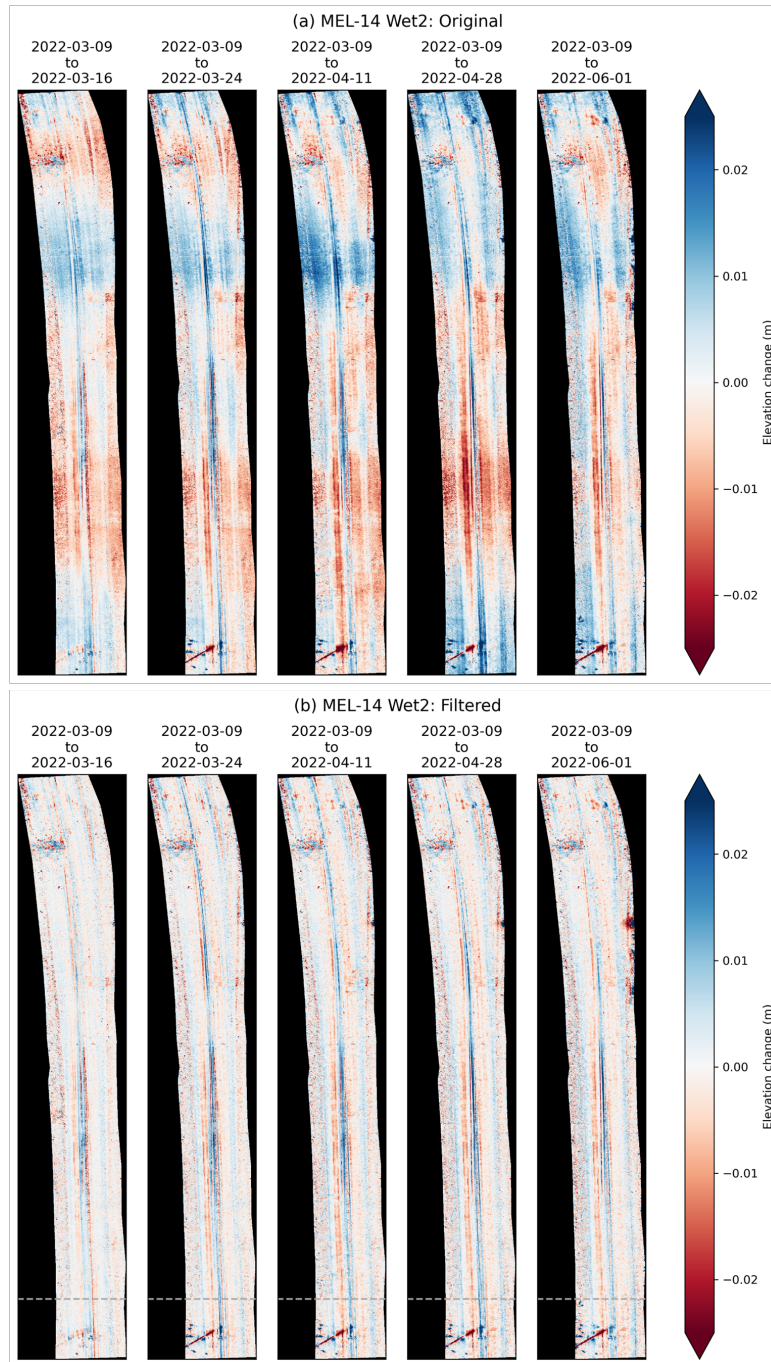
Figure 4.5: Example elevation change maps for the time series of the (a) original and (b) filtered surveys at MEL-14 during the second wet season (Wet2). The gray dashed lines in (b) denote the location of the cross section in Figure 4.6.

4.2.4 UAV DEM elevation change analysis

One potential method to examine the depth of wheel ruts is to look at cross-sectional profiles of the road surface at different longitudinal locations, such as in *Fannin and Sigurdsson* (1996). While the cross-sectional profiles do show the development of ruts (e.g., Figure 4.6), this method is insufficient and problematic for analyzing our surveys for several reasons. The vertical scale of ruts developing on our survey segments is small and highly variable along the longitudinal axis of the road (i.e., different cross sections have different rut magnitudes and shapes). This variation precludes a succinct description of road surface behavior with respect to rut development using cross sections alone. Additionally, the artificial longitudinal undulation pattern seen in Figure 4.5a is present in the cross-sectional profiles: where we expect the profile of 03-09-2022 to be the highest elevation, we instead see 03-16-2022 and 04-28-2022 plotting above 03-09-2022 (Figure 4.6). And lastly, cross-sectional analysis does not take advantage of the entire high-resolution data.

To examine how the entire road surface evolves over time, we used the filtered differenced DEMs to determine the empirical cumulative distribution functions (eCDFs) of elevation change across the full domain (Figure 4.7). For shorter survey time periods, the eCDF has a smaller variance, indicating minimal change to the road surface. Longer survey time periods, however, have a larger variance, indicating that the micro-topography of the road surface has become more heterogeneous (i.e., rutting has occurred).

Though we removed the longitudinal undulation pattern artifact with our high-pass Gaussian filter, other artifacts and random errors (i.e., noise) are still present in the differenced
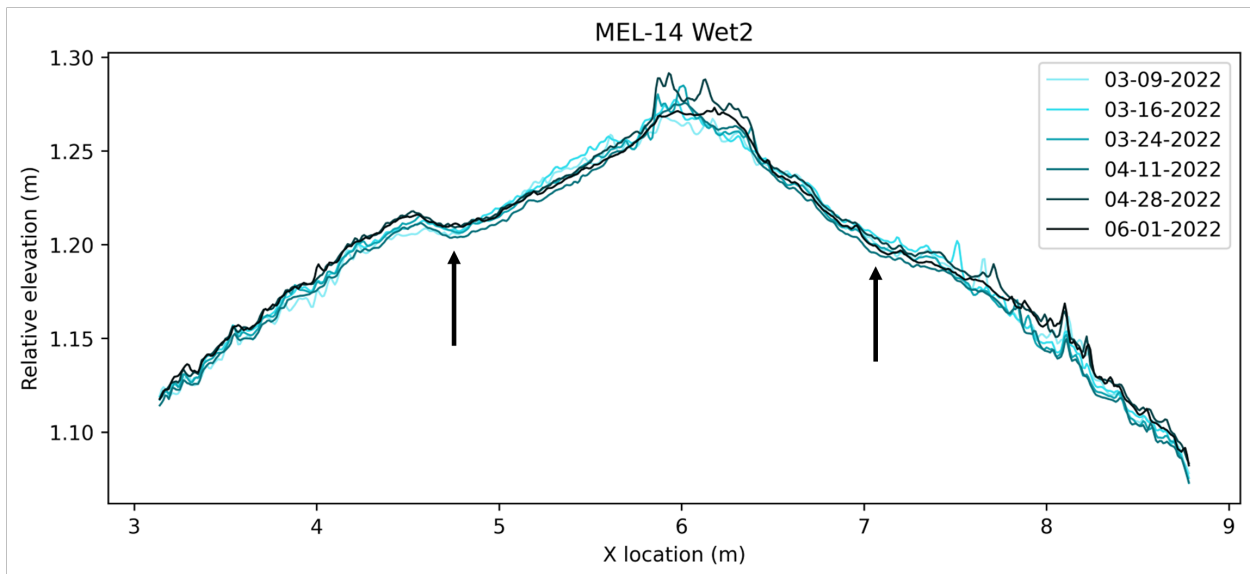
Figure 4.6: Cross-sectional profiles (location denoted by gray dashed line in Figure 4.5b) of unoccupied aerial vehicle (UAV)-derived digital elevation model (DEM) time series' at MEL-14 during the second wet season (Wet2). The development of ruts is denoted by the black arrows on either side of the road crown.

UAV-derived DEMs. To avoid these artifacts and errors—which exist on the extreme ends of our eCDFs of elevation change—we used the 5th percentile of the eCDF of elevation change as a measure for rut incision of a given time period. We chose the 5th percentile to represent rut incision as ruts tend to constitute the largest incisions in elevation change data and their depths are more uniform than rills caused by overland flow. As such, the cumulative rut incision depth over a given season is assumed to be the 5th percentile of elevation change for the final survey of the season.
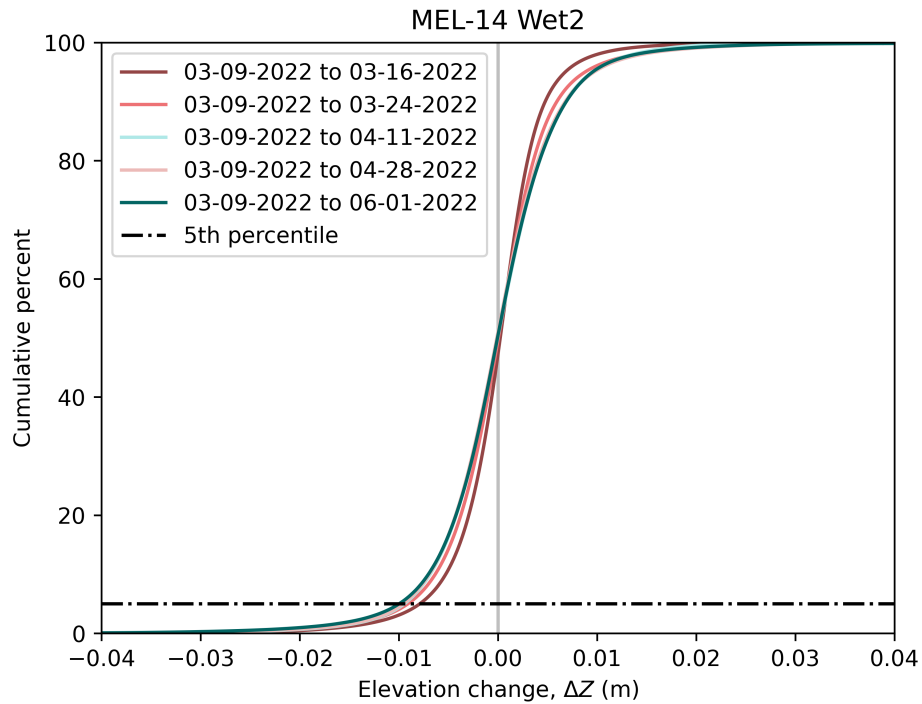
Figure 4.7: Empirical cumulative distribution function (eCDF) of elevation change at MEL-14 during the second wet season (Wet2). As the length of time between surveys increases, the variance of the elevation change also increases, indicating more heterogeneity in the micro-topography of the road surface. The 5th percentile of elevation change (denoted by the black dash-dotted line) is used as a measure of cumulative rut incision for a given survey time period.

4.2.5 Drainage system analysis

To examine the impacts of rutting on road surface flow pathways, we routed flow on the UAV-derived DEMs using Landlab, a Python toolkit for modeling earth surface processes (*Barnhart et al.*, 2020; *Hobley et al.*, 2017). In this drainage system analysis, we were less concerned with the longitudinal undulation pattern artifacts due to their relatively small impact on the slope of the road surface. As such, we resampled the raw UAV-derived DEMs from 0.01 m to 0.25 m resolution to attenuate excess noise, to smooth other potential artifacts, and to aid in maintaining reasonable processing times. Using a D8 flow routing algorithm, we routed runoff to the nodes of the survey grids. Each model run resulted in maps of the drainage system on the road surface (Figure 4.8).

As discussed in Chapter 4.2.1, a water bar is located near the bottom of each site's road segment. Without the presence of these water bars, water heading down road in a rut would continue down road and is thus considered part of our lowest boundary drainage for the following analyses. Note that these water bars were not always empty during a given UAV survey and therefore did not always have water draining through them.

We used the derived drainage areas for each survey to analyze the geomorphic outcome of rut incision (i.e., how wheel ruts evolve the drainage pattern of the road surface). To do so, we determined the average longitudinal location at which water leaves the road surface, weighted by drainage area at the edge of each longitudinal location. Because drainage area is proportional to discharge, we can use drainage area as a surrogate for discharge, and as such, the average longitudinal location at which water leaves the road surface can be thought
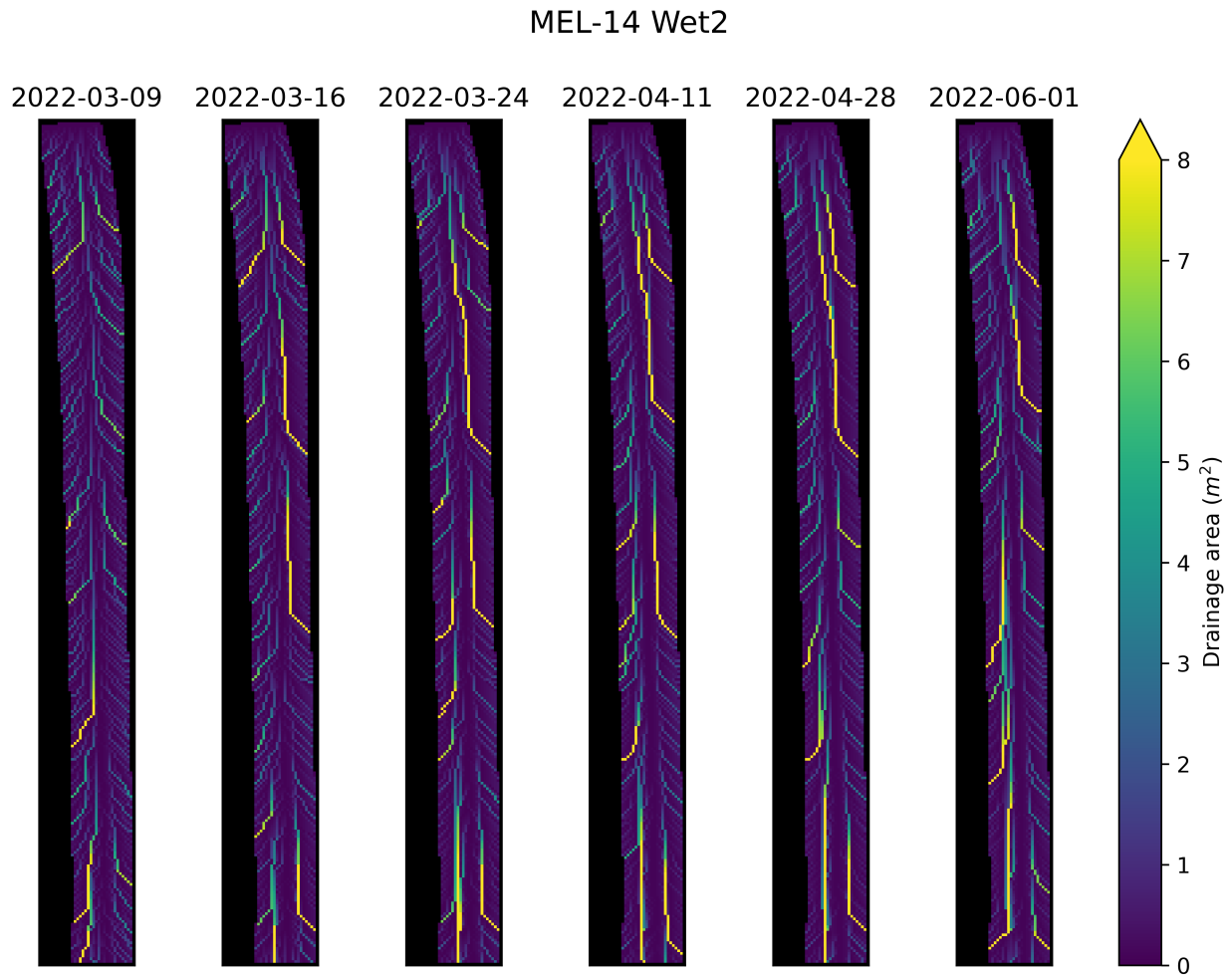
Figure 4.8: Time series maps of road surface drainage area at MEL-14 during the second wet season (Wet2). As time progresses, the drainage pathways increase in length and move farther down-road before veering off to the sides, which demonstrates the impacts of ruts on the road surface.

of as the center of mass of the drainage areas at the edges of the road surface. This center of

mass of drainage areas at the edges of the road surface allows us to quantify the down-road

shift due to rutting (see Chapter 4.1).

On a perfectly smooth (i.e., un-rutted), crowned road with no longitudinal slope, we

expect the center of mass of the drainage areas to be in the longitudinal middle of the road.

In this case, water would drain directly from the centerline to the sides as sheet flow. On an

un-rutted, crowned road with longitudinal slope, though, the center of mass of the drainage

areas will be shifted slightly down-road. The flow paths for this case would look more like

Figure 4.1a. Because the roads we used in this study have both longitudinal slope and crown

slope, we defined our "idealized" center of mass (i.e., the baseline to which we can compare

the actual center of mass) using the latter geometry. We use the width of the road at each

longitudinal location as a weight value for the center of mass calculation:

$$CM_{ideal} = \frac{\sum (w_y * y)}{a_{total}} - \frac{w_{avg}}{4} \frac{S_L}{S_x} \tag{4.1}$$

where CM_{ideal} is the idealized center of mass; w_y is the road width at a longitudinal location

along the road segment, y; a_{total} is the total road segment area; w_{avg} is the average road

width; S_L is the longitudinal slope of the road; and S_x is the average slope of the crown of

the road (approx. 6% at both KID-13 and MEL-14). The first term in Eq. 4.1 is used to

calculate the center of mass assuming no longitudinal slope. The second term in Eq. 4.1 is

used to shift CM_{ideal} down-road to account for the effect of slope. That shift can be derived

using basic trigonometry by taking the longitudinal slope and the crown slope as vectors to determine the downward shift angle and is a function of the average width of the road.

However, as roads rut, and with the natural roughness and longitudinal slope of the road, the drainage patterns tend to move downslope before curving toward the ditch, as can be seen in Figure 4.8. This leads to an even larger down-road shift of the center of mass of drainage areas than that of an idealized surface. As stated above, we use the sum of the drainage areas at the edge of each longitudinal location as a weight value for this center of mass calculation:

$$CM_a = \frac{\sum (a_y * y)}{a_{total}} \tag{4.2}$$

where CM_a is the center of mass of the drainage areas along the edges, a_y is the drainage area at a longitudinal location along the road segment y, and a_{total} is the total road segment area (i.e., the total drainage area).

To convert the center of mass values from an arbitrary coordinate system, we normalized both CM_a and CM_{ideal} by road location. These normalized values are dimensionless and on a scale of 0 to 1. We then compared CM_a to CM_{ideal} to give an approximation of the effect of ruts on the road flow pathways (i.e., downwards shift due to rutting; Figure 4.1b).

Additionally, we determined the fraction of the total drainage area leaving the road

through the bottom edge (i.e., leaving in ruts):

$$R_a = \frac{\sum (a_{bot}) + a_{wb}}{a_{total}} \tag{4.3}$$

where R_a is the fraction metric, a_{bot} is the drainage area along the bottom edge of the road

segment, a_{wb} is the drainage area at the water bar, and a_{total} is the total road segment area.

4.2.6 Erosion potential analysis

As an additional examination of the impacts of ruts on forest roads, we carried out a brief

analysis of the relative erosion potential of the flow pathways as ruts evolve. To do so,

we used an index of erosion potential based on excess shear stress. In excess shear stress

formulations of sediment transport and erosion, the excess shear stress is proportional to

both erosion and sediment transport potential:

$$\varepsilon_p \propto (\tau - \tau_c)^n \tag{4.4}$$

where ε_p is erosion potential, τ is the shear stress, τ_c is the critical shear stress (i.e., the

threshold at which sediment will start moving), and n is a constant. The value of n generally

ranges between 1.5 and 2.5 in the literature (e.g., *Govers*, 1992; *Meyer-Peter and Müller*,

1948). For our analysis, we defined the index of potential erosion as in Eq. 4.4, where n

is taken to be 2.0, and τ_c is taken to be 0.566 Pa based on an assumed d_{50} of 1 mm. The

formulation of shear stress we used (*Istanbulluoglu et al.*, 2002) brings in discharge, which,

as discussed in Chapter 4.2.5, is proportional to drainage area:

$$\tau = \beta q_o^m S^n \tag{4.5}$$

$$\Rightarrow \beta = \rho_w g n_b^{0.6}$$

where q_o is overland flow per unit width, S is slope, $m = 0.6$, $n = 0.7$, ρ_w is the density of water, g is the acceleration due to gravity, and n_b is Manning's roughness of the surface, which we take to be 0.05, based on results from *Alvis et al.* (2024).

Once we calculated the shear stress, we summed the indices of erosion potential for each survey in a time period and divided the summed index of a given survey $(t = t_n)$ by the summed index for the initial survey $(t = t_0)$ to obtain a normalized index of erosion potential, ε_i:

$$\varepsilon_i = \frac{\sum (\tau - \tau_c)_{t=t_n}^2}{\sum (\tau - \tau_c)_{t=t_0}^2} \tag{4.6}$$

This normalized index allows us to see the effect of ruts on the erosion potential of the road surface over time. A normalized index greater than 1 indicates an increase in erosion potential as compared to the initial time period, and a normalized index less than 1 indicates a decrease.

4.3   Results

4.3.1   Extent and rate of rutting

To address our first question of to what depth and how quickly ruts form on these mainline logging roads, we looked at elevation change data from three seasons at both KID-13 and MEL-14. Using the 5th percentile from our eCDFs of elevation change, we quantify the cumulative rut incision (Table 4.2) and rate (Figure 4.9) of rutting.

As seen in Table 4.2, the cumulative incision of ruts are variable across seasons and sites, falling between 0.7 cm and 2.0 cm. At KID-13, we see the largest cumulative incision of rutting of 1.97 cm during Wet1. With subsequent seasons, the cumulative incision of rutting decreases (i.e., a "shallowing" of rutting). At MEL-14, the largest cumulative incision of rutting occurs during Dry1 with a depth of 1.35 cm. Unlike at KID-13, however, MEL-14 shows no discernible pattern between subsequent seasons. The lack of a similar pattern is likely due to the fact that only two surveys were usable for Wet1. Interim road grading was carried out without our knowledge between 02/24/2021 and 04/12/2021, which led to 04/12/2021 being an unusable survey for our analyses.

To examine the rate at which rutting occurs, we plotted the 5th percentile of elevation change in centimeters (i.e., the cumulative rut incision) with respect to time since grading in months. At KID-13, we see that cumulative rut incision development has a nonlinear relationship with time since grading during all three seasons, with Wet2 showing the rut depth approximately approaching an asymptote of the deepest cumulative rut incision for

Table 4.2: Maximum rut incision in centimeters for all three seasons at both field study sites.

Site	Season	Maximum rut incision (cm)
KID-13	Wet1	1.97
	Dry1	1.30
	Wet2	0.75
MEL-14	Wet1	0.99
	Dry1	1.35
	Wet2	0.99

that season.

Note that the time since grading generally differs between field sites. The time between surveys at KID-13 was overall longer than that of MEL-14, which was intentional, specifically for Wet2 at MEL-14. We noticed that rut development tended to occur quickly, and we wanted to capture a finer temporal resolution at one of our field sites.
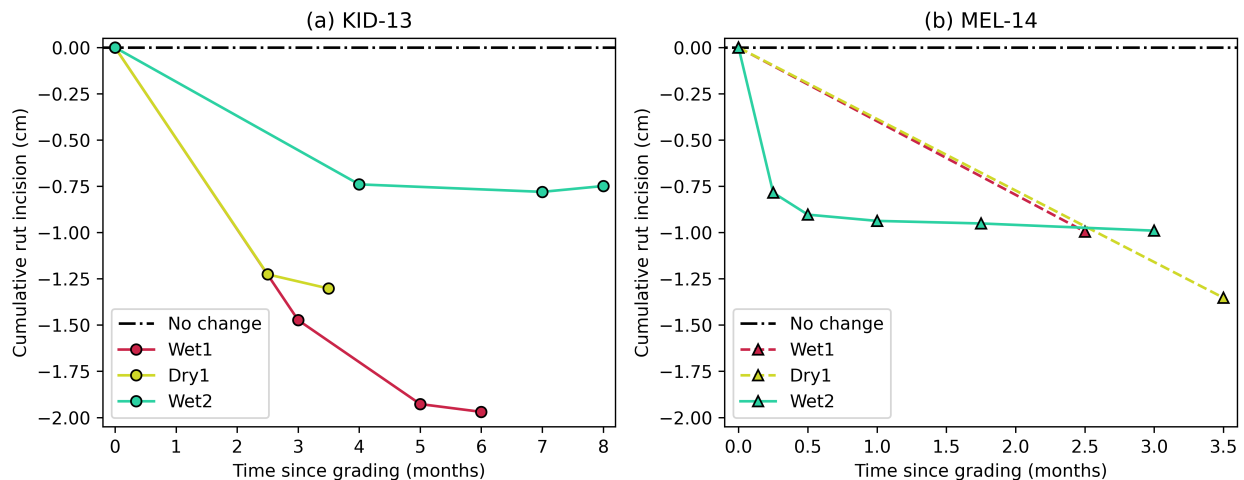
Figure 4.9: Relationship between cumulative rut incision depth in centimeters with respect to time since grading in months for (a) KID-13 and (b) MEL-14. Both KID-13 and MEL-14 demonstrate a nonlinear relationship between the variables.

4.3.2 Metrics of the drainage system

The cumulative incision depth and rate of rutting are important, but we are also interested in the implications: if ruts are present, what happens to the flow pathways on the road surface and how does that impact the drainage of the system? The capacity to measure this is a key advantage of aerial surveys over cross sections alone. To answer this question, we examined the results of our drainage area center of mass analysis discussed in Chapter 4.2.5. Specifically, we looked at where the center of mass of an idealized surface is located as compared to our rutted road surfaces, and we looked at the fraction of the road surface area that is draining through the lowest boundary of the road segment.

For our idealized road surfaces at KID-13 and MEL-14, the normalized values of CM_{ideal} are located at 0.501 and 0.482, respectively. For all seasons at both KID-13 and MEL-14, the normalized values of CM_a fall below the normalized values of CM_{ideal} (Figure 4.10), indicating a down-road shift due to rutting. The magnitude of the downward shift at KID-13 is less than that of MEL-14.

While our center of mass analysis utilized the drainage areas along all edges of the road surface, we were also interested in determining how much of the road surface contributed to only the lowest boundary. To show that we plotted the fraction of the total drainage area leaving the road through the bottom edge and included any drainage area exiting the plot through the lower water bar (see Chapter 4.2.5 for explanation). In this, we found that as ruts developed, the fraction of road surface draining through the lowest boundary of the road segment increased, with maximum fractions at KID-13 and MEL-14 being around 0.20 and
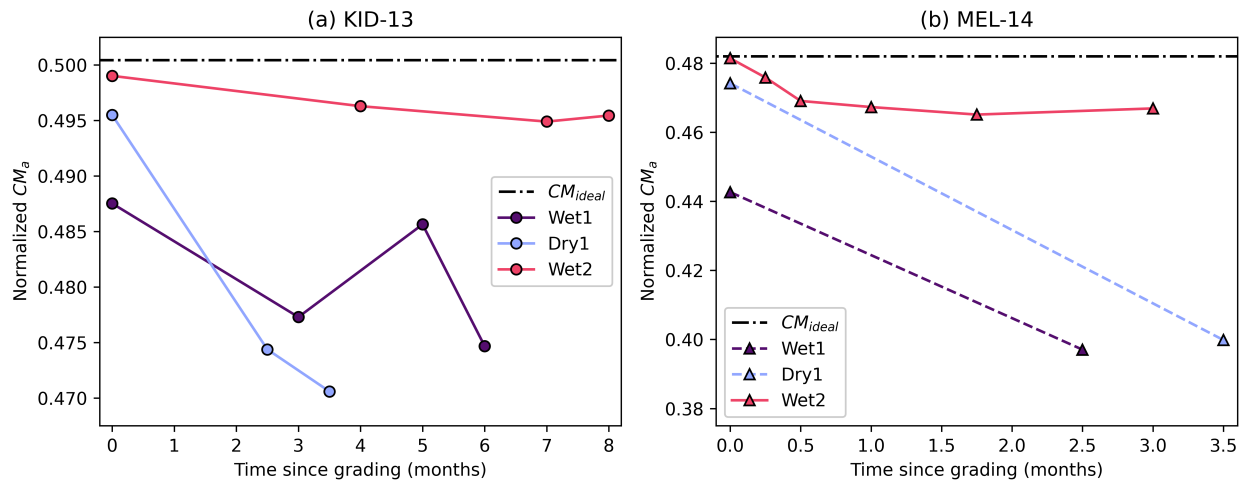
Figure 4.10: Relationship between the normalized drainage area center of mass and time since grading for (a) KID-13 and (b) MEL-14. Values falling below the ideal center of mass (CM_{ideal}) indicate a down-road shift due to rutting.

0.30, respectively (Figure 4.11). For less pronounced rut incisions (i.e., Wet2 at both sites), this fraction is the smallest.
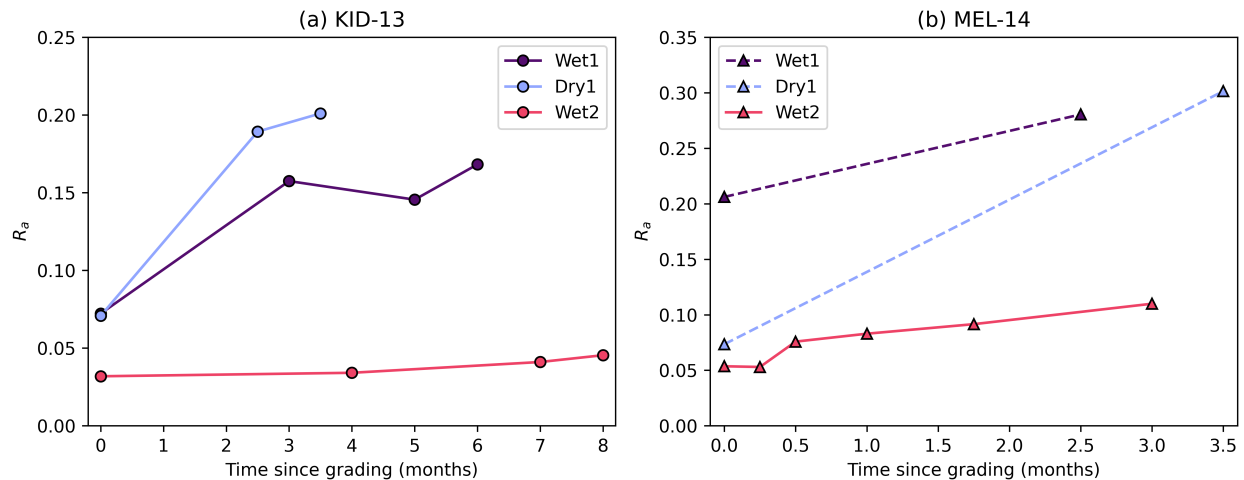
Figure 4.11: Relationship between fraction of total drainage exiting through the lowest boundary of the road segment and time since grading for (a) KID-13 and (b) MEL-14.

4.3.3 Erosion potential of the road surface

For the final piece of our analysis, we wanted to examine how rutting and drainage areas relate to erosion, since erosion is a key concern for forest roads. Our evaluation of the normalized index of potential erosion, ε_i, yielded somewhat similar patterns of results at each site (Figure 4.12). KID-13 (Figure 4.12a) presented interesting behavior where ε_i fell below 1 in both Wet1 and Wet2, which indicates a decrease in erosion potential as compared to the initial surface. During Wet2 at KID-13, that index of erosion potential remained below 1. For Wet1 and Dry1, however, KID-13 exhibited a net increase in erosion potential. MEL-14 (Figure 4.12b) demonstrated behavior more consistent with the expectation that rutting can cause an increase in erosion and overall exhibited higher relative erosion potentials for all seasons. At their maxima, KID-13 saw a 30% increase in erosion potential and MEL-14 saw a 120% increase in erosion potential.

4.4 Discussion

We found that the cumulative rut incision depth over the duration of a given survey season at both sites varied between 0.7 cm and 2.0 cm (Table 4.2). The magnitude of these depths is not as large as compared to other studies (e.g., *Fannin and Sigurdsson*, 1996; *Machuga et al.*, 2023; *Marra et al.*, 2018), but those studies were carried out on roads built in softer soils (sometimes with the intention of evaluating methods to control rutting in soft soils) or on non-mainline roads. On well-established mainline logging roads like these study sites, however, rut development appears to be less severe, probably because the subgrade of the
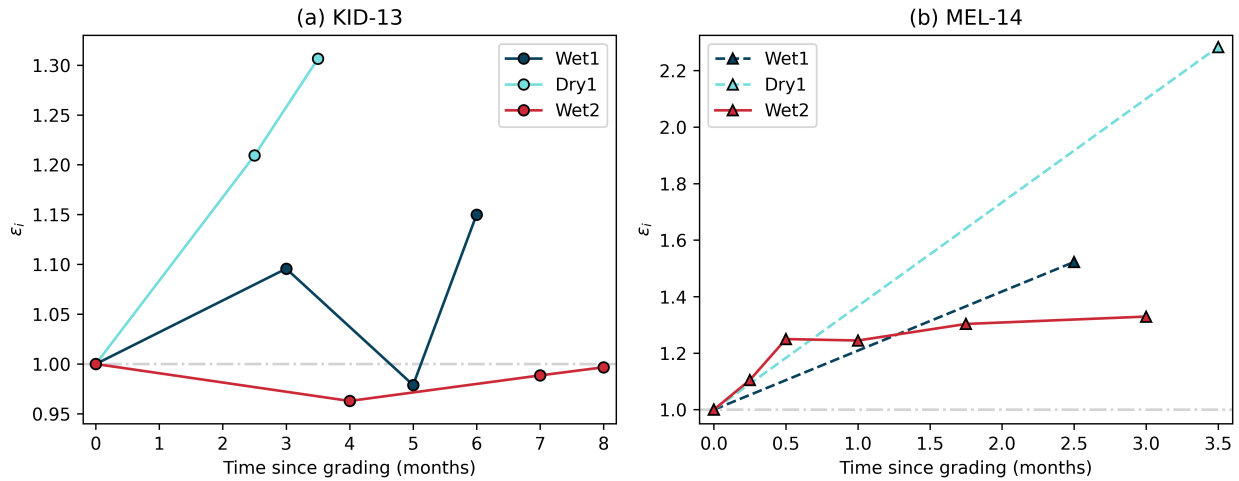
Figure 4.12: Relationship between the normalized index of erosion potential, ε_i, (Eq. 4.6) and time since grading at (a) KID-13 and (b) MEL-14. The dot-dashed gray line on both panels shows the threshold where the normalized index of erosion potential switches from a decrease to an increase as compared to the initial road surface.

road has been well-compacted by years of traffic.

At KID-13, all three seasons demonstrated a "slower" nonlinear relationship between cumulative rut incision and time since grading than that of Wet2 at MEL-14 (Figure 4.9). The rate of rutting is likely slower at KID-13 than MEL-14 due to the difference of longitudinal slopes at each site—MEL-14 is steeper than KID-13—and differences in traffic level at each of the sites—MEL-14 had, on average, more traffic than KID-13. The exponential decrease and subsequent asymptotic approach of the cumulative rut incision depth seen in a season is due to a feedback loop created by erosion processes and traffic. While traffic and rainfall/channelized flow both contribute to development and persistence of ruts, the expected continuing incision is negated by traffic serving as a stochastic variable that "smooths" the ruts and the large amount of compaction occurring (*Alvis et al.*, 2023). Additionally, at

KID-13 (and, to an extent, MEL-14), we see a "shallowing" of rut incisions with subsequent survey seasons (Table 4.2; Figure 4.9), which is likely due to the fact that, while the road was graded between seasons, no additional rock was added. The road hardened over time due to additional compaction from traffic.

While the rut depth magnitudes are relatively small, their impact is still noticeable. Both our center of mass analysis and our lowest boundary contribution analysis demonstrate the effects of ruts on road surface flow pathways. In an idealized situation, no ruts would exist, and flow would be directed off of the road surface to either side as sheet flow (e.g., Figure 4.1a, Figure 4.2a). With the development of ruts, the flow is directed down-road before being directed off to the sides or is not directed off to the sides and instead continues out of the lowest boundary of the road segment (e.g., Figure 4.1b, Figure 4.2b, Figure 4.2c). Essentially, the net vector of flow direction shifts down slope. All surveys for both KID-13 and MEL-14 demonstrate this downward shift, even the initial surveys for each season (Figure 4.10, Figure 4.11). The initial surveys were all carried out as soon as possible after grading the road surface. On average, the surveys occurred the day of or day after grading. The first survey at KID-13, however, was an exception, with the survey occurring one week after grading due to weather. Regardless, in most instances, rut development was in its beginning stages due to the grader tires coming behind the blade as well as other traffic running over the road surface and resulted in a down-road shift in the center of mass.

The center of mass metric not only tells us the shift of the average location at which water leaves the road surface, it also gives us an approximation of ditch line erosion control

treatment effectiveness. Flow that is directed down the road instead of into the roadside ditch does not utilize erosion control treatments present therein. Erosion control treatments in roadside ditch lines have been shown to be largely effective (e.g., *Aust et al.*, 2015; *Burroughs et al.*, 1984; *Luce and Black*, 1999; *Megahan et al.*, 2001). However, if flow is not traveling in the ditch, erosion control treatments are unable to aid in sediment transport reduction. With the down-road shift of flow pathways due to rutting, erosion control treatments in the ditch have less effectiveness potential as less of the ditch is utilized, as demonstrated in our results in Chapter 4.3.2 (Figure 4.10, Figure 4.11).

Additionally, flow that is channelized on the road surface due to rutting has a larger capacity for erosion than that of diffuse sheet flow (*Elliot et al.*, 1999; *Foltz and Burroughs*, 1990). We see evidence of a net increase in erosion potential as rut incision increases in our results (Figure 4.12). MEL-14 had a largely consistent increase in erosion potential over all three seasons. KID-13, however, demonstrated a slightly different story: for Wet1 and Wet 2, the erosion potential decreased as compared to the first survey of the seasons during at least one subsequent survey. A couple possible reasons for this exist: 1) the indices of erosion potential we calculated are a function of the entire road surface and not the ruts alone, so the road surface aside from the ruts played an important role and 2) KID-13 demonstrated very clear evidence of sediment displacement, so even though the rut incision depth increased, the rest of road surface could have smoothed out. Another important piece to note is that the model of shear stress used for our calculations assumes overland flow. This assumption does not necessarily hold for the ruts and rills on the road surface. If we included a more

sophisticated rill hydraulics model, we would likely have predicted more erosion potential both overall and, more specifically, at KID-13.

All told, the results of our analyses emphasize the importance of road maintenance on a regular basis. Ruts are quick to develop, especially if a new layer of aggregate is added to the road surface, but frequent grading can minimize the impacts of these ruts with respect to flow pathway alteration. However, as discussed in *Luce and Black* (2001b), road maintenance can also produce higher sediment yields shortly thereafter. As such, further work should be conducted to determine the relative increase in sediment yields due to rutting as compared to the increase in sediment yields due to road maintenance.

4.5   Conclusion

Overall, our two field sites yielded important information regarding rut formation on a sampling of mainline logging roads, especially with respect to flow pathways on the road surface. Our results demonstrate the advantage of using UAV-derived DEMs for analysis over cross-sections alone. Using UAV SfM surveys, with validation from TLS, we examined the evolution of ruts on two segments of mainline logging roads in western Washington. We found that:

1. the cumulative rut incision for a given season and field site varied between 0.7 cm and 2.0 cm;

2. the relationship between rut incision and time since grading is nonlinear at both sites for all seasons with sufficient data, with MEL-14 having a generally quicker rate of rutting than that of KID-13;

3. as ruts develop, the overall flow pathways shift down-road, which has implications on how much of the erosion control treatments in the roadside ditch lines are utilized; and

4. the erosion potential of our road surfaces tended to increase overall as ruts developed, with KID-13 seeing a maximum increase of 30% and MEL-14 seeing a maximum increase of 120%.

Chapter 5

CONCEPTUALIZATION OF A PROCESS-BASED FOREST ROAD EROSION MODEL

5.1 Current state of forest road erosion modeling

As discussed in Chapter 2, four main traffic-induced, erosion-enhancing processes have been anecdotally and experimentally described but not elaborately modeled in the literature. These four processes include: pumping, crushing, scattering, and rutting. Pumping is posited to occur when larger sediment that is layered over finer sediment gets pushed down by traffic, forcing the finer sediment to be "pumped" upwards. Crushing is caused by traffic breaking down larger sediment into finer sediment. Scattering is the lateral displacement of larger sediments armoring the road surface due to traffic, exposing the finer sediment below. Rutting is the deformation of the road surface caused by similar traffic patterns eroding and compacting wheel paths, which increases the capacity of water within those ruts to move sediment.

While a number of existing forest road erosion models are present in the literature (*Fu et al.*, 2010), most models lack a solid quantitative way to consider and incorporate traffic and its related erosion-enhancing processes. Of the models that do incorporate traffic, con-

sideration to traffic is given in either a strictly empirical manner or a semi-empirical manner, rather than explicitly representing traffic and its erosion-enhancing processes.

The strictly empirical incorporation of traffic in forest road erosion models involves using sediment and traffic data to determine a traffic factor. Traffic factors are used as a parameter to adjust the overall erosion over time based on road use. For example, the Washington Road Surface Erosion Model (WARSEM) is an empirically-based tool used to calculate average annual road surface erosion for forest roads in Washington state (*Dubé et al.*, 2004). WARSEM uses a traffic factor to adjust the total erosion based on level of traffic, which ranges from Abandoned (Inactive; 0.1) to Heavy ($\geq$5 passes/day; 120). These traffic factor values are based on data collected in *Reid* (1981), *Reid and Dunne* (1984), *Sullivan and Duncan* (1981), and *Foltz* (1996), which were studies carried out in Washington state. Accordingly, while WARSEM is a useful tool for estimating long term averages of total road erosion in Washington state, applications to other locations is difficult, and the model lacks a comprehensive treatment of traffic.

In semi-empirical models of forest road erosion, traffic and its related processes are typically incorporated through adjustment of the "erodibility" of a road surface. Erodibility is a measure of the road surface's resistance to erosion and is related to traffic through parameter fitting, which requires a fair amount of empirical data. A number of models that incorporate traffic in this way and are presented as physically- or process-based may perhaps be better described as semi-empirical in nature due to their reliance on an empirically-dependent variable such as erodibility. Two examples of such models are the Watershed Erosion Prediction

Project: Road (WEPP:Road; *Elliot*, 2004) and the Kinematic Runoff and Erosion Model (KINEROS2; *Ziegler et al.*, 2002). WEPP:Road uses a traffic level (High, Low, No) and the presence of ruts (or lack thereof) on the road surface to adjust the road surface erodibility, which is divided into rill and interrill erodibility values. The rill erodibility value is used for ruts on the road surface. For Low or No traffic, the rill erodibility value is reduced by 75% as compared to the typical rill erodibility value used for High traffic. Additionally, No traffic assumes that the road surface has 50% vegetation cover, which changes the erodibility of both rill and interrill areas. KINEROS2 uses the concept of interstorm surface preparation (i.e., surface change caused by road disturbances, such as traffic; *Ziegler et al.*, 2001b) to consider traffic's role in erosion. The interstorm surface preparation is incorporated into a storm-based dynamic erodibility formulation to account for the sediment readily available for transport. While these models do consider traffic in a more process-based way than strictly empirical models, room is left for future models to incorporate traffic and its related processes explicitly.

As such, we aim to develop a process-based model that incorporates traffic in a physically-based way. This sort of model can advance our scientific understanding of traffic's effects on forest road erosion and the sensitivities of underlying processes. While some amount of parameter fitting cannot be avoided, the physical basis of the discretized processes we model allows for a more explicit incorporation of traffic. In this chapter, we focus on the initial conceptualization and development of a model that estimates sediment generated from the forest road prism with special consideration to underlying physical processes induced by traf-

fic. The final model will integrate the four main traffic-induced, erosion-enhancing processes occurring within and on the road prism (*Foltz and Truebe*, 1995; *Rhee et al.*, 2018), as well as the transport of sediment on the surface and away from the road on a gridded representation of road topography. The initial model has been developed as a spatially-lumped model and includes mathematical formulations for the traffic-induced, erosion-enhancing processes of crushing and pumping, as well as shallow overland flow sediment transport.

5.2 Conceptual model for coupling sediment production and transport on a road surface

Below, we present our initial conceptual model for coupling sediment production and transport on a road surface using a spatially-lumped model domain. While most of this chapter focuses on the spatially-lumped model, we also discuss the incorporation of the remaining two traffic-induced, erosion-enhancing processes (i.e., scattering and rutting) into a spatially-distributed representation of the model.

5.2.1 Spatially-lumped model domain

We have hypothesized and developed a preliminary, spatially-lumped forest road sediment balance model that demonstrates the vertical sediment exchange among conceptual layers and the supply for lateral sediment transport on a representative road surface. The current spatially-lumped model incorporates the traffic-induced, erosion-enhancing processes of pumping and crushing. The domain of the topic spatially-lumped model is a 1-meter by 4.5-meter section within a larger road segment (Figure 5.1). Every meter-long section is

assumed to have the same characteristics such that sediment production in one section can

be extrapolated to every other section and summed to obtain the total sediment yield.
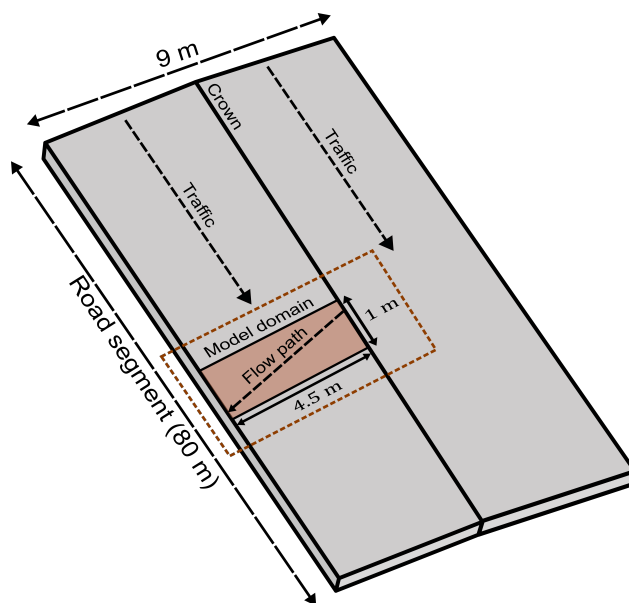
Figure 5.1: Schematic of spatially-lumped modeling domain within an 80 m by 9 m experimental road segment.

5.2.2 Tri-layer conceptualization

Because pumping and crushing occur vertically within road prism, we use a vertical tri-layered conceptualization (Figure 5.2) to model these processes. Scattering and rutting, however, occur laterally, and will be integrated to a future iteration of the model using a laterally distributed conceptualization. In addition to these erosion-enhancing processes, we incorporate water-driven sediment transport to model the erosion process itself.

The spatially-lumped tri-layered model conceptualization includes three layers for storage and five sediment fluxes. The three storage layers in this conceptualization are, from top to
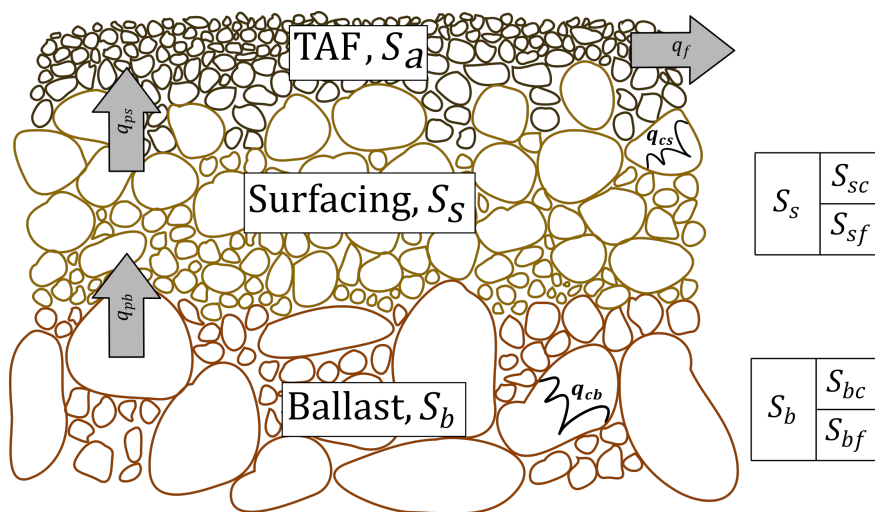
Figure 5.2: Tri-layered conceptualization used to model processes occurring vertically within the road prism.

bottom: the theoretical transport available fines (TAF) layer, S_a; the road surfacing layer, S_s; and the ballast layer, S_b (Figure 5.2). The five sediment fluxes include the pumping of fine sediment upwards between each of the layers of the road prism, crushing of larger sediments to form fine sediment in each of the layers, and the lateral transport of fine sediment from the transport available fines layer. This conceptualization is used to ensure conservation of mass.

For the lower storage layers, S_s and S_b are further divided into fine and coarse fractions of material such that:

$$S_s = S_{sf} + S_{sc} \tag{5.1}$$

$$S_b = S_{bf} + S_{bc} \tag{5.2}$$

where the f subscript denotes the fine fraction of material, and the c subscript denotes the coarse fraction of material. These sediment size fractions are grouped into buckets of "small enough for overland flow transport" (i.e., sand size or smaller) and "too big for overland flow transport" (i.e., larger than sand size) to simplify parameters. Additionally, each layer has a mass balance equation (Eq. 5.3-Eq. 5.7) to calculate its net storage flux.

The theoretical TAF storage layer is the uppermost road layer that contains only fine material (sand size or smaller) available for water-driven transport. This layer can be likened to an active layer of a riverbed (*Hirano*, 1971). The TAF layer connects the vertical conceptualization to the laterally-distributed conceptualization and is the layer in which sediment transport occurs. The two main fluxes acting on this layer are the TAF lateral transport flux, $q_{f_{out}}$, and the vertical surfacing pumping flux, q_{ps}. $q_{f_{out}}$ describes the fine sediment leaving the road prism and is governed by a common sediment transport equation. q_{ps} is an inter-layer transportive flux that describes the pumping of fine sediment from the surfacing layer, S_{sf}, into the TAF layer, S_a. The net storage flux of the TAF layer is defined as:

$$\frac{\Delta S_a}{\Delta t} = q_{ps} - q_{f_{out}} \tag{5.3}$$

where Δt is the time step.

The surfacing storage layer is the middle layer of the cross-section and is typically a mixture of approximately 80% gravel and 20% finer material that is between six and twelve inches deep. Within out conceptualization, this layer couples to both the TAF and the ballast

and is the most active layer in terms of the number of fluxes acting on and within it. The three fluxes acting on this layer are the surfacing pumping flux, q_{ps}; the surfacing crushing flux, q_{cs}; and the ballast pumping flux, q_{pb}. As described above, q_{ps} is an inter-layer transportive flux that describes the pumping of fine sediment from the surfacing layer, S_{sf}, into the TAF layer, S_a. q_{cs} is an intra-layer generative flux that describes the crushing of coarse surfacing material, S_{sc}, into fine surfacing material, S_{sf}. q_{pb} is an inter-layer transportive flux that describes the pumping of fine sediment from the ballast layer, S_{bf}, into the fine sediment of the surfacing layer, S_{sf}. The net storage flux of each sediment size fraction in the surfacing layer is defined as:

$$\frac{\Delta S_{sf}}{\Delta t} = q_{pb} - q_{ps} + q_{cs} \tag{5.4}$$

$$\frac{\Delta S_{sc}}{\Delta t} = -q_{cs} \tag{5.5}$$

The ballast storage layer is the lowest layer of this conceptualization and is typically larger material with interstitial space occupied by a fine material matrix. The ballast transitions to native material farther down the stratigraphic column, but the native material is not considered in this analysis. This layer couples to the surfacing via one of two fluxes. The two fluxes acting on this layer are the ballast crushing flux, q_{cs}, and the ballast pumping flux, q_{pb}. q_{cb} is an intra-layer generative flux that describes the crushing of coarse ballast material, S_{bc}, into fine ballast material, S_{bf}. q_{pb} is an inter-layer transportive flux that describes the pumping of fine sediment from the ballast layer, S_{bf}, into the fine sediment of the surfacing

layer, S_{sf}. The net storage flux of each sediment size fraction in the ballast layer is defined as:

$$\frac{\Delta S_{bf}}{\Delta t} = -q_{pb} + q_{cb} \tag{5.6}$$

$$\frac{\Delta S_{bc}}{\Delta t} = -q_{cb} \tag{5.7}$$

5.2.3 Layer flux equations

To model each of the fluxes described above, we use both previously developed equations, as well as equations we have developed based on hypotheses. Crushing and pumping are modeled via equations developed based on hypotheses from the literature and field observations (e.g., *Foltz and Truebe*, 1995; *Reid and Dunne*, 1984; *Rhee et al.*, 2018; *Ziegler et al.*, 2001b). At the interface of each layer, the transportive pumping flux moves fine sediment upwards. We have hypothesized the general form of the pumping flux to be:

$$q_p = u_p \frac{S_{xf}}{S_x} \frac{n_{\Delta t}}{\Delta t} \tag{5.8}$$

where u_p is the potential rate at which fine sediment is pumped between layers and is currently assumed to be a constant value per truck pass, $n_{\Delta t}$ is the number of truck passes occurring in a time step, and Δt is the time step. S_{xf} and S_x represent the fine fraction storage and total storage of a layer, respectively.

Within the lower two layers, the generative crushing flux decreases the supply of coarse

material while increasing the supply of fine sediment. We have hypothesized the general

form of the crushing flux to be similar to that of the pumping flux:

$$q_c = k_c \frac{S_{xc}}{S_x} \frac{n_{\Delta t}}{\Delta t} \tag{5.9}$$

where k_c is the potential rate at which coarse sediment is crushed (and therefore fine sediment

is generated) and is currently assumed to be a constant value per truck pass, $n_{\Delta t}$ is the

number of truck passes occurring in a time step, and Δt is the time step. S_{xc} and S_x

represent the coarse fraction storage and total storage of a layer, respectively.

The lateral transport capacity is modeled by Govers' equation for shallow overland flow

(*Govers*, 1992):

$$q_f = \frac{10^{-4.348}}{\rho_s d_{50}^{0.811}} \frac{(\tau_g - \tau_c)^{2.457}}{L} \tag{5.10}$$

where q_f is the average sediment transport capacity of overland flow per unit area, ρ_s is the

density of sediment, d_{50} is the median grain size in the TAF layer, τ_c is the critical shear

stress, τ_g is the grain shear stress, and L is the representative length of road over which we

are performing this calculation.

This transport capacity formulation is modified such that it partitions shear stress based

on how "full" the TAF layer is (i.e., uses grain shear stress instead of total bed shear stress).

If the fine sediment of the TAF layer fills only some of the voids between larger sediment in

the surfacing, the shear stress available to transport the sediment will be less because the

larger sediment acts as an "obstruction". The idea of using partitioning to account for the emergence of larger sediment particles that act as bedforms is based on the work of *Einstein and Barbarossa* (1952). We use a shear stress partitioning ratio, f_g, to determine the portion of the total bed shear stress acting on the sediment grains, τ_g (e.g., *Tiscareno-Lopez et al.*, 1994):

$$\tau_g = \tau_t * f_g \tag{5.11}$$

where f_g is typically defined as $\left(\frac{n_g}{n_t}\right)^{3/2}$, with n_g being the Manning's roughness of the fine sediment grains and n_t being the total Manning's roughness (see Appendix A.1 for a full derivation of this formulation). However, in our system, the partitioning fraction, f_g, is also dependent on the depth of fine sediment in the TAF layer. As such, we posit that:

$$f_g = \begin{cases} \left(\frac{n_g}{n_t}\right)^{3/2} \left(\frac{S_a}{d_{95_s}}\right) & \text{if } S_a \leq d_{95_s} \\ \\ 1 & \text{if } S_a > d_{95_s} \end{cases} \tag{5.12}$$

where d_{95_s} is the d_{95} of the surfacing layer. If the TAF layer depth is less than or equal to d_{95_s}, f_g plays a significant role due to the emergence of larger sediment particles acting as bedforms. As soon as the depth of the TAF layer overtakes the d_{95} of the surfacing layer, the shear stress acting on the grains, τ_g becomes the total shear stress.

Similar to f_g, n_t is also dependent on the depth of fine sediment in the TAF layer, and

we determine the total roughness using:

$$
n_t = \begin{cases} n_c + \frac{S_a}{d_{95_s}}(n_g - n_c) & \text{if } S_a \leq d_{95_s} \\ \\ n_g & \text{if } S_a > d_{95_s} \end{cases}
\tag{5.13}
$$

where n_c and n_g are the Manning's roughness of the coarse sediment grains and of the fine sediment grains, respectively. Values for both n_c and n_g used in the model are based on data from *Emmett* (1970).

In determining the actual sediment transport flux, $q_{f_{out}}$, we consider two conditions of the system: transport-limited and supply-limited. For the transport-limited condition to be met, the amount of available sediment generated by traffic (i.e., existing TAF storage S_a plus the sediment pumped from the surfacing into the TAF, q_{ps}) is greater than or equal to the sediment transport capacity, q_f. For the supply-limited condition to be met, the amount of available sediment generated by traffic is less than the sediment transport capacity. As such, we define the actual amount of sediment transported as:

$$
q_{f_{out}} = min(q_{ps} + S_a, q_f)
\tag{5.14}
$$

5.2.4 Incorporation of scattering and rutting

The next version of our process-based model will incorporate the final two traffic-induced, erosion-enhancing processes: scattering and rutting. The incorporation of scattering (and,

implicitly, rutting) can be seen in Figure 5.3. This updated conceptualization includes the pumping of fine sediment upwards between layers of the road prism, crushing of larger sediments to form fine sediment in each of the layers, scattering of larger sediments in the active layer, and the lateral transport of fine sediment from the active layer out of the system. Scattering occurs laterally and is denoted as q_{sa} in the updated tri-layered conceptualization. Rutting, rather than being a process caused by a specific flux, is caused by a combination of vertical and lateral movement of sediment and the presence of ruts enhances erosion, as discussed in Chapter 4. Ultimately, scattering and rutting will be the main link to the more spatially-distributed processes of the model.
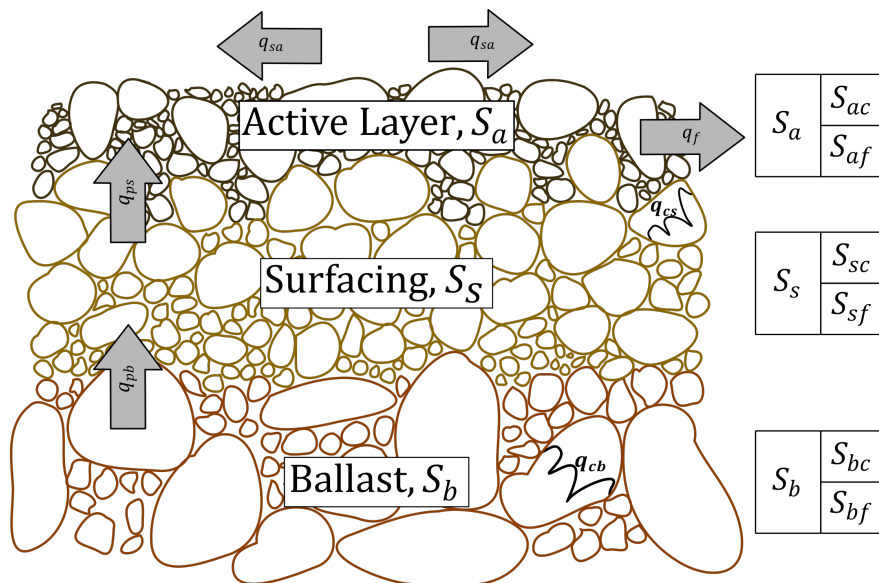
Figure 5.3: Updated tri-layered conceptualization used to model processes occurring within the road prism.

With the incorporation of scattering and rutting, we will fully convert the model to a spatially-distributed representation of the road surface, including the roadside ditch line.

The spatially-distributed model will be developed using Landlab—an Earth surface dynamics modeling framework (*Barnhart et al.*, 2020; *Hobley et al.*, 2017). Landlab is an open-source modular framework, offering different components to model earth surface processes that are easily combined to create a more complicated model. The road prism has numerous processes occurring therein, including, but not limited to: (1) the four traffic-induced, erosion-enhancing processes described in Chapter 2 and Chapter 5.1; (2) overland flow sediment transport; and (3) channelized flow in wheel ruts and the roadside ditch line. As such, Landlab is an ideal modeling framework for our spatially-distributed model.

In early conversations regarding the spatially-distributed model, we developed a sediment displacement component in Landlab. This component is a preliminary attempt at modeling scattering and rutting of the road surface using a stochastic traffic model in which the number of vehicle passes is a random number based on an exponential distribution with a mean of 5 vehicle passes per day. As a truck passes over the road, sediment is displaced to either side of and behind the tire, and when the road is not driven on, slight amounts of linear diffusion occur. As a proof-of-concept, we used a synthetic modeling domain (Figure 5.4a) of the road surface and roadside ditch line and ran the sediment displacement component for 10 model days. Wheel ruts develop on either side of the crown of the road surface (Figure 5.4b, Figure 5.5).

In addition to the processes described above, the spatially-distributed model will incorporate components modeling the effects of different erosion control treatments on road sediment yield. Once the the spatially-distributed model is finalized, we will apply the model to various
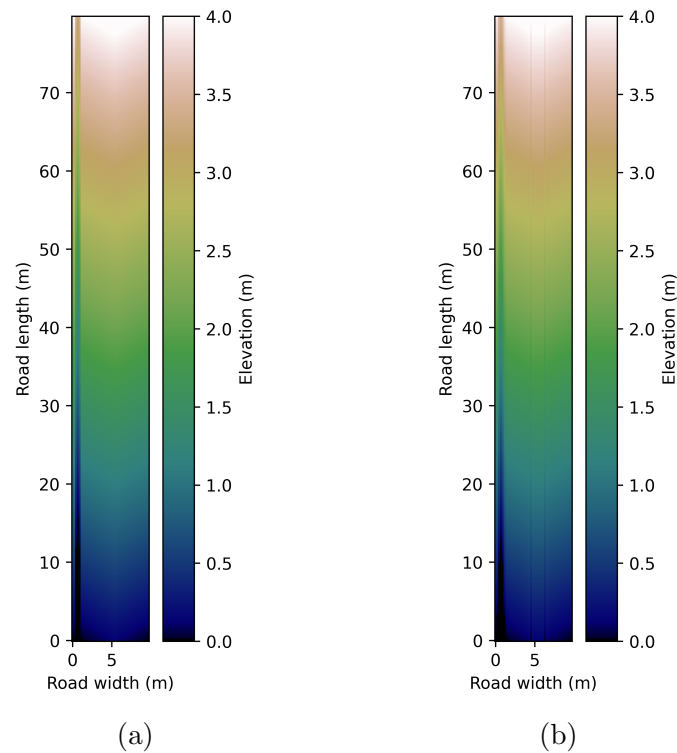
Figure 5.4: The current modeling domain as defined in Landlab showing (a) the initial road surface and (b) the road surface after running the in-progress sediment displacement component. Wheel ruts develop on either side of the road crown.
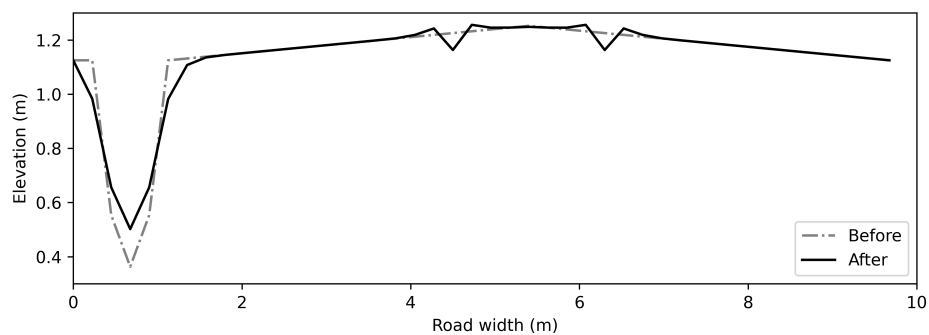
Figure 5.5: A cross-sectional profile of the road surface and ditch line before (gray dash-dotted line) and after (black line) running the in-progress sediment displacement Landlab component.

locations in western Washington using a range of climate and traffic conditions to examine estimates of forest road erosion. The model runs will be compared to sediment and runoff data collected during a broader study conducted by the Cooperative Monitoring Evaluation and Research Committee within the Washington Department of Natural Resources Adaptive Management Program (to be subsequently referred to as the WADNR Roads Project). These data will help calibrate and validate the model.

Because the WADNR Roads Project is utilizing a large number of field sites (78) to study multiple covariates affecting sediment production, we anticipate carrying out numerous model runs. Covariates that contribute to sediment production include traffic levels (high, medium, low), rainfall rates (high, medium, low), lithologies (volcanic, siltstone), road slopes (2.5–13%), rock surfacing qualities (marginal, good, high quality), and ditch line erosion control treatments (bare, eroded, grassed, wattled). We plan to run the process-based model using combinations of covariates in line with those seen at the 78 field sites, as well as a few other combinations.

The final model results from across sites will be presented in the limiting factor framing that relates erosion, supply, and energy seen in Chapter 2.4 to begin thinking about how different locations behave based on traffic and other covariates. If the energy is less than the supply, the erosion of the system will be dependent on energy, making the erosion process energy limited (e.g., a fully muddy road). However, once the energy is greater than the supply, the erosion of the system will be equal to the amount of supply available, making the erosion process supply limited (e.g., a rocky road). Based on this framing, we can classify

roads and think of potential mitigation strategies in terms of the road system type.

5.3   *Preliminary model results and discussion*

Below are preliminary results from example spatially-lumped model runs forced using rainfall data from a gage at Elk Rock near Mount St. Helens in Washington state. We carried out three model runs, each of which used a different level of traffic per day. The traffic level is modeled using a stochastic Poisson distribution centered around 5, 10, and 20 truck passes per day. Aside from the rainfall data, the model parameters are currently estimates based on limited information available in the literature, road surfacing practices, and field inferences (Table 5.1). As the model is further developed, the equations presented in this chapter and the parameter estimates used in the following results will be refined. Refinement of both will be determined based on small-scale field experiments (such as the experiments in Chapter 3 and Chapter 4) carried out as part the WADNR Roads Project.

In our model runs, the TAF layer has been initialized at "full" depth—a condition that corresponds to a road that has had many truck passes and no sediment transport due to rainfall—such that the model does not require a spin-up period (i.e., time to fill up the TAF layer to produce any sediment transport). A large storm occurs at the beginning of the period which flushes a lot of the fine sediment away—this is also called the "first flush" phenomenon (*Van Meerveld et al.*, 2014). The ups and downs of the fine sediment storage are due to traffic running over the road surface, causing a disturbance (increase), and then rainfall occurring, washing the fine sediment away (decrease) (Figure 5.6). As the traffic

Table 5.1: Parameter estimations used in the spatially-lumped model runs.

Parameter	Definition	Value(s)	Units
$S_{a_{initial}}$	Initial TAF layer depth	0.0275	m
$S_{s_{initial}}$	Initial surfacing layer depth	0.23	m
$S_{b_{initial}}$	Initial ballast layer depth	2.00	m
u_{ps}	Pumping rate in the surfacing layer	$5 * 10^{-7}$	m/truck pass
k_{cs}	Crushing rate in the surfacing layer	$1 * 10^{-7}$	m/truck pass
u_{pb}	Pumping rate in the ballast layer	$1 * 10^{-7}$	m/truck pass
k_{cb}	Crushing rate in the ballast layer	$1 * 10^{-7}$	m/truck pass
d_{50}	Median grain size in the TAF layer	$1.8 * 10^{-5}$	m
τ_c	Critical shear stress	0.055	Pa
Mean $n_{\Delta t}$	Center of a random Poisson distribution used to represent daily truck passes	5, 10, 20	truck passes/day

level increases, we see a higher overall TAF layer storage depth.

Figure 5.7 demonstrates the use of shear stress partitioning when modeling sediment transport for our three traffic levels. Here, we look at both the cumulative reference transport capacity and the cumulative actual transport. The cumulative reference transport capacity is the theoretical cumulative depth of domain-averaged erosion per storm had the shear stress not been partitioned (i.e., sum of q_f from Eq. 5.10 if τ_t had been used instead of τ_g). The red lines represent the cumulative reference transport capacity, and the bronze lines show the cumulative depth of sediment actually transported per storm (i.e., sum of $q_{f_{out}}$ from Eq. 5.14). The values of cumulative actual transport are much lower than the cumulative reference transport capacity because of shear stress partitioning. We see that as traffic level increases, the cumulative reference transport capacity decreases and the cumulative actual
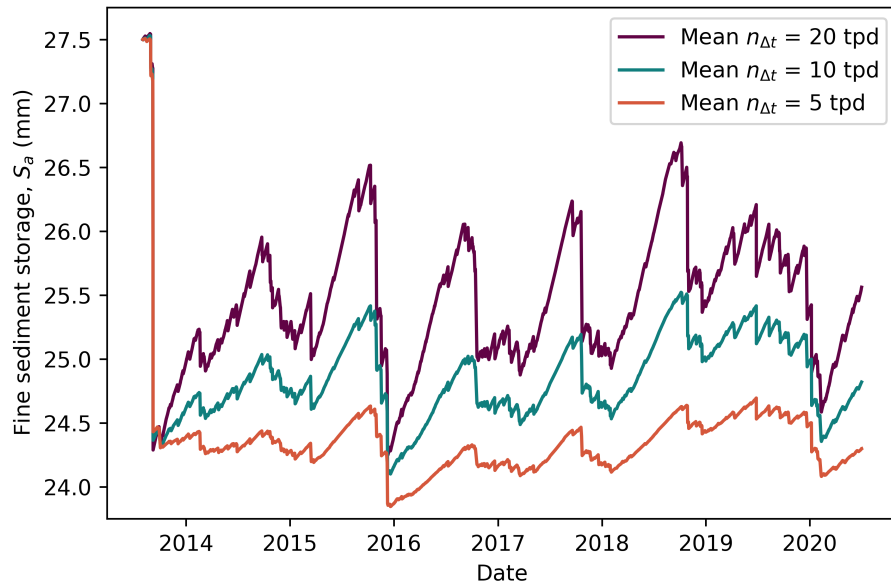
Figure 5.6: Fine sediment storage depth in the transport available fines (TAF) layer over time for three traffic levels (mean $n_{\Delta t} = 5$, 10, 20 truck passes per day). The TAF layer was initialized at 27.5 mm to avoid a model spin-up period.

transport increases. In other words, as traffic increases, the supply of readily-available fine sediment increases, which also causes an increase in actual sediment transported.
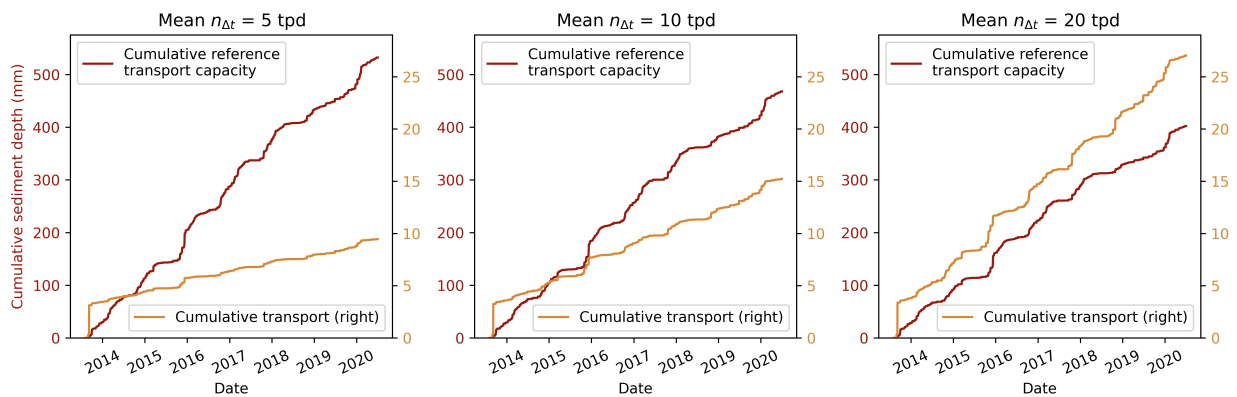
Figure 5.7: Cumulative reference transport capacity depth and cumulative actual transport depth over time for three traffic levels (mean $n_{\Delta t} = 5$, 10, 20 truck passes per day).

Lastly, we examine the annual sediment load per meter of road (Figure 5.8). Overall, the values of sediment mass per meter of road yielded by this model run are high compared to preliminary data collected as part of the WADNR Roads Project. This overestimation is likely due to a couple issues: (1) our parameters are only estimates currently and (2) this iteration of the spatially-lumped model includes only the road prism, whereas the data collected as part of the WADNR Roads Project includes the roadside ditch lines, which have grass linings serving as an erosion control treatment for sediment-laden water entering the ditches.
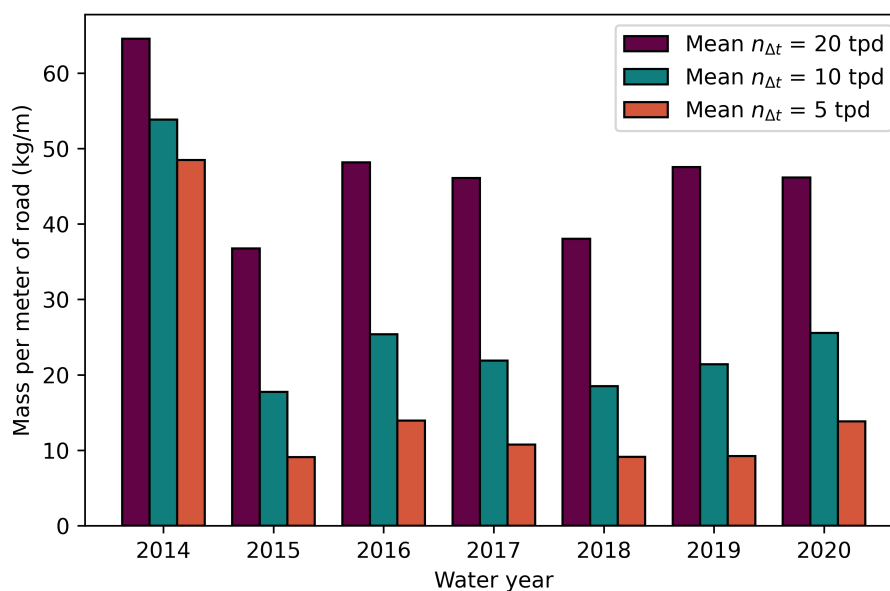
Figure 5.8: Sediment load per meter of road for each water year of the model run for three traffic levels (mean $n_{\Delta t} = 5,\ 10,\ 20$ truck passes per day).

5.4   Conclusion

In this chapter, we presented an initial spatially-lumped, process-based model for forest road erosion.

- The role of traffic within the model is conceptualized and mathematical representations are proposed for the two of the four processes.

- Results show how the uppermost layer evolves in relation to rainfall forcing and three different traffic levels.

- Sediment yield results broadly overestimate as compared with observations due to current estimations of model parameters. Refinement of parameters and mathematical representations will be based on small-scale field experiments carried out as part the WADNR Roads Project.

- This is the first model proposed to incorporate the discretized traffic-induced, erosion-enhancing processes seen in the literature. Ideally, this model will open doors for more physics-based thinking in estimating forest road erosion.

Acknowledgements

BIBLIOGRAPHY

Akay, A. E., O. Erdas, M. Reis, and A. Yuksel, Estimating sediment yield from a forest road network by using a sediment prediction model and GIS techniques, *Building and Environment*, *43*(5), 687–695, publisher: Elsevier, 2008.

Akgul, M., H. Yurtseven, S. Akburak, M. Demir, H. K. Cigizoglu, T. Ozturk, M. Eksi, and A. O. Akay, Short term monitoring of forest road pavement degradation using terrestrial laser scanning, *Measurement*, *103*, 283–293, doi:10.1016/j.measurement.2017.02.045, 2017.

Al-Hamdan, O. Z., F. B. Pierson, M. A. Nearing, C. J. Williams, J. J. Stone, Patrick R. Kormos, Jan Boll, and Mark A. Weltz, Risk Assessment of Erosion from Concentrated Flow on Rangelands Using Overland Flow Distribution and Shear Stress Partitioning, *Transactions of the ASABE*, *56*(2), 539–548, doi:10.13031/2013.42684, 2013.

Al-Hamdan, O. Z., F. B. Pierson, P. Robichaud, W. J. Elliot, and C. J. Williams, New Erodibility Parameterization for Applying WEPP on Rangelands Using ERMiT, *Journal of the ASABE*, *65*(2), 251–264, doi:10.13031/ja.14564, 2022.

Alvis, A. D., C. H. Luce, and E. Istanbulluoglu, How does traffic affect erosion of unpaved forest roads?, *Environmental Reviews*, *31*(1), 182–194, doi:10.1139/er-2022-0032, _eprint: https://doi.org/10.1139/er-2022-0032, 2023.

Alvis, A. D., C. H. Luce, E. Istanbulluoglu, T. Black, J. Dieu, and J. Black, Using additional roughness to characterize erosion control treatment effectiveness in roadside ditch lines, *Earth Surface Processes and Landforms*, *49*(4), 1255–1272, doi:10.1002/esp.5763, 2024.

Anderson, D. M., and L. H. Macdonald, Modelling road surface sediment production using a vector geographic information system, *Earth Surface Processes and Landforms*, *23*(2), 95–107, publisher: Wiley Online Library, 1998.

Arcement, G. J., and V. R. Schneider, Guide for selecting Manning's roughness coefficients for natural channels and flood plains, *USGS Numbered Series 2339*, U.S. Geological Survey, doi:10.3133/wsp2339, 1989.

Arnáez, J., V. Larrea, and L. Ortigosa, Surface runoff and soil erosion on unpaved forest roads from rainfall simulation tests in northeastern Spain, *Catena*, *57*(1), 1–14, doi:10.1016/j.catena.2003.09.002, publisher: Elsevier, 2004.

Aust, W. M., M. C. Bolding, and S. M. Barrett, Best Management Practices for Low-Volume Forest Roads in the Piedmont Region: Summary and Implications of Research, *Transportation Research Record*, *2472*(1), 51–55, doi:10.3141/2472-06, 2015.

Aydin, A., Y. Turk, and R. Eker, Pros and Cons of the Manual and Autonomous UAV Flights in Mapping of the Forest Road Surface Deformations: Preliminary Results, in *2nd International Symposium of Forest Engineering and Technologies*, pp. 47–52, Tirana, Albania, 2019.

Barnhart, K. R., E. W. H. Hutton, G. E. Tucker, N. M. Gasparini, E. Istanbulluoglu, D. E. J. Hobley, N. J. Lyons, M. Mouchene, S. S. Nudurupati, J. M. Adams, and C. Bandaragoda, Short communication: Landlab v2.0: a software package for Earth surface dynamics, *Earth Surface Dynamics*, *8*(2), 379–397, doi:10.5194/esurf-8-379-2020, publisher: Copernicus GmbH, 2020.

Barros, A. P., and J. D. Colello, Surface Roughness for Shallow Overland Flow on Crushed Stone Surfaces, *Journal of Hydraulic Engineering*, *127*(1), 38–52, doi:10.1061/(ASCE) 0733-9429(2001)127:1(38), 2001.

Bilby, R. E., K. Sullivan, and S. H. Duncan, The Generation and Fate of Road-Surface Sediment in Forested Watersheds in Southwestern Washington, *Forest Science*, *35*(2), 453–468, publisher: Oxford University Press, 1989.

Black, T., N. Nelson, R. Cissel, and C. Luce, Prediction of Erosion from Forest Road Networks, 2013.

Bloser, S., and B. E. Scheetz, Sediment Production from Unpaved Oil Well Access Roads in the Allegheny National Forest, *Tech. rep.*, The Center for Dirt and Gravel Road Studies at Pennsylvania State University, 2012.

Boston, K., Impact of the Ninth Circuit Court Ruling (Northwest Environmental Defense Center v. Brown) Regarding Forest Roads and the Clean Water Act, *Journal of Forestry*, *110*(6), 344–346, doi:10.5849/jof.11-069, 2012.

Boston, K., The potential effects of forest roads on the environment and mitigating their impacts, *Current Forestry Reports*, *2*(4), 215–222, publisher: Springer, 2016.

Boston, K., M. Pyles, and A. Bord, Compaction of forest roads in Northwestern Oregon–room for improvement, *International Journal of Forest Engineering*, *19*(1), 24–28, doi:10.1080/ 14942119.2008.10702556, publisher: Taylor & Francis, 2008.

Bradley, A. H., Reducing tire pressures lessens rutting on thawing forest roads: Results of two field trials, *SAE Technical Paper No. 942246*, Society of Automotive Engineers, Warrendale, PA, 1994.

Brown, K. R., W. Michael Aust, and K. J. McGuire, Sediment delivery from bare and graveled forest road stream crossing approaches in the Virginia Piedmont, *Forest Ecology and Management*, *310*, 836–846, doi:10.1016/j.foreco.2013.09.031, 2013.

Brown, K. R., K. J. McGuire, W. M. Aust, W. C. Hession, and C. A. Dolloff, The effect of increasing gravel cover on forest roads for reduced sediment delivery to stream crossings, *Hydrological Processes*, *29*(6), 1129–1140, doi:10.1002/hyp.10232, 2015.

Buffington, J. M., and D. R. Montgomery, A systematic analysis of eight decades of incipient motion studies, with special reference to gravel-bedded rivers, *Water Resources Research*, *33*(8), 1993–2029, doi:10.1029/96WR03190, 1997.

Burroughs, E. R., and J. G. King, Reduction of soil erosion on forest roads, *Tech. rep.*, U.S. Department of Agriculture, Forest Service, Intermountain Research Station, Ogden, UT, doi:10.2737/INT-GTR-264, 1989.

Burroughs, E. R., F. J. Watts, J. G. King, D. F. Haber, D. Hansen, and G. Flerchinger, Relative Effectiveness of Rocked Roads and Ditches in Reducing Surface Erosion, in *21st annual engineering, geology, and soils engineering symposium*, pp. 251–263, University of Idaho, Moscow, ID, 1984.

Cade, B. S., and B. R. Noon, A Gentle Introduction to Quantile Regression for Ecologists, *Frontiers in Ecology and the Environment*, *1*(8), 412–420, 2003.

Cambi, M., G. Certini, F. Neri, and E. Marchi, The impact of heavy traffic on forest soils: A review, *Forest Ecology and Management*, *338*, 124–138, doi:10.1016/j.foreco.2014.11.022, 2015.

Cao, L., Y. Wang, and C. Liu, Study of unpaved road surface erosion based on terrestrial laser scanning, *CATENA*, *199*, 105,091, doi:10.1016/j.catena.2020.105091, 2021.

Cartwright, N., Are RCTs the Gold Standard?, *BioSocieties*, *2*(1), 11–20, doi:10.1017/S1745855207005029, 2007.

Cederholm, C. J., and L. M. Reid, Impact of forest management on coho salmon (Oncorhynchus kisutch) populations of the Clearwater River, Washington: a project summary, in *Streamside Management: Forestry and Fishery Interactions, Proceedings of a Symposium held at University of Washington, 12-14 February 1986. Contribution no. 57, Institute of Forest Resources.*, edited by E. O. Salo and T. W. Cundy, pp. 373–398, Seattle, Washington, 1987.

Chen, Y., L. Xing-nian, and W. Xie-kang, Effects of roughness elements distribution on overland flow resistance, *Journal of Mountain Science*, *12*(5), 1145–1156, doi:10.1007/s11629-014-3391-8, 2015.

Cissel, R., T. Black, N. Nelson, and C. Luce, Southwest Crown of the Continent GRAIP Roads Assessment: Center Horse and Morrell/Trail Project Area, Poorman Creek, and Cold Creek. Lolo, Helena, and Flathead National Forests, Montana, *Tech. rep.*, US Department of Agriculture, Forest Service Rocky Mountain Research Station, Boise, ID, 2014.

Coker, R. J., B. D. Fahey, and J. J. Payne, Fine Sediment Production from Truck Traffic, Queen Charlotte Forest, Marlborough Sounds, New Zealand, *Journal of Hydrology (New Zealand)*, *31*(1), 56–64, publisher: New Zealand Hydrological Society, 1993.

Collins, L. M., and C. E. Johnston, Effectiveness of straw bale dams for erosion control in the Oakland Hills following the fire of 1991, in *Brushfires in California Wildlands: Ecology and Resource Management*, edited by J. E. Keeley and T. Scott, pp. 171–183, International Association of Wildland Fire, Fairfield, WA, 1995.

Cristan, R., W. M. Aust, M. C. Bolding, S. M. Barrett, J. F. Munsell, and E. Schilling, Effectiveness of forestry best management practices in the United States: Literature review, *Forest Ecology and Management*, *360*, 133–151, doi:10.1016/j.foreco.2015.10.025, 2016.

Cristan, R., W. M. Aust, M. C. Bolding, and S. M. Barrett, Estimated Sediment Protection Efficiencies for Increasing Levels of Best Management Practices on Forest Harvests in the Piedmont, USA, *Forests*, *10*(11), 997, doi:10.3390/f10110997, 2019.

Croke, J. C., and P. B. Hairsine, Sediment delivery in managed forests: a review, *Environmental Reviews*, *14*(1), 59–87, doi:10.1139/a05-016, publisher: NRC Research Press, 2006.

Dangle, C. L., M. C. Bolding, W. M. Aust, S. M. Barrett, and E. B. Schilling, Best Management Practices Influence Modeled Erosion Rates at Forest Haul Road Stream Crossings in Virginia, *JAWRA Journal of the American Water Resources Association*, *55*(5), 1169–1182, doi:10.1111/1752-1688.12762, 2019.

Darby, S. E., H. Q. Trieu, P. A. Carling, J. Sarkkula, J. Koponen, M. Kummu, I. Conlan, and J. Leyland, A physically based model to predict hydraulic erosion of fine-grained riverbanks: The role of form roughness in limiting erosion, *Journal of Geophysical Research*, *115*(F4), F04,003, doi:10.1029/2010JF001708, 2010.

Dawson, A., Rutting in unsurfaced roads - materials and structure interaction effects, in *International Symposium on Thin Pavements, Surface Treatments, Unbound Roads*, p. 9, Fredericton, New Brunswick, Canada, 1997.

Dawson, A., and P. Kolisoja, *Managing rutting in low volume roads: Executive summary*, Roadex III Project, 2006.

De Witt, A., K. Boston, and B. Leshchinsky, Predicting Aggregate Degradation in Forest Roads in Northwest Oregon, *Forests*, *11*(7), 729, doi:10.3390/f11070729, publisher: MDPI AG, 2020.

Dent, E. F., K. A. Mills, and J. Robben, Turbidity Off of Forest Roads in Oregon, in *Total Maximum Daily Load (TMDL) Environmental Regulations II*, American Society of

Agricultural and Biological Engineers, Albuquerque, New Mexico, USA, doi:10.13031/2013.15557, 2003.

Dobson, R. J., T. Colling, C. Brooks, C. Roussi, M. K. Watkins, and D. Dean, Collecting Decision Support System Data through Remote Sensing of Unpaved Roads, *Transportation Research Record: Journal of the Transportation Research Board*, *2433*(1), 108–115, doi:10.3141/2433-12, 2014.

Donald, W. N., W. C. Zech, X. Fang, and J. J. LaMondia, Evaluation of Wheat Straw Wattles for Velocity Reduction in Ditch Check Installations, *Transportation Research Record: Journal of the Transportation Research Board*, *2358*(1), 69–78, doi:10.3141/2358-08, 2013.

Dubé, K., W. Megahan, and M. McCalmon, Washington Road Surface Erosion Model, *Tech. rep.*, Washington Department of Natural Resources, Olympia, Washington, USA, 2004.

Dubé, K., A. Shelly, J. Black, and K. Kuzis, Washington road sub-basin scale effectiveness monitoring first sampling event (2006–2008) report, *Tech. rep.*, Washington Department of Natural Resources, Olympia, Washington, USA, 2010.

Edwards, P. J., F. Wood, and R. L. Quinlivan, Effectiveness of Best Management Practices that Have Application to Forest Roads, *General Technical Report NRS-163*, USDA Forest Service Northern Research Station, Parsons, West Virginia, USA, 2016.

Einstein, H. A., and R. B. Banks, Fluid resistance of composite roughness, *Transactions, American Geophysical Union*, *31*(4), 603, doi:10.1029/TR031i004p00603, 1950.

Einstein, H. A., and N. L. Barbarossa, River Channel Roughness, *Transactions of the American Society of Civil Engineers*, *117*(1), 1121–1132, doi:10.1061/TACEAT.0006666, publisher: American Society of Civil Engineers, 1952.

El Issaoui, A., Z. Feng, M. Lehtomäki, E. Hyyppä, H. Hyyppä, H. Kaartinen, A. Kukko, and J. Hyyppä, Feasibility of Mobile Laser Scanning towards Operational Accurate Road Rut Depth Measurements, *Sensors*, *21*(4), 1180, doi:10.3390/s21041180, 2021.

Elliot, W. J., WEPP Internet Interfaces for Forest Erosion Prediction, *JAWRA Journal of the American Water Resources Association*, *40*(2), 299–309, doi:10.1111/j.1752-1688.2004.tb01030.x, 2004.

Elliot, W. J., R. B. Foltz, and C. H. Luce, Modeling Low-Volume Road Erosion, *Transportation Research Record*, *1652*(1), 244–249, doi:10.3141/1652-64, publisher: SAGE Publications Inc, 1999.

Emmett, W. W., The hydraulics of overland flow on hillslopes, *Report 662A*, U.S. Govt. Print. Off., doi:10.3133/pp662A, edition: -, 1970.

Engman, E. T., Roughness Coefficients for Routing Surface Runoff, *Journal of Irrigation and Drainage Engineering*, *112*(1), 39–53, doi:10.1061/(ASCE)0733-9437(1986)112:1(39), 1986.

Fannin, R. J., and O. Sigurdsson, Field Observations on Stabilization of Unpaved Roads with Geosynthetics, *Journal of Geotechnical Engineering*, *122*(7), 544–553, doi:10.1061/(ASCE)0733-9410(1996)122:7(544), 1996.

Ferguson, R. I., R. J. Hardy, and R. A. Hodge, Flow resistance and hydraulic geometry in bedrock rivers with multiple roughness length scales, *Earth Surface Processes and Landforms*, *44*(12), 2437–2449, doi:10.1002/esp.4673, 2019.

Foltz, R. B., Sediment Reduction from the Use of Lowered Tire Pressures, *SAE Technical Paper No. 942244*, Society of Automotive Engineers, Warrendale, PA, 1994.

Foltz, R. B., Traffic and no-traffic on an aggregate surfaced road: Sediment production differences., in *The Seminar on Environmentally Sound Forest Road and Wood Transport*, FAO, Sinaia, Romania, 1996.

Foltz, R. B., and E. R. Burroughs, Sediment production from forest roads with wheel ruts, in *Watershed Planning and Analysis in Action Symposium. Proceedings of IR Conference Watershed Mgt/IR Div/ASCE in Durango, Colorado, July 9-11, 1990.*, edited by R. E. Riggins, E. B. Jones, R. Singh, and P. A. Rechard, pp. 266–275, American Society of Civil Engineers, 1990.

Foltz, R. B., and W. J. Elliot, Effect of lowered tire pressures on road erosion, *Transportation research record*, *1589*(1), 19–25, publisher: SAGE Publications Sage CA: Los Angeles, CA, 1997.

Foltz, R. B., and M. A. Truebe, Effect of aggregate quality on sediment production from a forest road, in *Proceedings of the Sixth International Conference on low-volume roads.*, vol. 1, pp. 49–57, Transportation Research Board, National Research Council, Washington, DC, USA, 1995.

Foltz, R. B., and M. A. Truebe, Locally available aggregate and sediment production, *Transportation Research Record*, *1819*(1), 185–193, publisher: SAGE Publications Sage CA: Los Angeles, CA, 2003.

Foltz, R. B., G. L. Evans, and M. Truebe, Relationship of forest road aggregate test properties to sediment production, in *Watershed Management and Operations Management 2000 in Fort Collins, Colorado, June 20-24, 2000.*, edited by M. Flug, D. Frevert, and D. W. Watkins, Jr., pp. 1–10, American Society of Civil Engineers, Reston, Virginia, USA, 2000.

Foster, G. R., L. J. Lane, M. A. Nearing, S. C. Finkner, and D. C. Flanagan, Erosion component, in *USDA-Water Erosion Prediction Project: Hillslope Profile Model Documentation*,

edited by L. J. Lane and M. A. Nearing, no. 2 in NSERL Report, pp. 1–12, National Soil Erosion Research Lab, West Lafayette, IN, 1989.

Fu, B., L. T. H. Newham, and C. E. Ramos-Scharron, A review of surface erosion and sediment delivery models for unsealed roads, *Environmental Modelling & Software*, *25*(1), 1–14, publisher: Elsevier, 2010.

Giroud, J. P., and J. Han, Design method for geogrid-reinforced unpaved roads. I. Development of design method, *Journal of Geotechnical and Geoenvironmental Engineering*, *130*(8), 775–786, doi:10.1061/(ASCE)1090-0241(2004)130:8(775), publisher: American Society of Civil Engineers, 2004.

Gnanendran, C. T., and C. Beaulieu, On the behaviour of low-volume unpaved resource access roads: effects of rehabilitation, *Canadian Journal of Civil Engineering*, *26*(3), 262–269, publisher: NRC Research Press Ottawa, Canada, 1999.

Govers, G., Evaluation of transporting capacity formulae for overland flow, in *Overland Flow: Hydraulics and Erosion Mechanics*, pp. 243–273, Chapman and Hall, New York, 1992.

Hanna, S., and K. Boston, Aggregate Performance on Forest Roads in the Pacific Northwest, *European Journal of Forest Engineering*, *4*(2), 43–49, 2018.

Hirano, M., RIVER-BED DEGRADATION WITH ARMORING, *Proceedings of the Japan Society of Civil Engineers*, *1971*(195), 55–65, doi:10.2208/jscej1969.1971.195_55, publisher: Japan Society of Civil Engineers, 1971.

Hobley, D. E. J., J. M. Adams, S. S. Nudurupati, E. W. H. Hutton, N. M. Gasparini, E. Istanbulluoglu, and G. E. Tucker, Creative computing with Landlab: an open-source toolkit for building, coupling, and exploring two-dimensional numerical models of Earth-surface dynamics, *Earth Surface Dynamics*, *5*(1), 21–46, doi:10.5194/esurf-5-21-2017, 2017.

Hrůza, P., T. Mikita, N. Tyagur, Z. Krejza, M. Cibulka, A. Procházková, and Z. Patočka, Detecting Forest Road Wearing Course Damage Using Different Methods of Remote Sensing, *Remote Sensing*, *10*(4), 492, doi:10.3390/rs10040492, 2018.

Indraratna, B., J. Lackenby, and D. Christie, Effect of confining pressure on the degradation of ballast under cyclic loading, *Geotechnique*, *55*(4), 325–328, publisher: Thomas Telford Ltd, 2005.

Istanbulluoglu, E., and R. L. Bras, Vegetation-modulated landscape evolution: Effects of vegetation on landscape processes, drainage density, and topography, *Journal of Geophysical Research*, *110*(F2), F02,012, doi:10.1029/2004JF000249, 2005.

Istanbulluoglu, E., D. G. Tarboton, R. T. Pack, and C. Luce, A probabilistic approach for channel initiation, *Water Resources Research*, *38*(12), 61–1–61–14, doi:10.1029/2001WR000782, 2002.

Istanbulluoglu, E., D. G. Tarboton, R. T. Pack, and C. Luce, A sediment transport model for incision of gullies on steep topography, *Water Resources Research*, *39*(4), doi:10.1029/2002WR001467, 2003.

Johnson, G., Minnesota's experience with thin bituminous treatments for low-volume roads, *Transportation research record*, *1819*(1), 333–337, publisher: SAGE Publications Sage CA: Los Angeles, CA, 2003.

Jordanova, A. A., and C. S. James, Experimental Study of Bed Load Transport through Emergent Vegetation, *Journal of Hydraulic Engineering*, *129*(6), 474–478, doi:10.1061/(ASCE)0733-9429(2003)129:6(474), 2003.

Jordán, A., and L. Martínez-Zavala, Soil loss and runoff rates on unpaved forest roads in southern Spain after simulated rainfall, *Forest Ecology and Management*, *255*(3-4), 913–919, doi:10.1016/j.foreco.2007.10.002, publisher: Elsevier, 2008.

Jordán-López, A., L. Martínez-Zavala, and N. Bellinfante, Impact of different parts of unpaved forest roads on runoff and sediment yield in a Mediterranean area, *Science of the Total Environment*, *407*(2), 937–944, doi:10.1016/j.scitotenv.2008.09.047, publisher: Elsevier, 2009.

Kemp, E., B. Leshchinsky, and K. Boston, Case Study: Evaluating Road Performance and Sediment Generation during Simulated Wet Weather Hauling, *European Journal of Forest Engineering*, *2*(1), 22–34, 2016.

Kemper, W. D., and R. C. Rosenau, Aggregate Stability and Size Distribution, in *Methods of Soil Analysis*, pp. 425–442, John Wiley & Sons, Ltd, doi:https://doi.org/10.2136/sssabookser5.1.2ed.c17, section: 17 _eprint: https://acsess.onlinelibrary.wiley.com/doi/pdf/10.2136/sssabookser5.1.2ed.c17, 1986.

Kochenderfer, J. N., Erosion Control on Logging Roads in the Appalachians, *Research Paper NE-158*, U.S. Department of Agriculture, Forest Service, Northeastern Forest Experiment Station., Upper Darby, PA, google-Books-ID: ZT0b3O9welMC, 1970.

Kochenderfer, J. N., and J. D. Helvey, Using gravel to reduce soil losses from minimum-standard forest roads, *Journal of Soil and Water Conservation*, *42*(1), 46–50, publisher: Soil and Water Conservation Society, 1987.

Kothyari, U. C., H. Hashimoto, and K. Hayashi, Effect of tall vegetation on sediment transport by channel flows, *Journal of Hydraulic Research*, *47*(6), 700–710, doi:10.3826/jhr.2009.3317, 2009.

Lackenby, J., B. Indraratna, G. McDowell, and D. Christie, Effect of confining pressure on ballast degradation and deformation under cyclic triaxial loading, *Géotechnique*, *57*(6), 527–536, doi:10.1680/geot.2007.57.6.527, publisher: Thomas Telford Ltd, 2007.

Lane, P. N. J., and G. J. Sheridan, Impact of an unsealed forest road stream crossing: water quality and sediment sources, *Hydrological processes*, *16*(13), 2599–2612, doi:10.1002/hyp.1050, publisher: Wiley Online Library, 2002.

Lane, S. N., Acting, predicting and intervening in a socio-hydrological world, *Hydrology and Earth System Sciences*, *18*(3), 927–952, doi:10.5194/hess-18-927-2014, 2014.

Laursen, E. M., The Total Sediment Load of Streams, *Journal of the Hydraulics Division*, *84*(1), 1–36, doi:10.1061/JYCEAJ.0000158, _eprint: https://ascelibrary.org/doi/pdf/10.1061/JYCEAJ.0000158, 1958.

Le Bouteiller, C., and J. G. Venditti, Sediment transport and shear stress partitioning in a vegetated flow, *Water Resources Research*, *51*(4), 2901–2922, doi:10.1002/2014WR015825, 2015.

Li, L., M. A. Nearing, V. O. Polyakov, M. H. Nichols, F. B. Pierson, and M. L. Cavanaugh, Evolution of rock cover, surface roughness, and its effect on soil erosion under simulated rainfall, *Geoderma*, *379*, 114,622, doi:10.1016/j.geoderma.2020.114622, 2020.

Li, T., J. G. Venditti, C. D. Rennie, and P. A. Nelson, Bed and bank stress partitioning in bedrock rivers, *Journal of Geophysical Research: Earth Surface*, *127*(2), e2021JF006,360, iSBN: 2169-9003 Publisher: Wiley Online Library, 2022a.

Li, X., Y. Zhang, X. Ji, P. Strauss, and Z. Zhang, Effects of shrub-grass cover on the hillslope overland flow and soil erosion under simulated rainfall, *Environmental Research*, *214*, 113,774, doi:10.1016/j.envres.2022.113774, 2022b.

Likitlersuang, S., K. Kounyou, and G. A. Prasetyaningtiyas, Performance of geosynthetic cementitious composite mat and vetiver on soil erosion control, *Journal of Mountain Science*, *17*(6), 1410–1422, doi:10.1007/s11629-019-5926-5, 2020.

Luce, C. H., Hydrological processes and pathways affected by forest roads: what do we still need to learn?, *Hydrological Processes*, *16*(1), 2901–2904, doi:10.1002/hyp.5061, 2002.

Luce, C. H., and T. A. Black, Sediment production from forest roads in western Oregon, *Water Resources Research*, *35*(8), 2561–2570, publisher: Wiley Online Library, 1999.

Luce, C. H., and T. A. Black, Effects of traffic and ditch maintenance on forest road sediment production, in *Proceedings of the Seventh Federal Interagency Sedimentation Conference*, pp. V67–V74, Reno, Nevada, 2001a.

Luce, C. H., and T. A. Black, Spatial and Temporal Patterns in Erosion from Forest Roads, *Land use and watersheds: Human influence on hydrology and geomorphology in urban and forest areas*, pp. 165–178, publisher: Wiley Online Library, 2001b.

Luce, C. H., and T. W. Cundy, Parameter identification for a runoff model for forest roads, *Water Resources Research*, *30*(4), 1057–1069, doi:10.1029/93WR03348, _eprint: https://onlinelibrary.wiley.com/doi/pdf/10.1029/93WR03348, 1994.

MacDonald, L. H., R. W. Sampson, and D. M. Anderson, Runoff and road erosion at the plot and road segment scales, St John, US Virgin Islands, *Earth Surface Processes and Landforms*, *26*(3), 251–272, publisher: Wiley Online Library, 2001.

Machuga, O., A. Shchupak, O. Styranivskiy, J. Krilek, M. Helexa, J. Kováč, T. Kuvik, V. Mancel, and P. Findura, Field and Laboratory Research of the Rut Development Process on Forest Roads, *Forests*, *15*(1), 74, doi:10.3390/f15010074, 2023.

Manga, M., and J. W. Kirchner, Stress partitioning in streams by large woody debris, *Water Resources Research*, *36*(8), 2373–2379, doi:10.1029/2000WR900153, 2000.

Marra, E., M. Cambi, R. Fernandez-Lacruz, F. Giannetti, E. Marchi, and T. Nordfjell, Photogrammetric estimation of wheel rut dimensions and soil compaction after increasing numbers of forwarder passes, *Scandinavian Journal of Forest Research*, *33*(6), 613–620, doi:10.1080/02827581.2018.1427789, 2018.

Megahan, W. F., Erosion over time on severely disturbed granitic soils: a model, *Research Paper INT-156*, U.S. Department of Agriculture Forest Service Intermountain Forest and Range Experiment Station, Ogden, Utah, 1974.

Megahan, W. F., and W. J. Kidd, Effect of logging roads on sediment production rates in the Idaho Batholith, *Research Paper INT-123*, U.S. Department of Agriculture Forest Service Intermountain Forest and Range Experiment Station, Ogden, Utah, doi:10.5962/bhl.title. 68728, 1972a.

Megahan, W. F., and W. J. Kidd, Effects of logging and logging roads on erosion and sediment deposition from steep terrain, *Journal of Forestry*, *70*(3), 136–141, publisher: Oxford University Press, 1972b.

Megahan, W. F., M. Wilson, and S. B. Monsen, Sediment production from granitic cutslopes on forest roads in Idaho, USA, *Earth Surface Processes and Landforms*, *26*(2), 153–163, doi:10.1002/1096-9837(200102)26:2⟨153::AID-ESP172⟩3.0.CO;2-0, 2001.

Meyer-Peter, E., and R. Müller, Formulas for bed-load transport, in *IAHSR 2nd meeting*, IAHSR, Stockholm, Sweden, 1948.

Moore, I. D., and G. J. Burch, Sediment Transport Capacity of Sheet and Rill Flow: Application of Unit Stream Power Theory, *Water Resources Research*, *22*(8), 1350–1360, doi:10.1029/WR022i008p01350, 1986.

Moore, R. D., Slug injection using salt in solution, *Streamline Watershed Management Bulletin*, *8*(2), 1–6, publisher: Citeseer, 2005.

Mueller, M. M., S. Dietenberger, M. Nestler, S. Hese, J. Ziemer, F. Bachmann, J. Leiber, C. Dubois, and C. Thiel, Novel UAV Flight Designs for Accuracy Optimization of Structure from Motion Data Products, *Remote Sensing*, *15*(17), 4308, doi:10.3390/rs15174308, 2023.

Nearing, M. A., G. R. Foster, L. J. Lane, and S. C. Finkner, A Process-Based Soil Erosion Model for USDA-Water Erosion Prediction Project Technology, *Transactions of the ASAE*, *32*(5), 1587–1593, doi:10.13031/2013.31195, place: St. Joseph, MI Publisher: ASAE, 1989.

Nepf, H. M., Flow and Transport in Regions with Aquatic Vegetation, *Annual Review of Fluid Mechanics*, *44*(1), 123–142, doi:10.1146/annurev-fluid-120710-101048, publisher: Annual Reviews, 2012.

Nevalainen, P., A. Salmivaara, J. Ala-Ilomäki, S. Launiainen, J. Hiedanpää, L. Finér, T. Pahikkala, and J. Heikkonen, Estimating the Rut Depth by UAV Photogrammetry, *Remote Sensing*, *9*(12), 1279, doi:10.3390/rs9121279, 2017.

Packer, P. E., Criteria for Designing and Locating Logging Roads to Control Sediment, *Forest Science*, *13*(1), 2–18, doi:10.1093/forestscience/13.1.2, 1967.

Pattison, J., K. Boston, and M. Pyles, Development of a correlation model between a 20-kg Clegg Hammer and field CBR for measuring subgrade strength in forest roads in western Oregon, *International Journal of Forest Engineering*, *21*(1), 12–19, doi:10.1080/14942119.2010.10702586, publisher: Taylor & Francis, 2010.

PRISM Climate Group, Mean annual precipitation time series, 2023.

Prosser, I. P., W. E. Dietrich, and J. Stevenson, Flow resistance and sediment transport by concentrated overland flow in a grassland valley, *Geomorphology*, *13*(1-4), 71–86, doi:10.1016/0169-555X(95)00020-6, 1995.

Ramos-Scharrón, C. E., and L. H. Macdonald, Measurement and prediction of sediment production from unpaved roads, St John, US Virgin Islands, *Earth Surface Processes and Landforms*, *30*(10), 1283–1304, doi:10.1002/esp.1201, 2005.

Reid, D. A., M. A. Hassan, and W. Floyd, Reach-scale contributions of road-surface sediment to the Honna River, Haida Gwaii, BC, *Hydrological Processes*, *30*(19), 3450–3465, doi:10.1002/hyp.10874, 2016.

Reid, L. M., Sediment Production from Gravel-Surfaced Roads, Clearwater Basin, Washington, Ph.D. thesis, University of Washington, Seattle, Washington, 1981.

Reid, L. M., and T. Dunne, Sediment production from forest road surfaces, *Water Resources Research*, *20*(11), 1753–1761, doi:10.1029/WR020i011p01753, 1984.

Reinhart, K. G., A. R. Eschner, and G. R. Trimble, *Effect on streamflow of four forest practices in the mountains of West Virginia*, vol. 1, Northeastern Forest Experiment Station, Forest Service, US Department of Interior, 1963.

Rhee, H., J. Fridley, and D. Page-Dumroese, Traffic-Induced Changes and Processes in Forest Road Aggregate Particle-Size Distributions, *Forests*, *9*(4), 181, doi:10.3390/f9040181, publisher: MDPI AG, 2018.

Schussler, J. C., B. Kazaz, M. A. Perez, J. Blake Whitman, and B. Cetin, Field Evaluation of Wattle and Silt Fence Ditch Checks, *Transportation Research Record: Journal of the Transportation Research Board*, *2675*(6), 281–293, doi:10.1177/0361198121992073, 2021.

Sheridan, G. J., and P. J. Noske, A quantitative study of sediment delivery and stream pollution from different forest road types, *Hydrological Processes: An International Journal*, *21*(3), 387–398, doi:10.1002/hyp.6244, publisher: Wiley Online Library, 2007.

Sheridan, G. J., P. J. Noske, R. K. Whipp, and N. Wijesinghe, The effect of truck traffic and road water content on sediment delivery from unpaved forest roads, *Hydrological Processes*, *20*(8), 1683–1699, doi:10.1002/hyp.5966, 2006.

Sojka, R. E., D. L. Bjorneberg, J. A. Entry, R. D. Lentz, and W. J. Orts, Polyacrylamide in Agriculture and Environmental Land Management, in *Advances in Agronomy*, vol. 92, edited by D. L. Sparks, pp. 75–162, Academic Press, doi:10.1016/S0065-2113(04)92002-0, 2007.

Sugden, B. D., and S. W. Woods, Sediment Production From Forest Roads in Western Montana, *JAWRA Journal of the American Water Resources Association*, *43*(1), 193–206, doi:10.1111j.1752-1688.2007.00016.x, publisher: Wiley Online Library, 2007.

Sullivan, K. O., and S. H. Duncan, Sediment yield from road surfaces in response to truck traffic and rainfall, *Weyerhaeuser Technical Report 042-4402.80*, Weyerhaeuser Company, Technical Center, Tacoma, WA, 1981.

Swift, L. W., Jr., Gravel and Grass Surfacing Reduces Soil Loss From Mountain Roads, *Forest Science*, *30*(3), 657–670, doi:10.1093/forestscience/30.3.657, 1984a.

Swift, L. W., Jr., Soil losses from roadbeds and cut and fill slopes in the southern Appalachian Mountains, *Southern Journal of Applied Forestry*, *8*(4), 209–216, publisher: Oxford University Press, 1984b.

Tarekegn, T. H., and T. Sayama, Correction of SRTM DEM Artefacts by Fourier Transform for Flood Inundation Modeling, *Journal of Japan Society of Civil Engineers, Ser. B1 (Hydraulic Engineering)*, *69*(4), I_193–I_198, doi:10.2208/jscejhe.69.I_193, 2013.

Thompson, A. M., B. N. Wilson, and B. J. Hansen, Shear stress partitioning for idealized vegetated surfaces, *Transactions of the ASAE*, *47*(3), 701–709, doi:10.13031/2013.16102, 2004.

Tiscareno-Lopez, M., V. L. Lopes, J. J. Stone, and L. J. Lane, Sensitivity Analysis of the WEPP Watershed Model for Rangeland Applications II: Channel Processes, *Transactions of the ASAE*, *37*(1), 151–158, 1994.

Tollner, E. W., B. J. Barfield, C. Vachirakornwatana, and C. T. Haan, Sediment Deposition Patterns in Simulated Grass Filters, *Transactions of the ASAE*, *20*(5), 940–0944, doi: 10.13031/2013.35679, place: St. Joseph, MI Publisher: ASAE, 1977.

Toman, E. M., and A. E. Skaugset, Reducing Sediment Production from Forest Roads during Wet-Weather Hauling, *Transportation Research Record: Journal of the Transportation Research Board*, *2203*(1), 13–19, doi:10.3141/2203-02, 2011.

Trimble, G. R., Logging Roads in Northeastern Municipal Watersheds, *American Water Works Association*, *51*(3), 407–410, publisher: American Water Works Association, 1959.

Trimble, G. R., and R. S. Sartz, How Far from a Stream Should a Logging Road Be Located?, *Journal of Forestry*, *55*(5), 339–341, doi:10.1093/jof/55.5.339, 1957.

Türk, Y., A. Aydin, and R. Eker, Comparison of Autonomous and Manual UAV Flights in Determining Forest Road Surface Deformations, *European Journal of Forest Engineering*, *8*(2), 77–84, doi:10.33904/ejfe.1206846, 2022.

United States Bureau of Reclamation (USBR), Water Measurement Manual, 2001.

Uusitalo, J., J. Ala-Ilomäki, H. Lindeman, J. Toivio, and M. Siren, Predicting rut depth induced by an 8-wheeled forwarder in fine-grained boreal forest soils, *Annals of Forest Science*, *77*(2), 42, doi:10.1007/s13595-020-00948-y, 2020.

Van Meerveld, H. J., E. J. Baird, and W. C. Floyd, Controls on sediment production from an unpaved resource road in a Pacific maritime watershed, *Water Resources Research*, *50*(6), 4803–4820, doi:10.1002/2013WR014605, publisher: Wiley Online Library, 2014.

Venanzi, R., F. Latterini, V. Civitarese, and R. Picchio, Recent Applications of Smart Technologies for Monitoring the Sustainability of Forest Operations, *Forests*, *14*(7), 1503, doi: 10.3390/f14071503, 2023.

Visser, R., K. Brown, and B. Tinnelly, Geogrid for unsealed forest roads: installation considerations and bearing capacity testing in New Zealand, *International Journal of Forest Engineering*, *28*(2), 106–115, doi:10.1080/14942119.2017.1317132, publisher: Taylor & Francis, 2017.

Wemple, B. C., and J. A. Jones, Runoff production on forest roads in a steep, mountain catchment, *Water Resources Research*, *39*(8), 17, doi:10.1029/2002WR001744, publisher: Wiley Online Library, 2003.

Wemple, B. C., J. A. Jones, and G. E. Grant, Channel Network Extension by Logging Roads in Two Basins, Western Cascades, Oregon, *JAWRA Journal of the American Water Resources Association*, *32*(6), 1195–1207, doi:10.1111/j.1752-1688.1996.tb03490.x, _eprint: https://onlinelibrary.wiley.com/doi/pdf/10.1111/j.1752-1688.1996.tb03490.x, 1996.

Whitman, J. B., J. C. Schussler, M. A. Perez, and L. Liu, Hydraulic Performance Evaluation of Wattles Used for Erosion and Sediment Control, *Journal of Irrigation and Drainage Engineering*, *147*(7), 04021,028, doi:10.1061/(ASCE)IR.1943-4774.0001586, 2021.

Wilkinson, M., R. Jones, C. Woods, S. Gilment, K. McCaffrey, S. Kokkalas, and J. Long, A comparison of terrestrial laser scanning and structure-from-motion photogrammetry as methods for digital outcrop acquisition, *Geosphere*, *12*(6), 1865–1880, doi:10.1130/GES01342.1, 2016.

Wright, K. N., Evaluation of check dams for sediment control on disturbed land surfaces, Master's thesis, University of Illinois at Urbana-Champaign, Urbana, IL, 2010.

Yager, E. M., J. W. Kirchner, and W. E. Dietrich, Calculating bed load transport in steep boulder bed channels, *Water Resources Research*, *43*(7), iSBN: 0043-1397 Publisher: Wiley Online Library, 2007.

Yetemen, O., P. M. Saco, and E. Istanbulluoglu, Ecohydrology controls the geomorphic response to climate change, *Geophysical Research Letters*, *46*(15), 8852–8861, iSBN: 0094-8276 Publisher: Wiley Online Library, 2019.

Yurtseven, H., M. Akgul, A. O. Akay, S. Akburak, H. K. Cigizoglu, M. Demir, T. Ozturk, and M. Eksi, High accuracy monitoring system to estimate forest road surface degradation on horizontal curves, *Environmental Monitoring and Assessment*, *191*(1), 32, doi:10.1007/s10661-018-7155-8, 2019.

Ziegler, A. D., and T. W. Giambelluca, Importance of rural roads as source areas for runoff in mountainous areas of northern Thailand, *Journal of Hydrology*, *196*(1-4), 204–229, publisher: Elsevier, 1997.

Ziegler, A. D., R. A. Sutherland, and T. W. Giambelluca, Partitioning total erosion on un-paved roads into splash and hydraulic components: The roles of interstorm surface preparation and dynamic erodibility, *Water Resources Research*, *36*(9), 2787–2791, publisher: Wiley Online Library, 2000.

Ziegler, A. D., T. W. Giambelluca, and R. A. Sutherland, Erosion prediction on unpaved mountain roads in northern Thailand: validation of dynamic erodibility modelling using

KINEROS2, *Hydrological Processes*, *15*(3), 337–358, publisher: Wiley Online Library, 2001a.

Ziegler, A. D., R. A. Sutherland, and T. W. Giambelluca, Interstorm surface preparation and sediment detachment by vehicle traffic on unpaved mountain roads, *Earth Surface Processes and Landforms*, *26*(3), 235–250, publisher: Wiley Online Library, 2001b.

Ziegler, A. D., T. W. Giambelluca, and R. A. Sutherland, Improved method for modelling sediment transport on unpaved roads using KINEROS2 and dynamic erodibility, *Hydrological Processes*, *16*(15), 3079–3089, publisher: Wiley Online Library, 2002.

Appendix A

SHEAR STRESS PARTITIONING RATIOS, APPENDIX FOR CH. 3

Shear stress partitioning ratios

As discussed in Chapter 3.2.1 of the main text, *Einstein and Barbarossa* (1952) proposed to partition shear stress into various components such as the shear stress that acts upon sediment grains and the shear stress that acts upon forms in the channel (e.g., bed forms and vegetation).

$$\tau_t = \rho_w g R S \tag{A.1}$$

$$\tau_t = \tau_g + \tau_a \tag{A.2}$$

where τ_g is the grain shear stress and τ_a is the additional shear stress. ρ_w is the density of water, g is the acceleration due to gravity, R is the hydraulic radius, and S is the channel slope.

In this Appendix, we take this knowledge and look at the partitioning ratio of grain shear stress to total bed shear stress (Chapter 3.2.1; Eq. 3.2) using different approximations.

A.1   General form with velocity term

Starting with Manning's equation and rearranging, we can obtain the hydraulic radius, R, of the channelized flow as a function of flow velocity, U, roughness, n, and slope, S:

$$U = \frac{R^{2/3}S^{1/2}}{n} \tag{Manning}$$

$$\Rightarrow R = \left(n\frac{U}{S^{1/2}} \right)^{3/2} \tag{A.3}$$

Following the logic of *Laursen* (1958), Eq. A.3 can be used for obtaining the grain component hydraulic radius, R_g, given an average flow velocity in the channel:

$$R_g = \left(n_g\frac{U}{S^{1/2}} \right)^{3/2} \tag{A.4}$$

where n_g is the grain roughness.

In the same form as Eq. A.1, the effective shear stress acting on the grains, τ_g, can be written as:

$$\tau_g = \rho_w g R_g S$$

$$\tau_g = \rho_w g n_g^{3/2} \, U^{3/2} S^{1/4} \tag{A.5}$$

where ρ_g is the density of water and g is the acceleration of gravity.

For the shear stress partitioning ratio ($f_g = \frac{\tau_g}{\tau_t}$), we combine Equations A.1, A.3, and A.5

to get:

$$\frac{\tau_g}{\tau_t} = \frac{n_g^{3/2} \rho_w g U^{3/2} S^{1/4}}{n_t^{3/2} \rho_w g U^{3/2} S^{1/4}}$$

$$\frac{\tau_g}{\tau_t} = \left(\frac{n_g}{n_t}\right)^{3/2} \tag{A.6}$$

Using this standard form of shear stress partitioning ratio maintains a dependency on constant velocity, and the resulting shear stress partitioning ratio is proportional to the ratio of grain roughness to total roughness raised to the 1.5 power.

A.2 General form with no velocity term

In this section, we take the general form of the shear stress partitioning ratio and remove the dependency on constant velocity to get the equation in terms of fewer dependent variables. To do so, we write velocity as $U = \frac{Q}{A}$ and substitute in $A = \frac{R^2}{C^2}$ (sensu *Istanbulluoglu et al.*, 2003; *Moore and Burch*, 1986), where C is a constant that is based on channel shape:

$$U = \frac{QC^2}{R^2} \tag{A.7}$$

Using these substitutions, we can rewrite Manning's equation for Q and solve for R:

$$Q = \frac{1}{nC^2} R^{8/3} S^{1/2}$$

$$\Rightarrow R = \left[\frac{nC^2}{S^{1/2}}\right]^{3/8} Q^{3/8} \tag{A.8}$$

Again, following the logic of *Laursen* (1958), R can be written for grain or total roughness

as:

$$R_g = \left[\frac{n_g C^2}{S^{1/2}}\right]^{3/8} Q^{3/8}$$

$$R_t = \left[\frac{n_t C^2}{S^{1/2}}\right]^{3/8} Q^{3/8} \tag{A.9}$$

Recalling Eq. A.7, we can now express U as a function of Q, n, and S:

$$U = \frac{C^{1/2}}{n^{3/4}} Q^{1/4} S^{3/8} \tag{A.10}$$

We now have all the pieces needed to calculate the shear stress partitioning ratio. From Eq.

A.2 and *Manga and Kirchner* (2000), we have:

$$\tau_t = \tau_g + \tau_a$$

$$\rho_w g R_t S = \rho_w C_{dg} U^2 + \rho_w C_{da} U^2$$

or

$$\rho_w g R_t S = \rho_w C_{dt} U^2 \tag{A.11}$$

where $C_{dt} = C_{dg} + C_{da}$. And for bare conditions, we have:

$$\tau_t = \tau_g$$

$$\rho_w g R_g S = \rho_w C_{dg} U^2 \tag{A.12}$$

which we can use to solve for C_{dg} (and C_{dt}):

$$C_{dg} = \frac{g R_g S}{U^2} \tag{A.13}$$

Substituting Eq. A.9 and Eq. A.10:

$$C_{dg} = \frac{g \left[\frac{n_g C^2}{S^{1/2}}\right]^{3/8} Q^{3/8} S}{\left[\frac{C^{1/2}}{n_g^{3/4}} Q^{1/4} S^{3/8}\right]^2}$$

$$C_{dg} = \frac{g \left[\frac{n_g^{3/8} C^{3/4}}{S^{3/16}}\right] Q^{3/8} S}{\frac{C}{n_g^{3/2}} Q^{1/2} S^{3/4}}$$

$$C_{dg} = g n_g^{15/8} C^{-1/4} Q^{-1/8} S^{1/16} \tag{A.14}$$

And it follows that C_{dt} takes on the same form:

$$C_{dt} = n_t^{15/8} C^{-1/4} Q^{-1/8} S^{1/16} g \tag{A.15}$$

Our shear stress partitioning ratio, then, is:

$$\frac{\tau_g}{\tau_t} = \frac{\rho_w g n_g^{15/8} C^{-1/4} Q^{-1/8} S^{1/16} U^2}{\rho_w g n_t^{15/8} C^{-1/4} Q^{-1/8} S^{1/16} U^2}$$

$$\frac{\tau_g}{\tau_t} = \left(\frac{n_g}{n_t}\right)^{15/8} \tag{A.16}$$

The resulting shear stress partitioning ratio here is proportional to the ratio of grain roughness to total roughness raised to the 1.875 power.

A.3 Parabolic channel approximation with reduced dimensionality

In this section, we again take the general form of the shear stress partitioning ratio and remove the dependency on constant velocity to get the equation in terms of fewer dependent variables. Additionally, we use a parabolic approximation to further reduce the required variables.

In this case, we will follow a similar set of steps to Appendix A.2, but instead of using $A = \frac{R^2}{C^2}$ to calculate A, we instead use two simplifications: one for a parabolic channel's area, A, and one for the parabolic approximation of wetted perimeter, P, and hydraulic radius, R, assuming that the shape of water flow is wide and shallow:

$$A = \frac{a}{6} w^3 \tag{A.17}$$

$$P \approx w \tag{A.18}$$

$$R = \frac{A}{P} \approx \frac{a}{6} w^2 \tag{A.19}$$

where a is the parameter that determines the shape of a parabola and w is the top width of

the channel flow. We can substitute $w = \sqrt{\frac{6}{a}R}$ into Eq. A.17:

$$A = \frac{a}{6}\left(\frac{6}{a}R\right)^{3/2}$$

$$A = \sqrt{\frac{6}{a}}R^{3/2} \tag{A.20}$$

which we can substitute into Manning's equation and solve for R:

$$Q = \frac{1}{n}\sqrt{\frac{6S}{a}}R^{3/2}R^{2/3} = \frac{1}{n}\sqrt{\frac{6S}{a}}R^{13/6} \tag{A.21}$$

$$\Rightarrow R = \left(\frac{nQ}{\sqrt{\frac{6S}{a}}}\right)^{6/13} \tag{A.22}$$

Plugging Eq. A.22 back into Eq. A.20 to get A in terms of n, Q, S, and a:

$$A = \sqrt{\frac{6}{a}}\left(\frac{nQ}{\sqrt{\frac{6S}{a}}}\right)^{6/13*3/2} = \sqrt{\frac{6}{a}}\left(\frac{nQ}{\sqrt{\frac{6S}{a}}}\right)^{9/13} \tag{A.23}$$

Getting the velocity, U, in the same terms:

$$U = \frac{Q}{A} = Q\sqrt{\frac{a}{6}}\left(\frac{nQ}{\sqrt{\frac{6S}{a}}}\right)^{-9/13} \tag{A.24}$$

And calculating U^2 for ease of future arithmetic:

$$U^2 = Q^2 \frac{a}{6} \left(\frac{nQ}{\sqrt{\frac{6S}{a}}} \right)^{-18/13}$$

$$U^2 = \frac{Q^2 S^{9/13} \left(\frac{6}{a} \right)^{9/13}}{n^{18/13} Q^{18/13} \left(\frac{6}{a} \right)}$$

$$U^2 = \frac{Q^{8/13} S^{9/13}}{n^{18/13} \left(\frac{6}{a} \right)^{4/13}} \tag{A.25}$$

Following the logic of Appendix A.2 and using the forms of Eq. A.12 through Eq. A.14, we can get C_{dg} in terms of n, Q, S, and a, too:

$$C_{dg} = \frac{g R_g S}{U^2}$$

$$C_{dg} = \frac{g \left(\frac{n_g Q}{\sqrt{\frac{6S}{a}}} \right)^{6/13} S}{\frac{Q^{8/13} S^{9/13}}{n_g^{18/13} \left(\frac{6}{a} \right)^{4/13}}}$$

$$C_{dg} = \frac{g n_g^{6/13} Q^{6/13} S n_g^{18/13} \left(\frac{6}{a} \right)^{4/13}}{Q^{8/13} S^{9/13} S^{3/13} \left(\frac{6}{a} \right)^{3/13}}$$

$$C_{dg} = g n_g^{24/13} Q^{-2/13} S^{1/13} \left(\frac{6}{a} \right)^{1/13} \tag{A.26}$$

And it follows that C_{dt} takes on the same form:

$$C_{dt} = n_t^{24/13} Q^{-2/13} S^{1/13} \left(\frac{6}{a} \right)^{1/13} g \tag{A.27}$$

Our shear stress partitioning ratio, then, is:

$$\frac{\tau_g}{\tau_t} = \frac{\rho_w g n_g^{24/13} Q^{-2/13} S^{1/13} \left(\frac{6}{a}\right)^{1/13} U^2}{\rho_w g n_t^{24/13} Q^{-2/13} S^{1/13} \left(\frac{6}{a}\right)^{1/13} U^2}$$

$$\frac{\tau_g}{\tau_t} = \left(\frac{n_g}{n_t}\right)^{24/13} \tag{A.28}$$

The resulting shear stress partitioning ratio here is proportional to the ratio of grain roughness to total roughness raised to the 1.85 power.